NATIONAL TECHNICAL UNIVERSITY OF ATHENS
SCHOOL OF NAVAL ARCHITECTURE & MARINE ENGINEERING
LABORATORY OF MARINE ENGINEERING

LAMPROS RIZOS

DIPLOMA THESIS

DESIGN AND EXPERIMENTAL STUDY OF AN AIR CURTAIN ARRANGEMENT FOR PROTECTION FROM SOOT LOADING OF A SOLID STATE NO_X SENSOR PERMANENTLY INSTALLED IN THE EXHAUST GAS DUCT OF A DIESEL ENGINE

SUPERVISOR: PROFESSOR N. P. KYRTATOS

ATHENS, JULY 2014

AKNOWLEDGEMENTS

I would like to thank the supervisor professor N. Kyrtatos for giving me the opportunity to work in the facilities of Laboratory of Marine Engineering of National Technical University of Athens (NTUA – LME) and for his guidance given. I would, also, like to thank Dr - Ing N. Alexandrakis for his useful advice and his experience shared throughout the implementation of this thesis. In addition, I would like to thank Mr. S. Glaros and N. Vrettakos for their assistance in every step of the work done and especially for their help referring my familiarization with the facilities of LME – NTUA. Finally, I would like to thank NTUA – LME technicians, Mr. I. Daliapes and C. Sarris for their cooperation during the construction of the models designed and every technical matter occurred.

ABSTRACT

This thesis refers to the design and experimental study of an air curtain arrangement that would protect an amperometric NO_X sensor, initially designed for automotive applications, from excessive soot loading. The sensor is purposed to be permanently installed in the engine exhaust duct and it would be protected by the air curtain flow when it does not record measurements. Two types of this arrangement which consisted of a dummy sensor and an air nozzle were tested, for different values of air pressure. The amount of soot deposition was evaluated through processing techniques of dummy sensors' images, in order to define the most effective arrangement. The final structure which consists of the actual NO_X sensor and the selected air nozzle was tested. The sensor readings were compared to simultaneous measurements of a CLD type analyzer, specified by IMO. Moreover, NO_X measurements by the sensor were recorded with the air curtain device switched on, in order to investigate the impact of the arrangement's operation on the sensor's output.

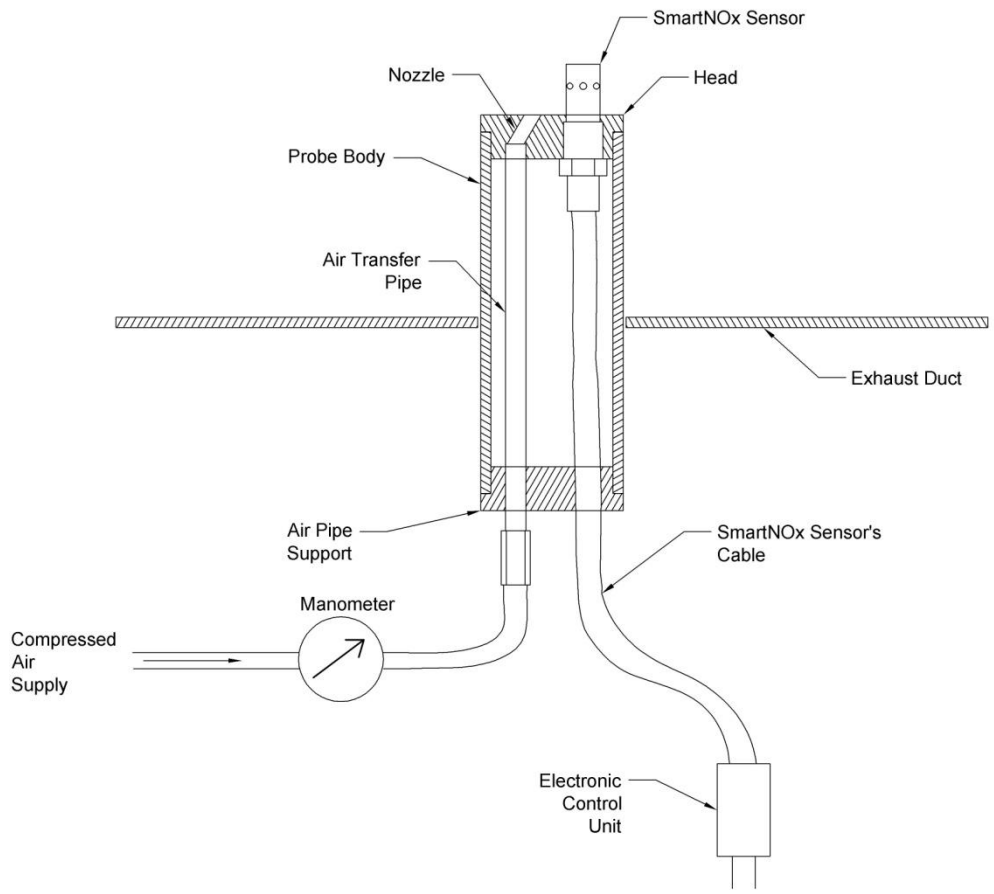

Figure 1. Schematic representation of an air curtain arrangement

TABLE OF CONTENTS

NOTATIONS

CLD – Chemiluminescence Detection

CO – Carbon Monoxide

CO_2 – Carbon Dioxide

DAQ – Data acquisition

ECU – Electronic Control Unit

GVC – Gross Calorific Value

HC - Hydrocarbons

HFO – Heavy Fuel Oil

IMO – International Maritime Organization

NVC – Net Calorific Value

NO – Nitrogen Monoxide

NO_2 – Nitrogen Dioxide

NO_x – Nitrogen Oxides

NTUA-LME – National Technical University of Athens / Laboratory of Marine Engineering

O_2 – Oxygen

O_3 – Ozone

PMD – Paramagnetic Detection

PMT – Photomultiplier Tube

RGB – Red Green Blue

SNS – SmartNO_X Sensor

SO_2 – Sulphur Dioxide

TIG – Tungsten Inert Gas

ZrO_2 – Zirconium Dioxide

1. INTRODUCTION - OBJECTIVES

The last few years, pollutant emissions from land – based human activities have been gradually reduced. On the contrary, pollutant emissions from shipping are continuously increasing. Apart from greenhouse gases, pollutants like sulphur and nitrogen oxides cause serious problems in the natural habitat like soil and water acidification, eutophication (over – fertilization) and ground – level ozone formation. Sea areas around Europe (Baltic and North Sea, North – Eastern Atlantic, the Mediterranean and the Black Sea) are suffering from millions tonnes of sulphur dioxide (SO_2) and nitrogen oxides (NO_X) in a yearly basis. Under a business-as-usual scenario these amounts of shipping emissions are expected to increase by 40-50 per cent during the time period between the year 2000 and 2020. By the end of that time period, shipping emissions around Europe are expected to surpass the total emissions from land-based sources in the 27 EU states, as shown in Figure 1.1 [1].

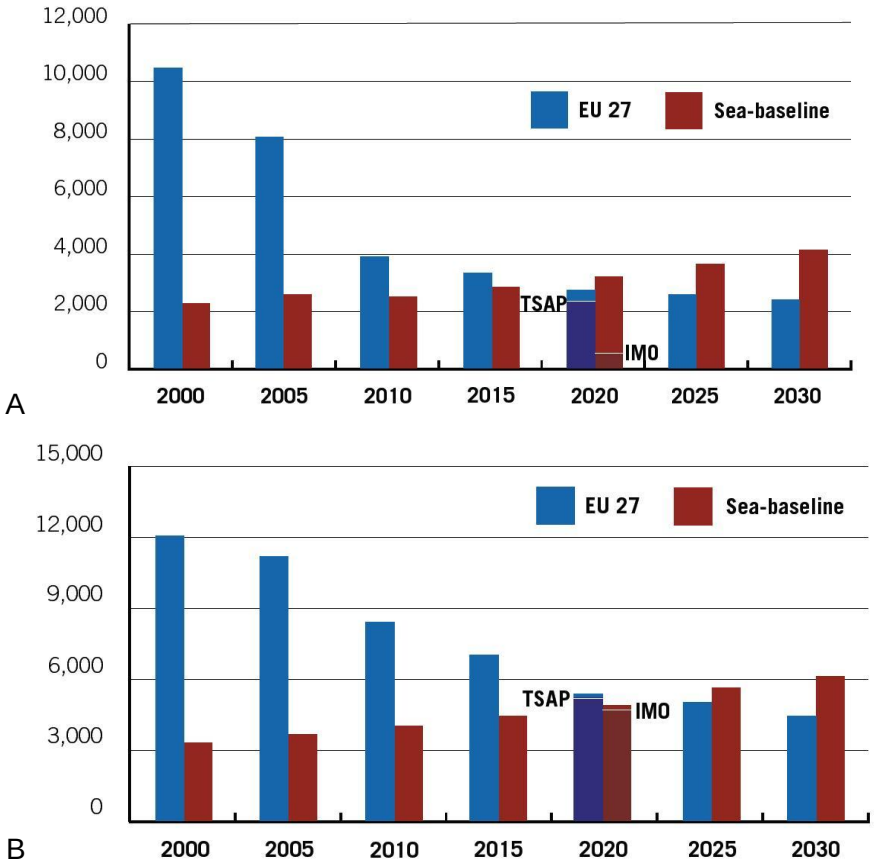

EU27: Emissions from land – based sources (incl. domestic shipping)
Sea: Emissions from international shipping in European sea areas
TSAP: Target in line with the EU's Thematic Strategy on Air Pollution
IMO: Expected outcome from implementing the revised IMO MARPOL Annex VI

Figure 1.1 (A): Emissions of SO_2 2000-2030 (ktonnes), (B): Emissions of NOx 2000-2030 (ktonnes) [1].

Therefore, the International Maritime Organization (IMO) has imposed emission standards, commonly referred to as Tier I, II and III. Tier III enters into force on year 2016 and includes the introduction of NO_X Emission Control Areas, in which NO_X emission limit is reduced by 74%, as shown in Figure 1.2.

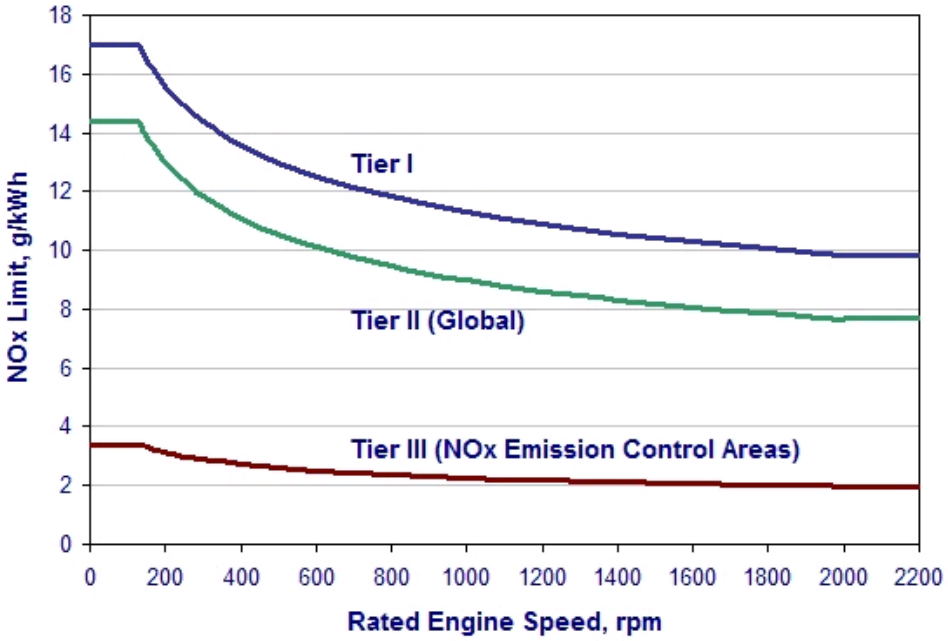

Figure 1.2. MARPOL Annex VI NO_X Emission Limits [1]

As regards the economy, on one hand, fuel prices have increased significantly during the last decade but, on the other hand, “Economy of Scale” imposes greater cargo intakes and service speeds.

All the aforementioned facts are revealing the need for the main engine to run at minimum fuel consumption levels, while at the same time satisfying the emission limits. Therefore, the design of a novel control system capable of operating the engine at optimal conditions is of outmost importance. Such a control system requires sensors and diagnostic routines which will also support the engine monitoring and diagnostic systems. One of the parameters to be monitored is the nitrogen oxide emissions (NO_X).

After several engine tests at NTUA – LME, it has been proved that a relatively cheap, compact and easy to operate NO_X sensor taken from the automotive industry (“Smart-NO_X” sensor - SNS) can take accurate measurements compared to those of reference type analyzers specified by IMO. However, it has been revealed that soot deposition can affect the sensor’s performance and shorten its life span.

The objective of this diploma thesis was the design of an air curtain arrangement which protects SNS from soot loading when it is switched off, so that the SNS can be

permanently installed in the exhaust duct. The layout of the air curtain device is shown in Figure 2.5.2. The idea is to create a cross flow of compressed air which disrupts the flow of the exhaust gas and prevents soot reaching the surface of the sensor.

To evaluate the performance of this device, engine tests were performed in which the SNS's output will be compared to the output of analyzers specified by IMO. These analyzers are already part of the NTUA – LME portable emissions measurement unit.

2. LITERATURE REVIEW

2.1 Introduction

The NO_X Technical Code, adopted by MARPOL - Annex VI, specifies that nitrogen oxide analyzers must be of the ChemiLuminescent Detector (CLD) type. The NTUA – LME mobile emission measurement unit features a NO_X analyzer of the CLD type (EcoPhysics CLD700) and an amperometric NO_X sensor created for automotive industry applications (Continental SmartNO_x Sensor). In this chapter, the operating principles of the aforementioned measurement devices will be presented in detail. Moreover, simultaneous measurements from both the sensor and the analyzer, already taken at the NTUA – LME test bed will be presented, in order to demonstrate the performance of the amperometric sensor in comparison with this of the CLD analyzer. Finally, indicative parts of the theory of *jets in cross flow,* on which the concept of the air-curtain device was based, will be described.

2.2 Amperometric sensors measurement principle

The operating principle of the amperometric sensor for the direct measurement of the NO_X-concentration in exhaust gases is based on the measurement of the resulting current when constant voltage is applied. The resulting current is directly proportional to the oxygen concentration in the exhaust gases.

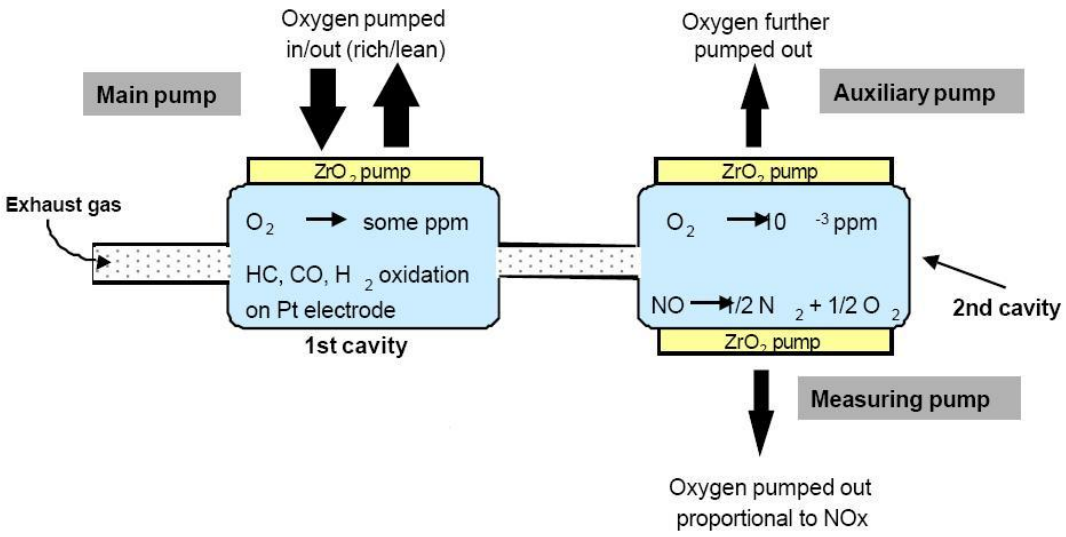

Figure 2.2.1. Schematic diagram of NO_X Sensor [2]

The sensor consists of a pumping cell and a diffusion barrier which limits oxygen transfer rate from the ambient air to the cathode of the pumping cell. The pumping cell typically

consists of two cavities, each of which has an ion conducting electrolyte made of solid ceramic material (in this case ZrO_2).

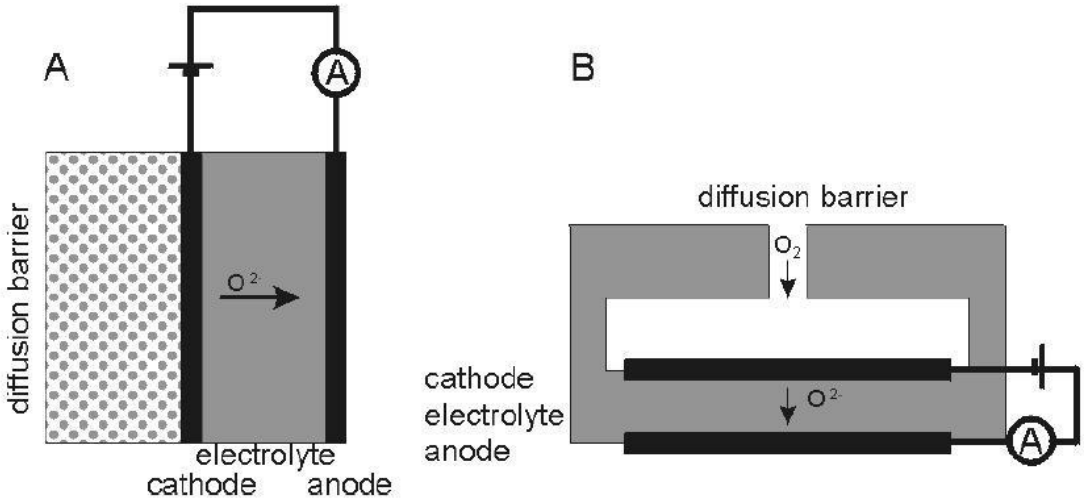

Figure 2.2.2. Schematic representations of a limiting current amperometric sensor. (A) porous diffusion barrier and, (B), a diffusion channel as a diffusion barrier. [3]

Due to the applied voltage and the different O_2 concentration between the sensor cavities and ambient air, the O_2 molecules break down into oxygen ions, as shown in the following electrochemical reaction.

$$O_2(g) + 4e^-(electrode) \rightarrow 2O^{2-}(electrolyte) \quad (2.2.1)$$

The ions move from the cathode electrode of the electrolyte to the anode electrode, passing through the ion conducting electrolyte. This flow of oxygen ions produces a current along the electrolyte which reduces the current produced by the applied voltage. The limiting current i_l is related to the oxygen concentration of the ambient air c_O according to the following equation.

$$i_l = \frac{4FD_O A c_O}{L} \quad (2.2.2)$$

Where, F is the Faraday constant,

D_O is the diffusion coefficient of oxygen in the gas phase,

A is the cross-sectional area of the diffusion barrier hole and

L is the length of the diffusion hole.

Except for the reduction of oxygen, oxidation of other compounds of the gas mixture (HC, CO, H_2 etc.) takes place. In addition Nitrogen dioxide is decomposed to NO and O_2

$$NO_2 \rightarrow NO + 1/2O_2. \quad (2.2.3)$$

Therefore, the gas mixture that reaches the second cavity, which consists of two pairs of electrodes, is composed of NO and a few ppm of O_2. This small concentration of O_2 is further reduced in the first pair of electrodes of the second cavity according to the electrochemical procedure described for the first cavity. Then, the gas in the second cavity only consists of NO which breaks down to N_2 and O_2 due to the catalytic action of the second pair of electrodes.

$$NO \rightarrow {}^{1}/_{2}\ N_2 + {}^{1}/_{2}\ O_2 \qquad (2.2.4)$$

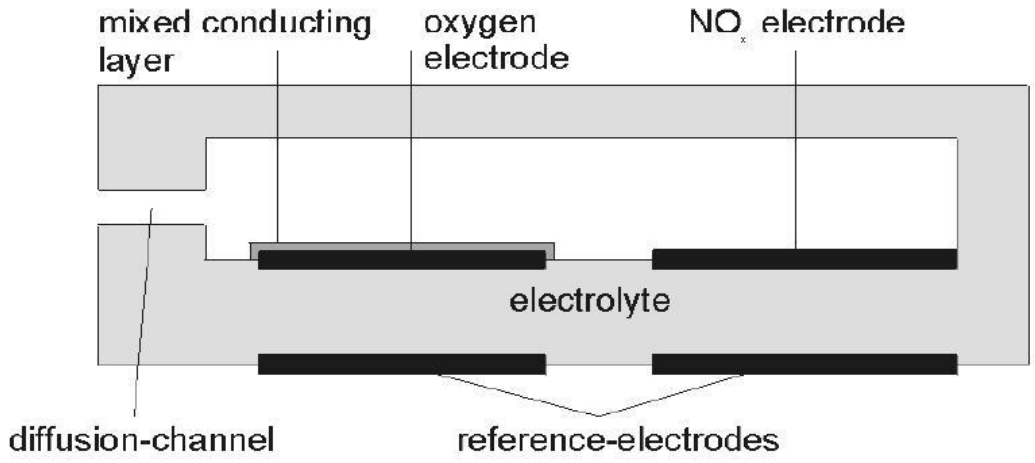

Figure 2.2.3. Overview of an amperometric two - electrode NO_X sensor [3]

The current generated by the produced O_2 from the above reaction is directly related to the NO_X concentration in the gas. [3]

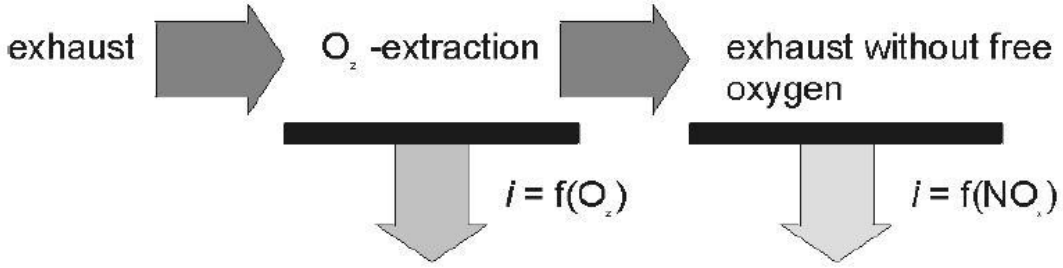

Figure 2.2.4. Schematical representation of an amperometric NO_X sensor operating method [3]

2.3 Chemiluminescence measurement principle [4]

The following reaction takes place, when sample gas is mixed with internally-produced ozone into the chamber of a CLD type analyzer.

$$NO + O_3 \rightarrow NO_2^* + O_2 \quad \text{(Approx. 20\%)} \qquad (2.3.1)$$

$$NO + O_3 \rightarrow NO_2 + O_2 \qquad (2.3.2)$$

In reaction (2.2.1) only the 20% of NO is converted into the excited state of NO_2 (NO_2*), which returns to ground state according the following reactions.

$$NO_2^* \rightarrow NO_2 + hv \qquad (2.3.3)$$

$$NO_2^* + M \rightarrow NO_2 + M \qquad (2.3.4)$$

The electromagnetic radiation emission has a wave length range between 600-3000mm and maximum intensity of 1200nm (approx.). Due to collisions with other molecules (M), the largest portion of the NO_2* reverts back to the ground state without radiation emission (2.3.4). This unwanted phenomenon is known as quenching and the extent to which it occurs depends on the character of the colliding molecule M. Also, the portion of NO_2* subjected to quenching, increases proportionally with the pressure in the chamber. Therefore, the pressure in the reaction chamber is reduced.

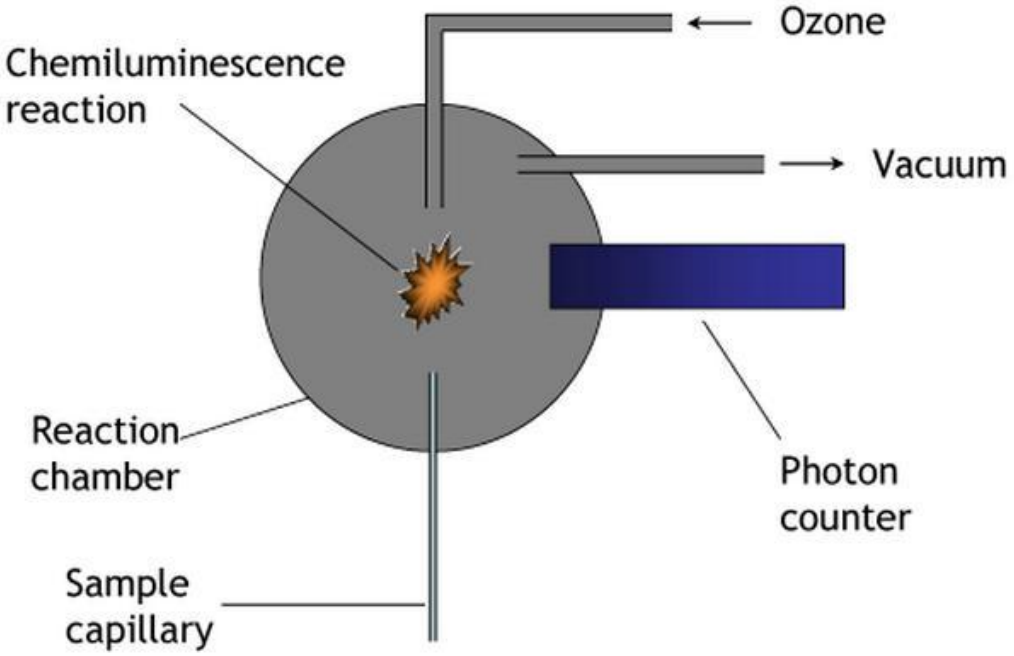

Figure 2.3.1. Chemiluminescence mechanism [5]

In order to include the concentration of NO_2 in the measurement, it is reduced to NO according the following reaction (2.3.5.).

$$NO_2 + C \rightarrow NO + CO \qquad (2.3.5)$$

In the reaction above, the sample gas passes through a converter heated up to 415^{o}C and carbon (C) is the reducing agent of the converter.

The concentration of NO generated according to the reaction (2.3.5) undergoes the mechanism described above (eqs. 2.3.1 – 2.3.4).
The chemiluminescence signal is detected photo-electrically by a multiplier. In the reaction chamber, the pressure remains constant and the O_3 concentration is in excess, so the signal is proportional to the NO- concentration of the sample gas.

2.4 Past activities of NTUA – LME related to the SmartNO$_X$ Sensor.

Several engine tests were conducted at the NTUA – LME test bed as a part of a comparative study, in order to evaluate the performance of a SmartNO$_X$ Sensor. The measurements of the SNS were compared to those of EcoPhysics CLD700 analyzer that measured NO$_X$ using the chemiluminescence principle. The engine was operated at various conditions in order to investigate the output of the SNS in different case scenarios and compare it directly to those of CLD analyzer.

- Constant load tests

During constant load tests (25, 50, 75 and 90%) the outputs of SNS and CLD700 showed great consistency and repeatability. More specifically, the deviation of the measurements from the mean value that was recorded from both the sensor and the analyzer was limited to ±3.4%[6]. Moreover, the output of the SNS was very close to the output of the CLD700.

- Transient load tests

During these tests the engine load was charged from 25% to 90% and back. It was observed that the SNS responded immediately to the load changes, while the CLD700 had a small delay. As in constant load tests, both the sensor's and the analyzer's output were consistent and repeatable. So the dynamic performance of the SNS was rather satisfactory[7].

- Engine shut down tests

In these tests, the engine was initially operated at idle state and then it was switched off. The data acquisition system continued to take measurements, even with the engine turned off. Once the engine was turned off, the NO$_X$ concentration dropped, then immediately showed a small increase and then reduced again to reach its lowest value, as it was

expected. The sensor's and analyzer's output was once again repeatable in all tests. The small increase of the NO_X concentration was attributed to exhaust gases that were trapped in the exhaust duct.

- Soot loading

Since the SNS is located into the exhaust gas duct, it is subjected to continuous soot deposition. The soot deposition contributes to the ageing of the sensor, reducing its life span and affecting its performance. To evaluate the rate of soot deposition, it was decided to make a dummy sensor of identical dimensions and install it on the exhaust duct. The dummy sensors had the same geometric features as the actual sensors with regards to the area exposed to the exhaust gases. Great detail was given in the holes on the sensor's tip, in order to investigate the rate of soot deposition in these areas that are essential to the actual sensor's performance.

Before the installation on the exhaust duct, the dummy sensor was weighed on a high precision weighting balance. After 83 hours of engine run the dummy sensor was removed from the exhaust duct and weighed, again, in order to evaluate the amount of soot that was deposit to the dummy sensor's surface. The dummy sensor weighed almost 9 mgr heavier and some of its holes were blocked, due to soot deposition [6].

It must be mentioned, that during all these tests the engine used diesel fuel oil. It is expected that in marine diesel engines, which use Heave Fuel Oil, soot deposition will be significantly higher.

Consequently, the issue of soot deposition has raised concern about its impact on the sensor's performance. Further investigation needed to be done, in order to find a way to suppress this phenomenon and its effects. Given the fact, that the sensor must be constantly installed in the exhaust duct for on-board measurements, the idea of a flow externally supplied that would prevent the soot loading was conceived. This could take the form of an air curtain arrangement that protect the SNS from soot deposition through an air jet that enters the area of the exhaust gases (cross flow).

2.5 Jet in cross flow

The term 'Jet in cross flow' refers to a jet of fluid that passes through a nozzle to interact with the surrounding cross flowing fluid. Jets in cross flow find practical application in pollutant dispersal among other engineering problems.

The flow field of a jet in cross flow is strongly influenced by the effective velocity ratio:

$$r = \sqrt{\frac{\rho_j u_j^2}{\rho_{cf} u_{cf}^2}} \qquad (2.5.1)$$

Where, u_j is the jet velocity, u_{cf} is the velocity of the crossflow, ρ_j is the density of the jet fluid and ρ_{cf} is the cross flow fluid density.

Many investigators have studied the mean jet trajectory and suggested analytical models to estimate it. As shown below, all models of the mean jet trajectory are functions of the effective velocity ratio. The most common models use the jet exit as a point source of momentum and the product *r·d,* where *d* is the diameter of the orifice, as the global length scale in the flow for the region away from the jet exit. The use of this length scale is shown in the following equation.

$$\frac{y}{rd} = A\left(\frac{x}{rd}\right)^B \qquad (2.5.2)$$

Where, A and B are constants.

Pratte and Baines (1967) obtain A=2.05 and B=0.28 using their experimental data.

Margarson's (1993) experimental results obtain 1.2 < A < 2.6 and 0.28 < B < 0.34.

Hasselbrink & Mungal (2001) scale the mean jet trajectory as

$$\frac{y}{rd} = \left\{\frac{2}{c_{ej}}\frac{x}{rd}\right\}^{1/2} \text{(in the near field)} \qquad (2.5.3)$$

$$\frac{y}{rd} = \left\{\frac{3}{c_{ew}}\frac{x}{rd}\right\}^{1/3} \text{(in the wake-like region)} \qquad (2.5.4)$$

Where, c_{ej} and c_{ew} are the entrainment coefficients in the jet region and the wake – like region respectively.

Figure 2.5.1 presents jet trajectories scaled with *r d* derived from experimental results using different values for effective velocity ratio.[8]

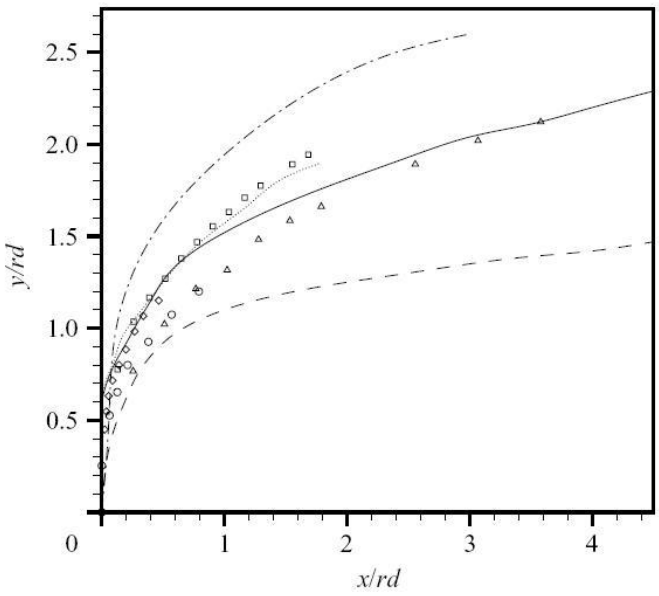

Figure 2.5.1. Jet trajectories from different experiments scaled by rd: ○, r=4.0 (Keffer & Baines 1963); ◊, r=6.0 (Keffer & Baines 1963); ∆, r=3.9 (Kamotani & Greber 1972); □, r=7.7 (Kamotani & Greber 1972); ——, r=10 (Smith & Mungal 1998); - - -, r=5 (Smith & Mungal 1998); ·····, r=5.81 (Chochoua et al. 2000);—·— , r=5.7 (Su & Mungal 2000)[8]

Having regard to the above jet trajectories, the idea of an air curtain device to prevent the sensor from soot loading was implemented. According to this concept, the compressed air exits the orifice and prevents the exhaust gas flow to reach the sensor when it does not take measurements. A preliminary sketch of such a device is shown in Figure 2.5.2.

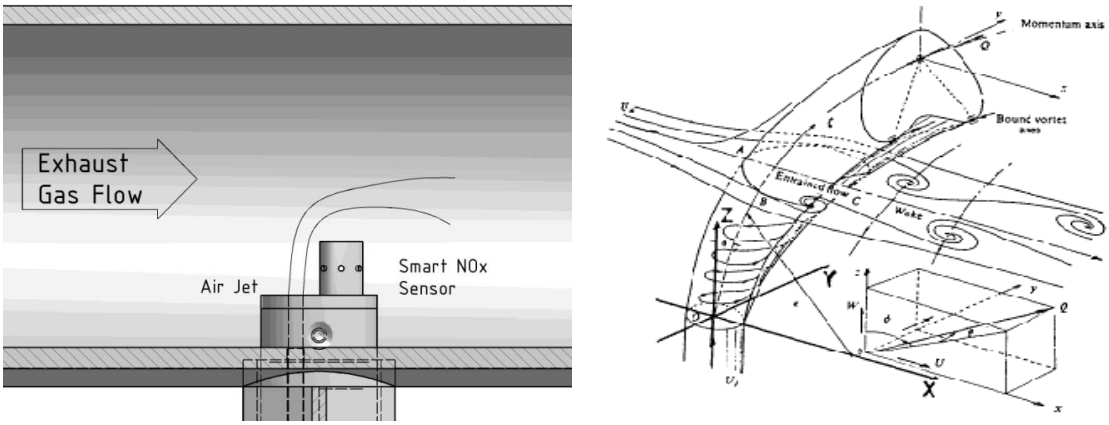

Figure 2.5.2. Basic concept of the air curtain device (left), flow field description of a jet in cross flow [9] (right)

3. DESIGN AND MANUFACTURING OF TRIAL AIR CURTAIN ARRANGEMENTS

3.1 Introduction

In order to investigate the effectiveness of an air-curtain device and evaluate the rate of soot loading, preliminary experiments needed to be conducted. Therefore, trial air – curtain devices were designed and manufactured at the NTUA – LME workshop. The matrix of experiments contained two parameters: the pressure of the air jet flow and the direction of the jet flow in relation to the dummy sensor's axis (parallel or inclined). This chapter refers to the second parameter and demonstrates the design and construction of two trial air-curtain arrangements with dummy sensors attached. It, also, presents the modifications made on the exhaust duct in order to make the installation of the dummy sensors (and later on the sensors and analyzers) feasible.

3.2 Design of trial air curtain arrangement with a nozzle parallel to the dummy sensor.

The arrangement with an air nozzle parallel to the dummy sensor's axis creates an air jet in the exhaust cross flow when it is installed to the exhaust duct, as shown in Figure 2.5.2. It is expected that the flow of compressed air around the sensor will create a layer which will deter the exhaust gas particles to reach the surface of the sensor. The whole structure consists of parts that are described below.

- Probe body (Fig. 3.2.2)

Since the SNS is created for automotive applications, it is designed to be installed directly in the exhaust duct as shown in the diagram below (Figure 3.2.1).

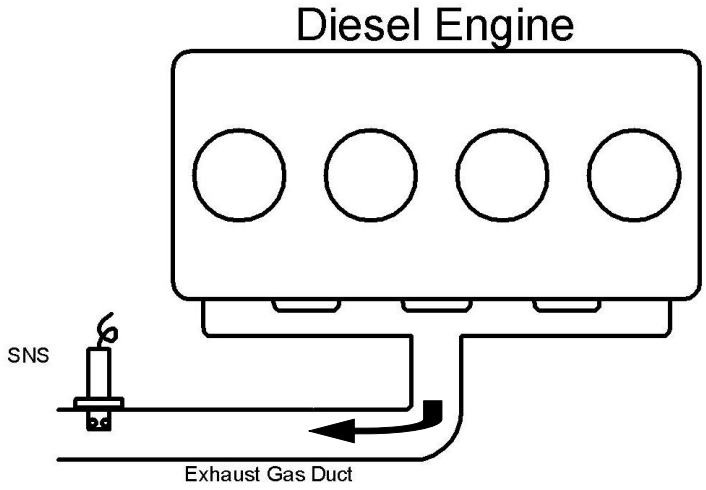

Figure 3.2.1. SmartNOx sensor installed in the exhaust duct of an automotive diesel engine.

The NO_X Technical code, adopted by MARPOL Annex VI, designate that a NO_X measurement instrument must be able to reach exhaust gases from an area between 10% and 90% of the diameter of the exhaust duct [10]. Due to its small size, the SNS can not comply with the aforementioned specification of the NO_X Technical Code, when it is installed in the exhaust duct as shown above (Figure 3.2.1). Therefore, the SNS must be fitted in a probe, with the shape of a hollow cylinder, which would place the sensor in the specified area of the exhaust duct and protect the sensor's wiring from the exhaust gases. Regarding the air – curtain device, this probe would, also enclose the air supply pipe. Apart from the appropriate length, the probe has an external diameter of 42 mm, due to the already existing experimental facilities specifications. Moreover, it has 4 holes with chamfered edges for M5 flathead screws that would hold the head of the dummy SNS and the air pipe support.

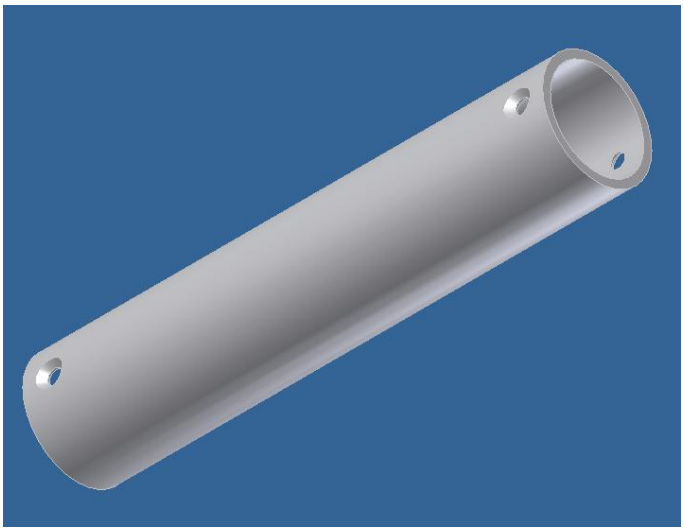

Figure 3.2.2. Design of sensor's probe body

- Head of the dummy SNS with an air nozzle (Fig. 3.2.3)

In this part of the device, the air pipe and the dummy sensor would be fitted. It bears an air nozzle which, in fact, is a hole, with 5mm diameter, homocentric to the hole where the air pipe is fitted. Moreover, the head has two threaded holes, in order to be bolted to the front tip of the probe body. Since it would be exposed to the exhaust gases the head was made by stainless steel.

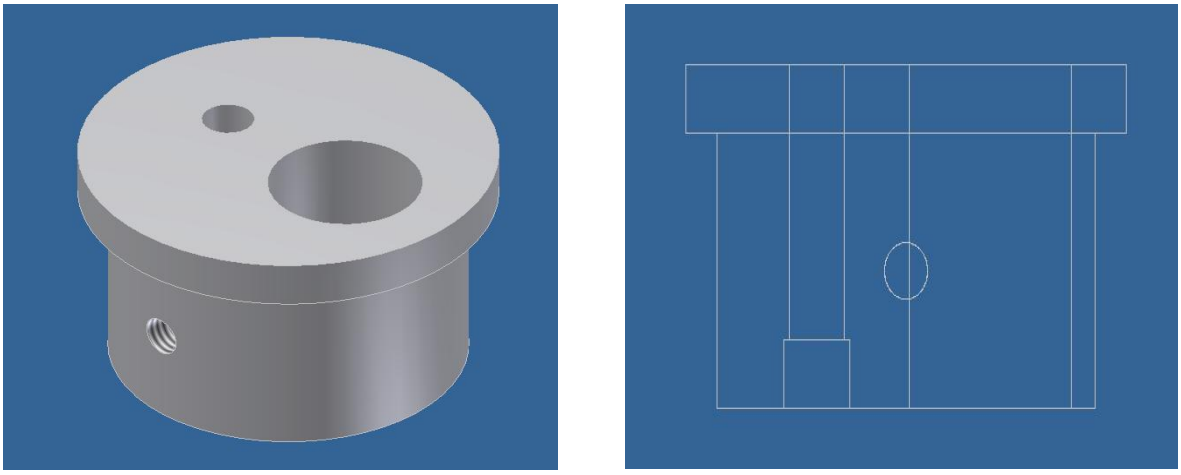

Figure 3.2.3. Design of head with the axial nozzle

- Compressed air transfer pipe (Fig. 3.2.4)

The air that would create the protective layer is transferred into the exhaust duct through a 300mm long pipe and has an external diameter of 6mm. The air pipe would be fitted tightly in the head of the dummy with the air nozzle and not by welding because its thin wall would be destroyed due to high temperature. On its other tip the pipe would be connected to a hose through a quick release fitting.

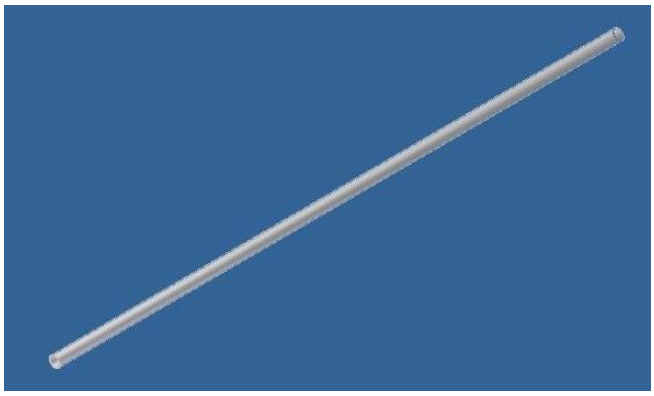

Figure 3.2.4. Design of compressed air transfer pipe

- Dummy sensor (Fig. 3.2.5)

As described above, it was needed to replicate the external geometry of the sensor in the area that is exposed to exhaust gases. Apart of the main dimensions, great attention was given to the holes on the tip of the sensor, because it was observed that they can be blocked due to soot deposition, as discussed in §2.4. In addition, it was manufactured by the same material as the real sensor (stainless steel ANSI 304 [6]).The dummy sensor was fitted in the head using welding.

Figure 3.2.5. Design of dummy sensor.

- Air transfer pipe support (Fig 3.2.6)

Taking into consideration the relatively long length of the air pipe and the weight of the hose with the quick release fitting, it was decided to design a support of the air pipe that would be fitted in the back tip of the probe. This support would protect the compressed air pipe from distortion that would lead to leakage or create additional losses for the internal compressed air flow. Furthermore, it bears two threaded holes for M5 screws, in order to be bolted to the back tip of the probe.

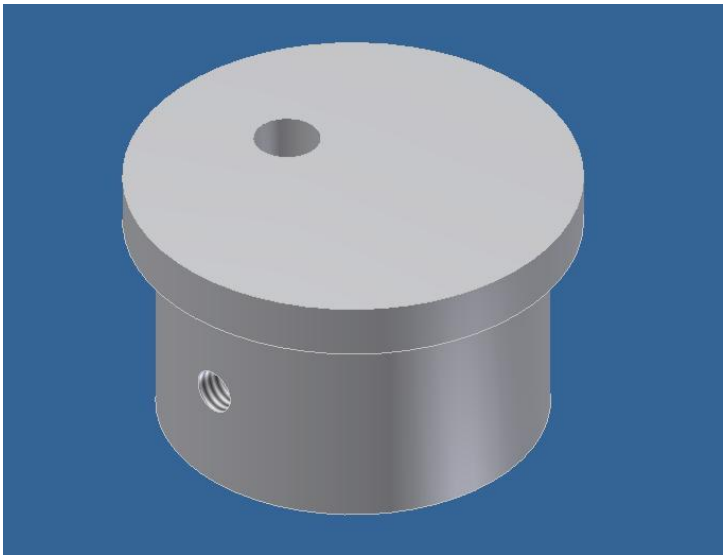

Figure 3.2.6. Design of air transfer pipe support

- Fitting BSP G 1 1/2” (Figs. 3.2.7, 3.2.8)

The air curtain can be installed in the exhaust duct via a fitting bolted in a duct’s socket. In fact, this fitting is a slightly modified hydraulic connector. Its internal diameter was to be

widened to 42mm, so that the device could fit in it. Also, a threaded hole for a M5 socket screw was designed in order to hold the device stable.

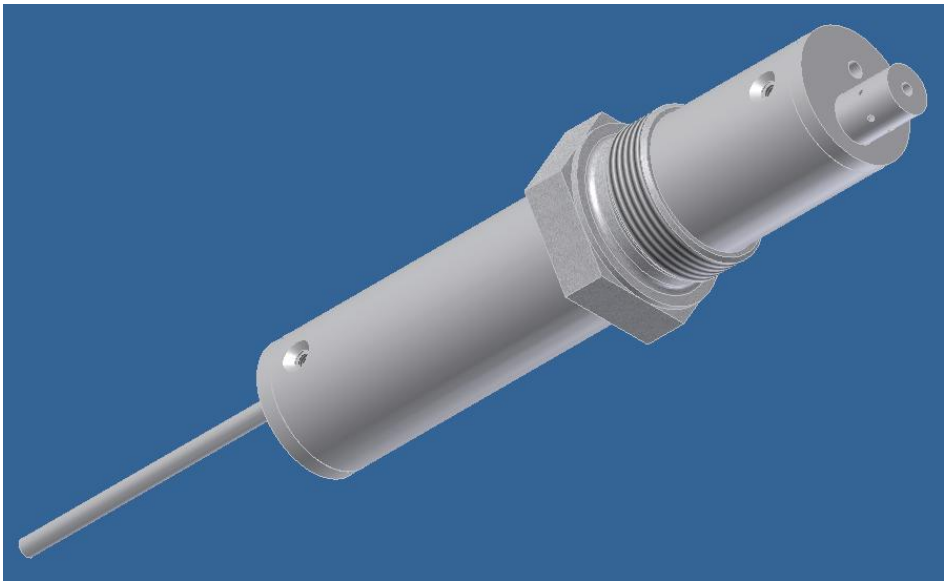

Figure 3.2.7. Design of the trial air curtain device assembled

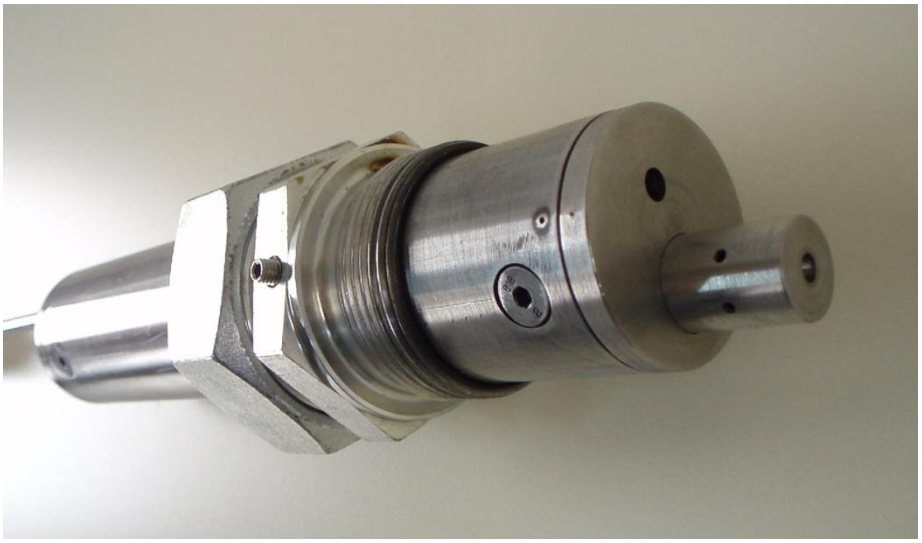

Figure 3.2.8. Trial air curtain device with axial nozzle

3.3 Design of trial air curtain arrangement with an inclined nozzle. (Fig. 3.3.2)

Apart from an orifice parallel to the sensor, an orifice that drives the air jet to the sensor's surface can create a protective air – curtain. The only part of the structure that differs significantly from the trial device that was described above is the head that bears the orifice. In this case, the air flow is driven to a nozzle which's axis is inclined by 30° from the air pipe. Also, an inclined by 60° plane was designed on the external surface of the head,

in order to be feasible for the drill to create the nozzle. Furthermore, emphasis was given to the length of the nozzle. More specifically, the socket for the air pipe was placed in such position so that the nozzle has the longest possible length, so that the air flow could be driven to the selected direction more effectively.

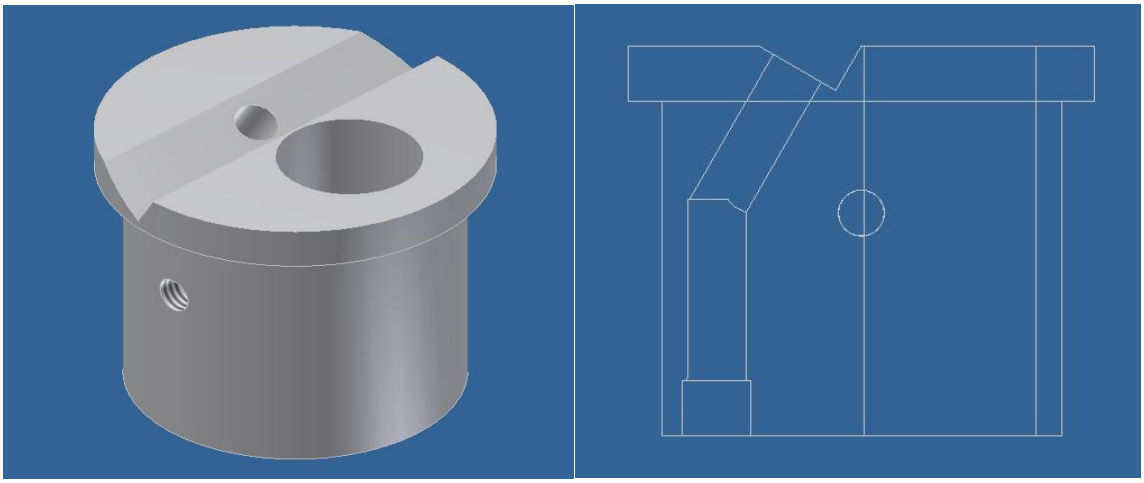

Figure 3.3.1. Design of head with inclined nozzle

Due to the change of the position of the socket for the transfer pipe, the design of the air pipe support needed to be slightly modified. The hole in which the air pipe is placed was moved so as to allow pipe alignment.

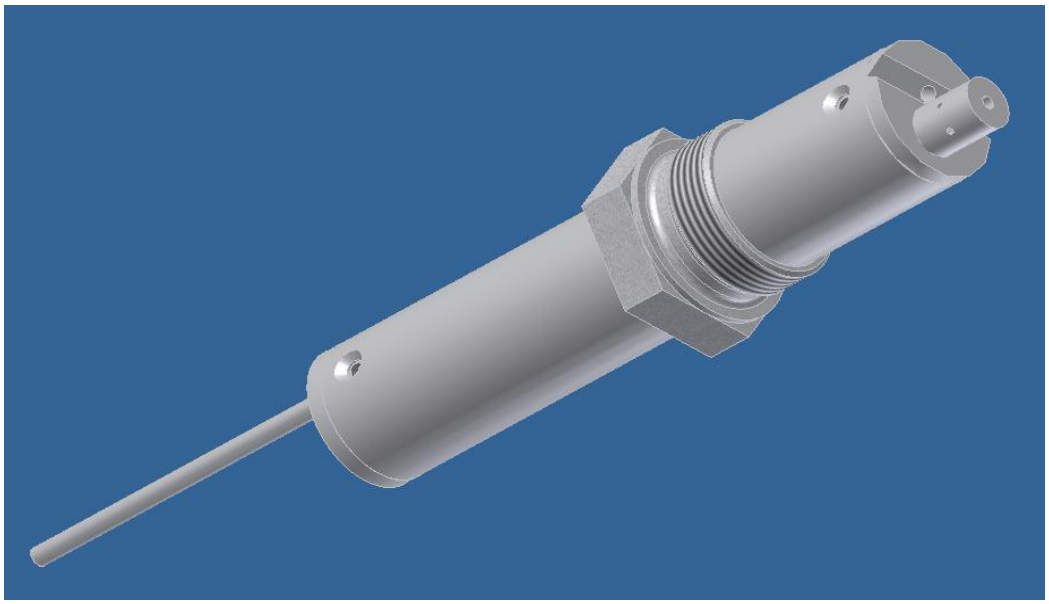

Figure 3.3.2. Design of the trial air curtain device assembled

Figure 3.3.3. Trial air curtain device with inclined nozzle

3.4 Modification of the lab engine's exhaust duct.

The exhaust duct of the lab engine used for the experimental investigations of this thesis did not have the appropriate sockets in order to install the sensors and the analyzer. It was, therefore, needed to design these sockets and determine their position along the exhaust duct. The available length of the duct is downstream the turbocharger and, as shown in figure 3.4.1, is rather limited.

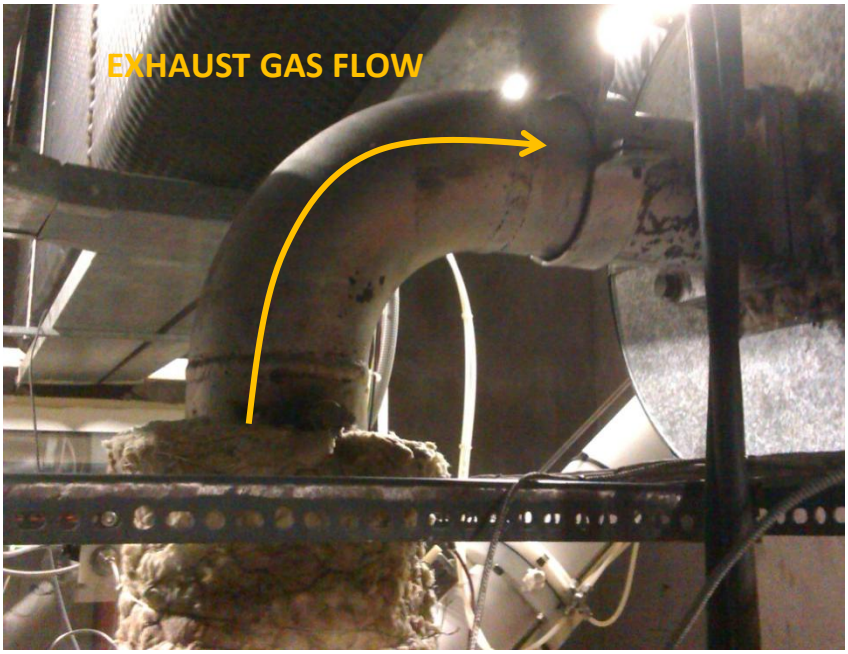

Figure 3.4.1 Initial state of the exhaust duct and exhaust gas flow direction.

Three sockets were needed to be installed in the exhaust duct. Two of them were designed for the dummy SNS and one for the analyzer's probe. The sockets for the SNS bear thread of BSP G 1 ½ type and the socket for the analyzer's probe bear thread of BSP G ½. Their location along the duct was an issue of outmost importance.

The operation of the air curtain device must not affect any other measurement instrument or dummy sensor. Therefore, it was impossible to place the sockets in the same transverse section of the duct. The socket for the CLD analyzer's probe was located downstream of the turbine outlet, one of the sockets for the SNS was located upstream of the elbow shown in Figure 3.4.1 and the second was located downstream of the elbow.

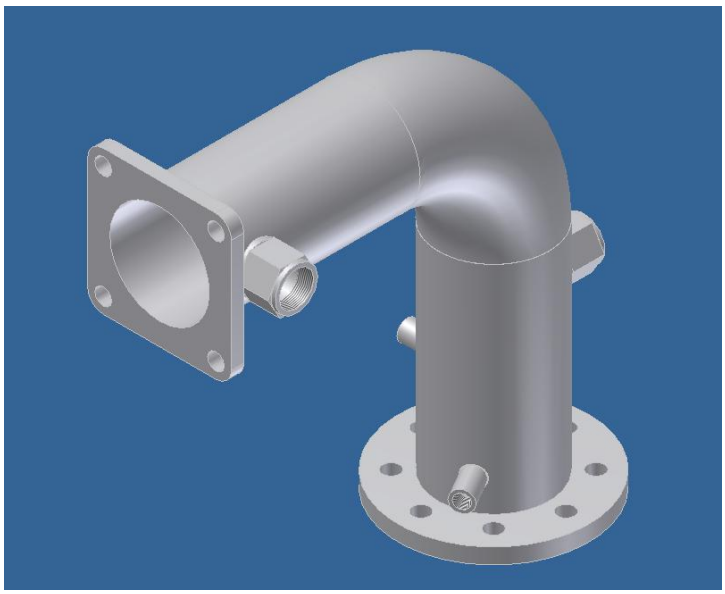

Figure 3.4.2. Drawing of the modified exhaust gas duct

The part of the exhaust duct, that was to be modified, was disassembled from the engine room. The holes, in which the sockets were fitted, were created using hole saws as shown in Figure 3.4.3.

Figure 3.4.3. Drilling holes on the exhaust duct.

The sockets were installed in the exhaust duct by welding of TIG type. Finally, threaded caps and metallic ring were installed, in order to secure duct's sealing.

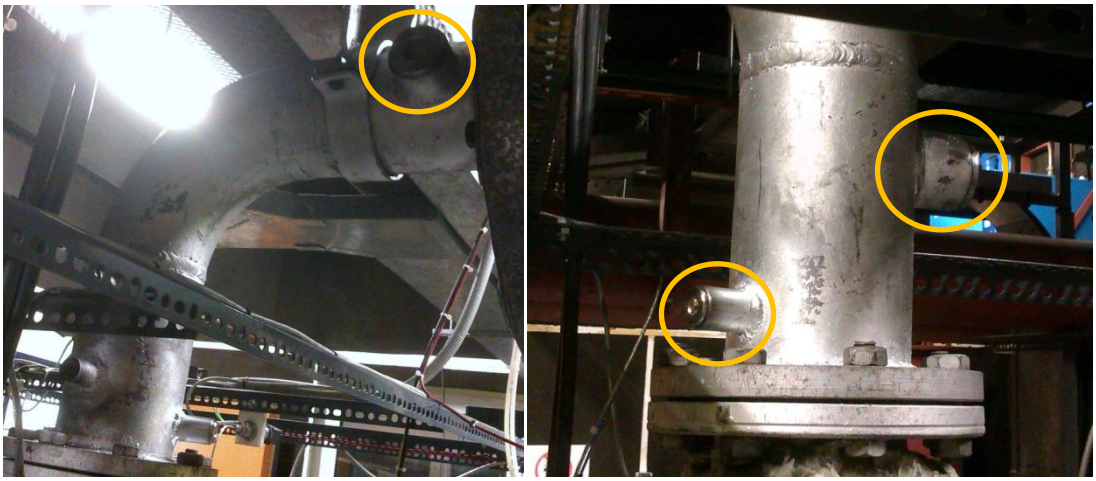

Figure 3.4.4. Modified exhaust duct including sockets for installation of exhaust gas sensor.

3.5 Conclusions

The objective of the activities described in this chapter was to set up a facility to be used for experimental investigations regarding the effectiveness of an air curtain device. These facilities consist of two trial air curtain devices and their sockets on research engine's exhaust duct. The trial devices were designed to be compact and easy to operate as the final air curtain device should be. These devices are, in fact, assembles of easily manufactured parts made by steel or stainless steel. A complete list of these parts is presented in Table 3.5.1.

No	Item	Quantity	Material
1	Probe	1	St. 37-2
2	Head of the dummy SNS with a parallel nozzle (0 deg)	1	DIN X5CrNi18.9
3	Head of the dummy SNS with an inclined nozzle (30 deg)	1	DIN X5CrNi18.9
4	Air pipe	1	DIN X5CrNi18.9
5	Dummy sensor	2	DIN X5CrNi18.9
6	Air transfer pipe support (0 deg)	1	St. 37-2
7	Air transfer pipe support (30 deg)	1	St. 37-2
8	Fitting BSP G1 1/2	1	St. 37-2
9	M5 Flathead allen screw	4	DIN 912
10	M5 socket allen screw	1	DIN 912
11	Socket for SmartNOx Sensor	2	St. 37-2
12	Socket for EcoPhysics CLD700	1	St. 37-2

Table 3.5.1. List of manufactured parts

4. EXPERIMENTS USING TRIAL AIR CURTAIN ARRANGEMENTS

4.1 Introduction

The objective of the activities described in this chapter is the experimental investigation of the air – curtain device's effectiveness. As already mentioned in §3.1, the matrix of experiments consists of two parameters: the air nozzle angle in relation with the sensor and the compressed air pressure. The cases of the first parameters were settled in Chapter 3. In this Chapter the compressed air pressure values are defined. For this purpose, two engine tests were needed in order to evaluate properties that are related to the engine's operation at 50% load and to measure the exhaust gas velocity in several positions along the centerline of a duct's cross section. Having defined the air pressure values, engine tests were conducted with a dummy sensor and the trial air curtain devices installed in the exhaust duct.

4.2 Description of the research engine

The engine tests were performed on the MAN B&W D2866 LE four-stroke diesel engine. The specifications of this engine are shown below:

Bore/Stroke	128 / 155 mm
Configuration	6cylinders, in-line
Compression ratio	15.5:1
Rating	230 kW at 1500rpm
Exhaust Gas Mass Flow	1500 kg/h
Exhaust Gas Temperature	600 ^{o}C

Table 4.2.1. Specifications of MAN B&W D2866 LE at 100% load

The research engine is connected with an AVK electric generator which has a performance ratio equal to 0.92 (approx.) and operates constantly at 1500rpm.

During the tests, the engine was running at 50% of the nominal load. Before conducting any experiment, it was needed to acquire data from the engine that correspond to this load. Therefore, the engine was set to run at this load and data were recorded from the sensors already installed.

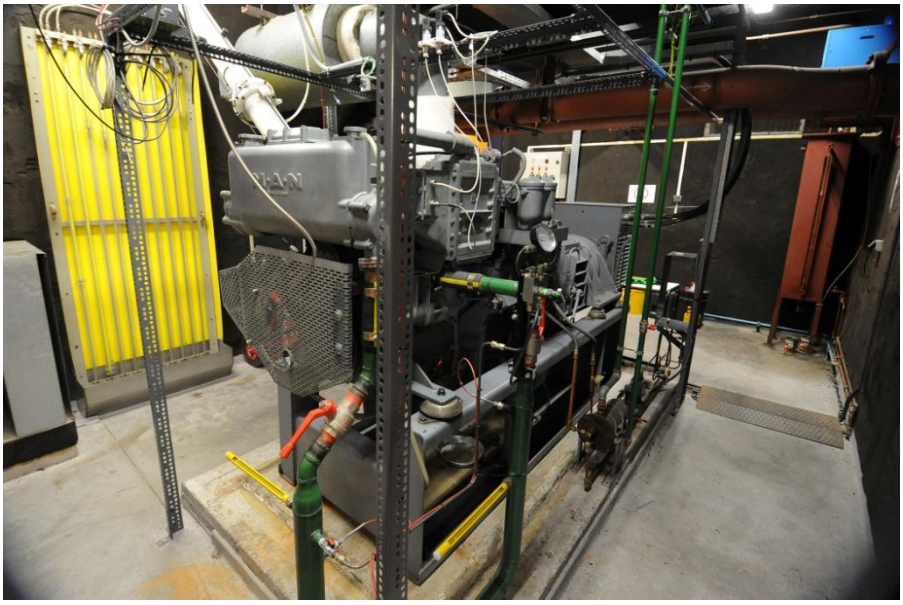

Figure 4.2.1. MAN B&W D2866 LE in NTUA - LME

Property	**Unit**	**Average Value**
Inlet air temperature	K	300.6
Inlet air temperature upstream of the intercooler	K	336.5
Inlet air temperature downstream of the intercooler	K	301.2
Exhaust gas temperature downstream of the turbocharger	K	629.3
Exhaust gas temperature upstream of the turbocharger	K	684.9
Inlet air pressure downstream of the intercooler	kPa	124.3
Fuel mass flow	Kg/min	0.487
Exhaust gas pressure upstream of the turbocharger	kPa	129.7
Inlet air pressure upstream of the intercooler	kPa	125.9
Inlet air diaphragm differential pressure	kPa	1.58

Table 4.2.2. Data of MAN B&W D2866 LE at 50% load

Inlet air mass flow and exhaust gas density were calculated, using the data above and following the formulas and the tables of ISO 5167 – 2 [11].

Inlet air mass flow	Kg/s	0.256
Exhaust gas constant R	m^2/s^2K	287.38
Exhaust gas density	Kg/m^3	0.608
Exhaust gas flow	m^3/s	0.434
Exhaust gas mean velocity	m/s	33.7

Table 4.2.3. Exhaust gas calculated properties

During all tests, the engine was operated on diesel oil with fuel properties listed below.

Property	Unit	Quantity
Density (at 15°C)	Kg/lt	0.8347
Viscocity (at 40°C)	cSt	3.32
S	ppm	22
C	%w/w	86.65
H	%w/w	13.37
N	%w/w	0.0014
GCV	kcal/kg	11056
NCV	kcal/kg	10378

Table 4.2.4. Fuel oil properties

4.3 Exhaust gases velocity measurements

In order to have an indicative estimate of the exhaust gas flow, it was decided to evaluate the velocity of the exhaust gases. This evaluation procedure featured velocity measurements in seven points along a cross section of the exhaust duct. The measurement instrument was installed in the research engine's exhaust duct downstream of the turbocharger. Between the socket, in which the velocity measurement device was installed, and the turbocharger, an elbow is interposed. Given that the length of the duct downstream of the elbow is less than 4 times its diameter, it is expected that the resulting velocity profile would roughly approximate the profile of turbulent flow.

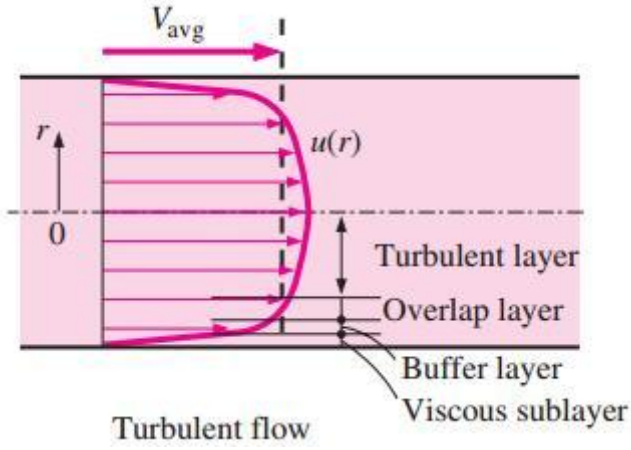

Figure 4.3.1. Velocity profile of turbulent flow in a pipe.[12]

The measurement instrument was the ZS25 Vane Wheel Sensor of Höntzsch® Flow Measuring Technology, which calculates the velocity of the ambient gas by scanning the vane rotation. The sensor is corrosion resistant and can operate in temperatures up to 500°C, therefore it was considered suitable for this set of measurements.

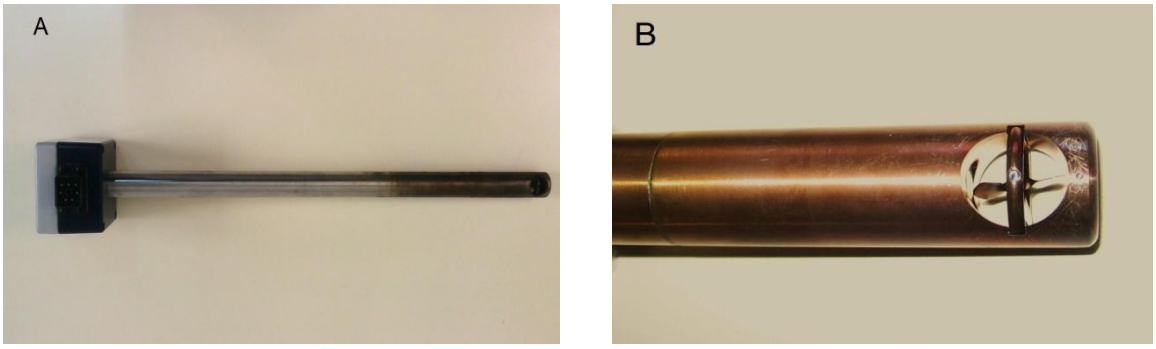

Figure 4.3.2. (A) Höntzsch Gas flow sensor, (B) Flow sensor's vane wheel

Regarding the installation of the sensor in the exhaust duct, there are some requirements so that the measurements are reliable. Obviously, in terms of safety, there must be no leaks of exhaust gas. In addition, the vane's rotational axis must be aligned in the direction of the flow. If this requirement is not fulfilled, the sensor's output is distorted in a way shown in Figure 4.3.3.

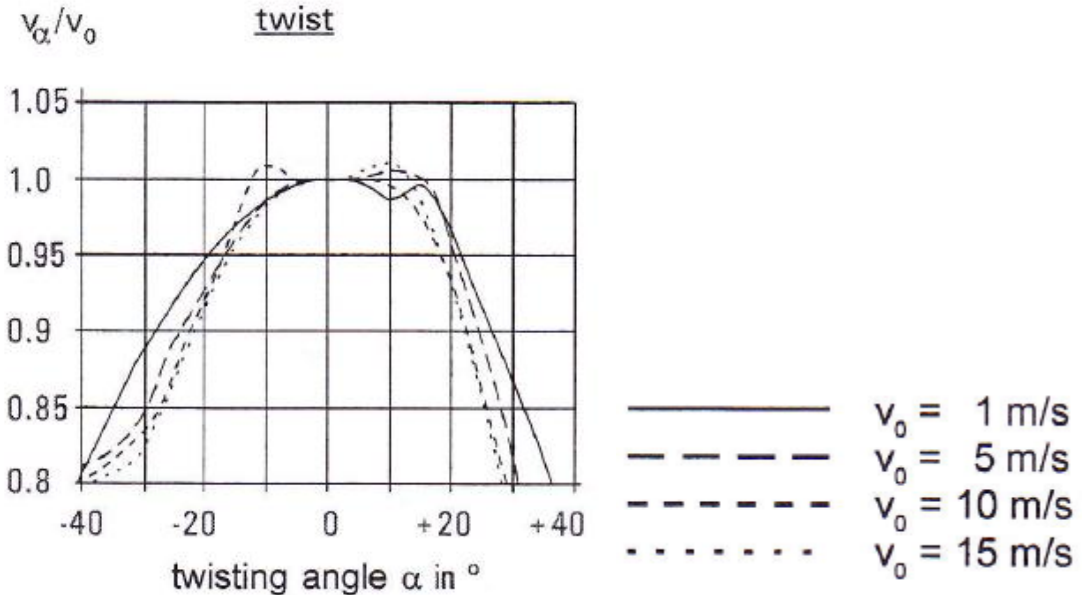

Figure 4.3.3. Diagram of flow meter measurements' twist in relation to twisting angle for several reference velocity values [13]

To satisfy the aforementioned requirements, an adaptor, shown in Figure 4.3.4, was used so that the gas flow meter can be installed in a socket initially purposed for the SmartNO_X Sensor. The adaptor is attached to the sensor through tight fitting and relative movements are prevented because of a socket M4 screw that bolts in the adaptor and presses the sensor's probe.

Figure 4.3.4. Adaptor for installation of velocity meter.

During these measurements, the engine was operated constantly at 50% of nominal load. As mentioned, the gas velocity was measured in seven points along the centerline of a duct's cross section. Therefore, the sensor's probe was marked, in order to control the sensor's position along the centerline of the duct's cross section. The transition from one point to the next was done by loosening the screw of the adaptor. In every measuring point, values of velocity had been recorded for several minutes. The results of the measurements are presented below.

Measur. point	**1**	**2**	**3**	**4**	**5**	**6**	**7**
x [mm]	25	34	43	53	64	85	108
V_{min} [m/s]	28.39	8.51	5.97	5.66	40.46	42.21	44.96
V_{max} [m/s]	30.29	9.18	7.02	6.48	41.08	43.22	45.54
V_{aver} [m/s]	29.37	8.83	6.37	6.09	40.69	42.73	45.24

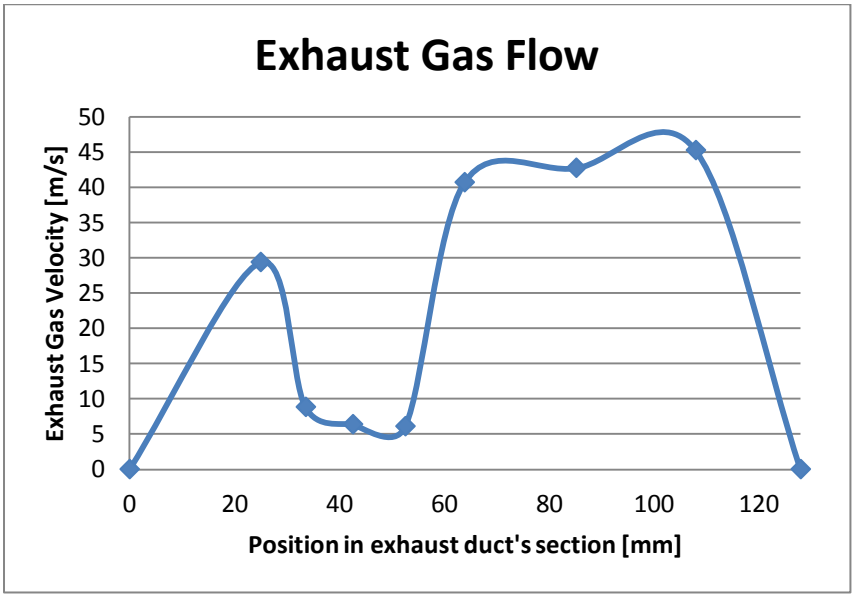

Figure 4.3.5. Exhaust gas velocity measurements along exhaust duct cross section.

As it is shown above, there is a large fluctuation in the values of gas velocity along the centerline of the duct's cross section. This can be explained by the fact that there is limited length of straight duct upstream of the measuring position. Obviously, the velocity profile cannot be approximated by that of turbulent flow. The data points No 2, 3 and 4 have almost 10 mm spacing between one another, while points 1, 5, 6 and 7 have almost 20 mm. Therefore, their contribution to the final average value is not equal. More specifically, the weights corresponding to points 2, 3 and 4 are half the weights of points 1, 5, 6 and 7. The weighted mean of the exhaust gas velocity values is equal to $30.7 m/s$, and is calculated according to the following formula.

$$\bar{v}_{exhaust} = \frac{\sum_{i=1}^{7} w_i \cdot v_i}{\sum_{i=1}^{7} w_i} \qquad (4.3.1)$$

The mean exhaust gas velocity calculated in §4.2 was equal to $33.7\ m/s$ (Table 4.2.3) which is almost 10% higher than the weighted value calculated in this section.

4.4 Definition of compressed air pressure values

The definition of compressed air pressure values would be based on the formulas presented in §2.5. The mean trajectory of a jet in cross flow is a function of the effective velocity ratio (eqs 2.5.2 – 4.). The effective velocity ratio is related to the velocity and density of the jet flow. A single value of pressure for the air jet corresponds to a value of air velocity and density. Having the cross flow (exhaust gas flow) and the jet (compressed air) velocity and density calculated, a mean jet trajectory can be defined.

Two types of jet trajectories that correspond to two values of compressed air pressure were to be investigated. The first type is shown in Figure 2.5.2., in which the jet surpasses the sensor. In the second type of mean jet trajectory the jet exits the orifice and impinges the sensor's surface. Obviously, in the second case the compressed air pressure is lower than in the first case.

However, the large fluctuations in the exhaust gas velocity measured make the aforementioned procedure have questionable reliability in the results with regards to jet trajectories.

Based on the values of gas temperature downstream of the turbine outlet, density and gas constant *R* calculated in §4.2, the exhaust gas pressure is equal to a value near atmospheric pressure (1,1 bar approx.) according to the following equation.

$$p = \rho\, RT \qquad (4.4.1)$$

As it is known, in gas flow through an orifice the gas velocity reaches sonic conditions when the absolute pressure ratio is equal to 0.528. Consequently, in this case, for air pressure values beyond 2.3 bar the air flow is chocked. This means that an increase of air pressure would not affect the air velocity. Of course, the air density would increase too, but the impact of this increase in the effective velocity ratio is relatively smaller.

Taking all the aforementioned facts into account, it was decided to investigate the air curtain effectiveness for two values of compressed air pressure. In the first case the compressed air pressure will be set at 4 bar (>2.3) and in other one will be set at 2 bar (< 2.3).

2 bar of air pressure corresponds to air flow rate equal to $6.9\ g/s$ and air velocity equal to $156\ m/s$, while 4 bar air pressure corresponds to $16.7\ g/s$ and $346.14 m/s$ respectively (Appendix 1). Using the values of exhaust gas properties shown in Table (4.2.3) the mean jet trajectories for 2 and 4 bar of air pressure were exported, according to equation 2.5.2.

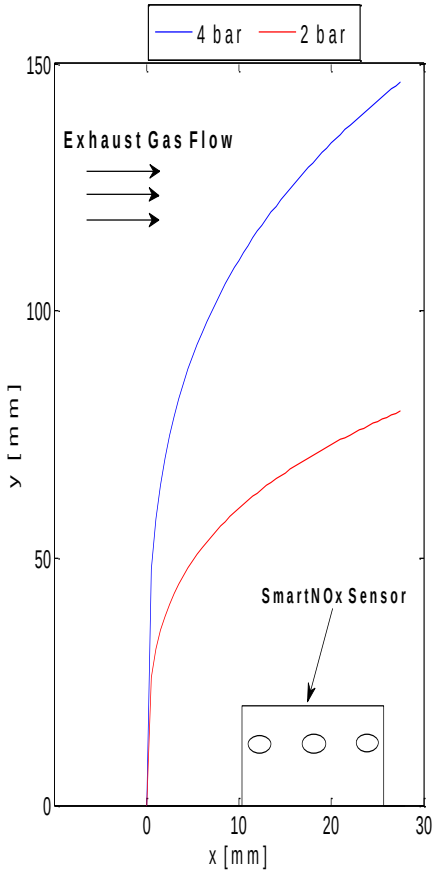

Figure 4.4.1. Mean jet trajectories corresponding to air pressure values of 2 and 4 bar.

4.5 Compressed air supply system

As shown in Figure 1, a compressed air supply system is a major part of the air curtain arrangement. A typical schematical representation of such a system is shown below.

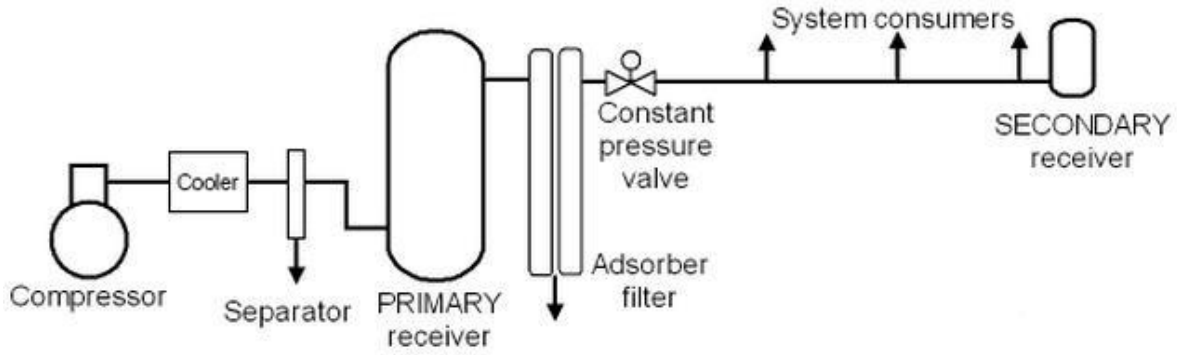

Figure 2.5.1. Typical compressed air system [14]

NTUA – LME air system features a three – stage reciprocating compressor that produces 82.5 m^3/h of air of 30 bar pressure with a power demand of 15 kW and an air receiver of 350 lt capacity. The range of air pressure inside the primary receiver was set to be 25 – 30 bar. When the air pressure reaches its minimum value (25 bar), due to compressed air demand, the compressor is switched on automatically until the pressure inside the receiver reaches its maximum value (30 bar). Apparently, the frequency under which this procedure takes place is related to the demand of compressed air. The time for the air pressure to drop from the upper to its lower limit is calculated according to the following formula [14].

$$t = V \cdot \frac{p_1 - p_2}{C \cdot p_{atm}} \quad \text{(min)} \quad (4.5.1)$$

Where, V is the volume of the receiver tank (cu ft)
C is the free air needed (cu ft/min)
p_a is the atmosphere pressure (14.7 psia)
p_1 is the maximum tank pressure (psia)
p_2 is the minimum tank pressure (psia)

For NTUA – LME facilities: $V = 350\ lt = 12.36\ ft^3$,
$p_1 = 30\ bar = 435.11\ psia$ and $p_2 = 25\ bar = 362.6\ psia$

For supplied compressed air of 2 bar, $C_1 = 11.01\ {}^{m^3}/_{h} = 6.48\ {}^{ft^3}/_{min}$ (Appendix 1), and therefore, $t_{2\ bar} = 9.4\ min$.

For supplied compressed air of 4 bar, $C_2 = 24.4\ {}^{m^3}/_{h} = 14.5\ {}^{ft^3}/_{min}$ (Appendix 1), and therefore, $t_{4\ bar} = 4.3\ min$.

Consequently, when the air curtain arrangement demands compressed air of 2 bar, the compressor is switched on almost every 9 minutes and for compressed air of 4 bar the compressor is switched on every 4 minutes. For both cases of compressed air pressure, the refill of the air receiver lasts almost 45 seconds. Given the fact that the arrangement is to be permanently installed in the exhaust duct, it can be concluded that for both cases of air pressure the power demand, and, therefore the running costs, of such an arrangement is significant.

4.6 Experimental investigation of soot deposition.

Having the trial devices manufactured and the values of air pressure defined, the experiments for the investigation of the air – curtain device's performance proceeded. The evaluation of the performance was done through visual observation of the soot deposition. Therefore, a dummy SmartNO_X Sensor was installed in the exhaust duct and the research engine was set to run at 50% of nominal load for two hours. This engine test was conducted to evaluate the hours of engine run needed in order to see satisfying amount of soot deposition.

The dummy SNS had been manufactured for past activities of NTUA – LME, referred in §2.4. Due to soot deposition and oxidation, the dummy SNS needed to be cleaned and polished (Figure 4.5.1.).

Figure 4.6.1. Initial state of dummy SmartNO_X Sensor

After two hours of engine operation, the amount of soot deposition was significant. The resulting view of the dummy sensor is shown in Figure 4.4.2. This view was set as reference for future comparisons between the amounts of soot deposition on the trial air – curtain devices.

In the tests that followed, the engine was set to run at 50% of nominal load for two hours. In each test, each trial air – curtain device was tested for one value of air pressure. Obviously the devices were installed in the same position along the exhaust duct.

Figure 4.6.2. Dummy SNS after two hours of engine operation.

As discussed in §4.2, the exhaust gas temperature downstream of the turbocharger at 50% load surpasses 350°C. Consequently, the metal surfaces of the devices would raise high temperature which may affect severely the elastic air hose to which they are connected. For this reason, it was decided that a heat extractor is needed to be fitted to the air pipe. Therefore, a corrugated cylinder made from aluminium was manufactured in NTUA – LME and fitted to the device as shown in Figure 4.5.3.

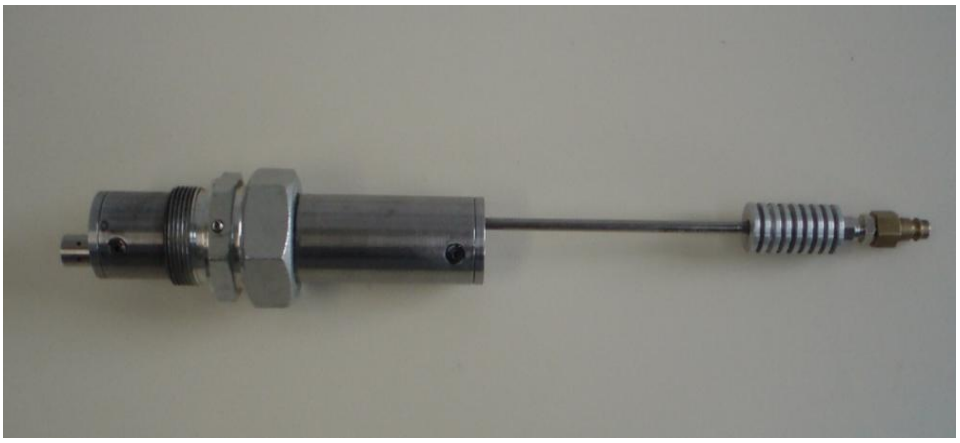

Figure 4.6.3. Heat extractor fitted to the trial air - curtain

During the tests that followed, it was observed that, the temperature of the pipe's surface was high but this temperature would not affect the integrity of the hose. As it may seems the relatively large surface of the support that is in touch with the air pipe had absorbed most of the heat.

In all tests, the period during which the engine was at idle state, in order to warm up and the transition to 50% load lasted the same. This was done in order to secure that the engine operation would produce the same amount of soot during all tests.

4.7 Results from the experiments

After each test the trial device, was uninstalled from the exhaust duct and photographed. Great attention was given to depict the surface of the dummy sensors. More specifically, the surface was divided in two parts: the one that is adjacent to the nozzle and the part that is opposite to the nozzle. Having the photo shooting of each test completed, the devices were polished using light grained sandpaper. This was necessary, so that the devices start each test in the same condition without any deposits.

Some pictures of the devices taken after the engine tests are presented below.

- Initial state of trial air – curtain devices

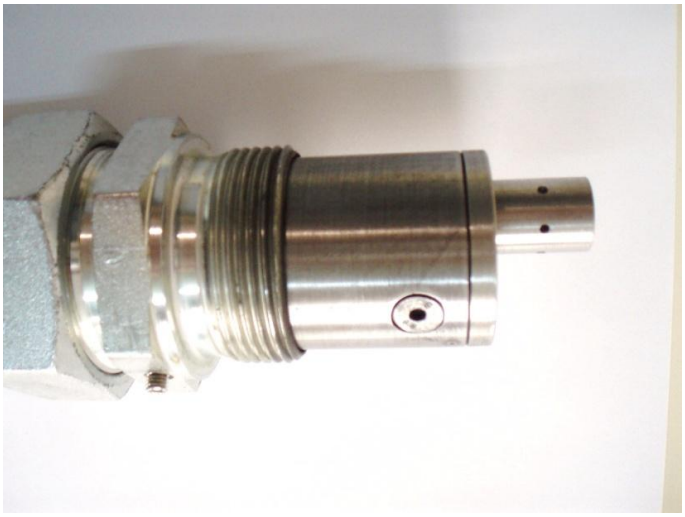

Figure 4.7.1. Initial state of trial device with parallel nozzle

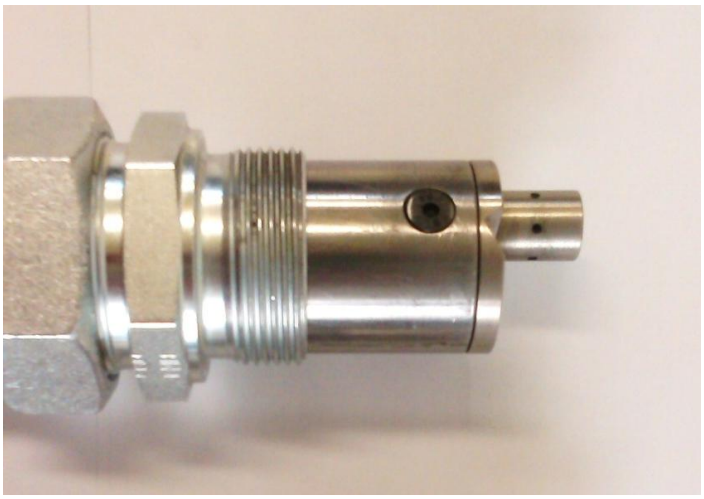

Figure 4.7.2. Initial state of trial device with inclined nozzle

- Test No1: Trial device with nozzle parallel to the dummy SNS – 2bar air pressure

Figure 4.7.3. Test No1. View adjacent to nozzle

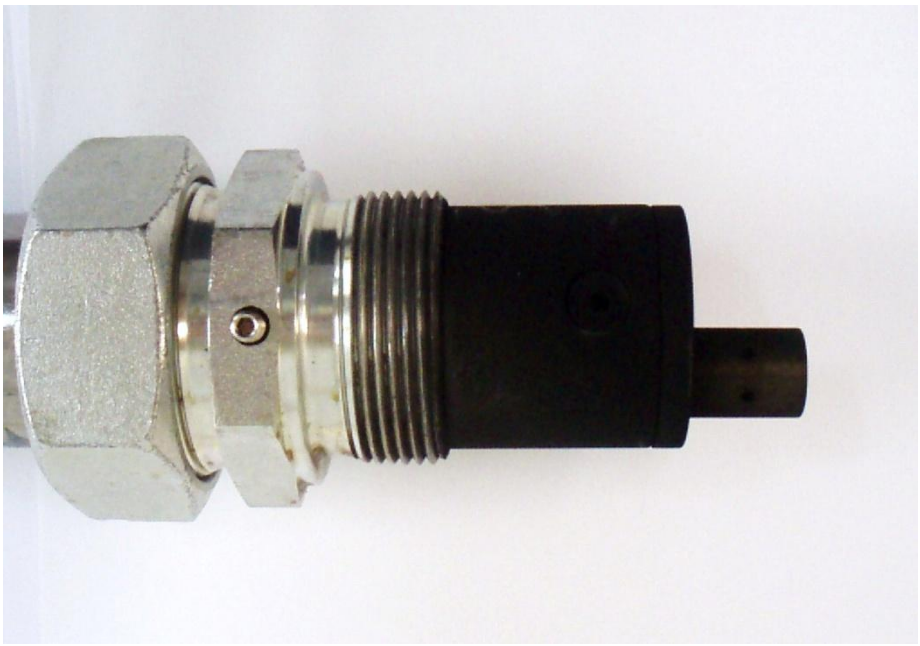

Figure 4.7.4 Test No1. View opposite to nozzle

- Test No2: Trial device with nozzle parallel to the dummy SNS – 4bar air pressure

Figure 4.7.5. Test No2. View adjacent to nozzle

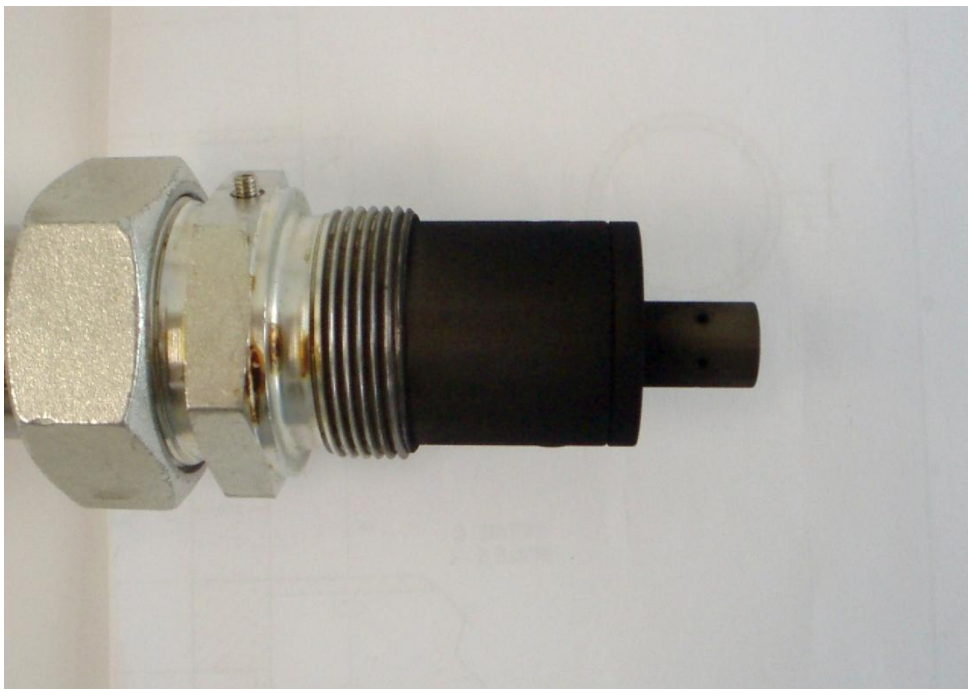

Figure 4.7.6. Test No2. View oppposite to nozzle

- Test No3: Trial device with inclined nozzle – 2bar air pressure

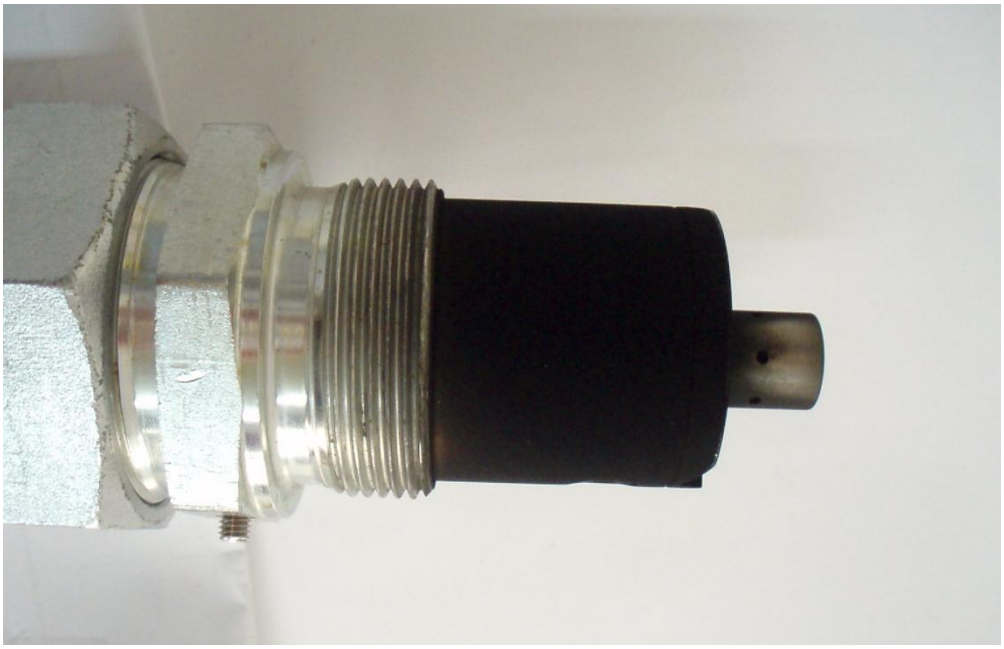

Figure 4.7.7. Test No3. View adjacent to nozzle

Figure 4.7.8. Test No3. View opposite to nozzle

- Test No4: Trial device with inclined nozzle – 4bar air pressure

Figure 4.7.9. Test No4. View adjacent to nozzle

Figure 4.7.10. Test No4. View opposite to nozzle

4.8 Conclusions.

The objective of this chapter was to investigate the rate of soot deposition on the trial air curtain arrangements. Before this procedure takes place, the values of compressed air pressure supplied to the air curtain arrangement had to be defined. For this purpose, it was needed to acquire an indicative estimate of the exhaust gas flow. The mean exhaust gas velocity was approached with two different ways. The results differed by almost 10% which is an acceptable deviation. The second way, which involved velocity measurements at different points along the centerline of an exhaust duct's cross section, revealed that there are large fluctuations in the exhaust gas flow at this location. Given this fact, it was decided to examine the air curtain's effectiveness for two values of compressed air pressure: 2 and 4 bar.

Each trial arrangement was tested for both air pressure values for two hours. The results shown in §4.5 reveal that the operation of the trial devices has an impact on the soot deposited on the dummy SNS's surface at all cases. The trial device with the parallel nozzle showed better effectiveness at 4bar of compressed air. On the contrary, the trial device with inclined nozzle showed the same effectiveness for both cases of air pressure. However, as shown in Figures 4.5.7 – 10, there is significant difference in the amount of soot deposition between the adjacent and the opposite to the nozzle view of the dummy SNS.

5. INVESTIGATION OF SOOT DEPOSITION USING IMAGE PROCESSING TECHNIQUES

5.1 Introduction

In order to evaluate the trial devices' performance it was decided to process the images shown at §4.5. The image processing technique that is presented in this chapter was done using Matlab® Image Processing Toolbox. This software can provide a quantitative comparison, as regards soot deposition, among the pictures of the devices. Apart from visual observations, the results from this comparison were used to define the values of the parameters set (angle of nozzle and air pressure) that offer better performance in soot deposition avoidance.

5.2 Image processing

The only part of the device that has to be protected from soot deposition is, obviously, the sensor's tip. The image process that is discussed in this chapter involves, only the area of the images which depicts the dummy sensor.

Therefore, all images were cropped in order to isolate the area of the dummy sensor not including a single pixel of the background or other part of the device. Then, these new images were imported to Matlab® environment.

The basic data structure in Matlab® is the array. Matlab® stores truecolor (RGB) images as three dimensional arrays. For example, an image that is composed of 500 rows and 800 columns of different colored dots would be stored in Matlab® as a 500x800x3 array, where the first plane in the third dimension represents the red pixel intensities, the second plane represents the green pixel intensities, and the third plane represents the blue pixel intensities.

In order to process the images of dummy sensors, it was needed to convert RGB images to "intensity images". An intensity image is a data matrix, whose values represent intensities within some range. An intensity image is represented as a single matrix, with each element of the matrix corresponding to one image pixel. The value of each element corresponds to the color intensity of the pixel. This color belongs to a selected color map. The most appropriate color map for the images involved in this process was the grayscale color map.

Having all images converted, histograms that give a schematic presentation of distribution of depicted colors along grayscale color map were generated. More specifically, the values on the horizontal axis of the histograms correspond to a color of the grayscale color map. Zero corresponds to total black and 250 corresponds to white. The height of the bars represents the number of pixels that have the specific color. The red shaded areas enclose all bars and represent the range of depicted colors along grayscale color map.

The processed pictures were taken in the same ambient lighting. Moreover, in all these images two holes of dummy SNS's tip are depicted. In this way, the comparison among the histograms is more reliable.

5.3 Histograms

Below are presented the histograms exported from Matlab for the dummy SNS (reference histogram), the adjacent and the opposite to the nozzle view of each device for the two air pressure cases.

- Initial state of dummy SNS

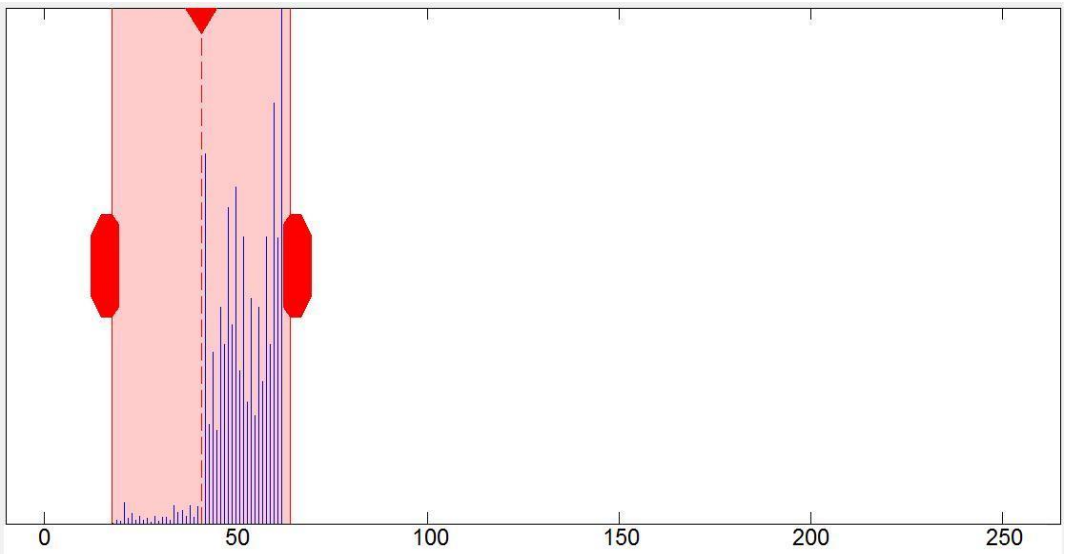

Figure 5.3.1. Histogram corresponding to Figure 4.6.1.

- Dummy SNS – Reference model

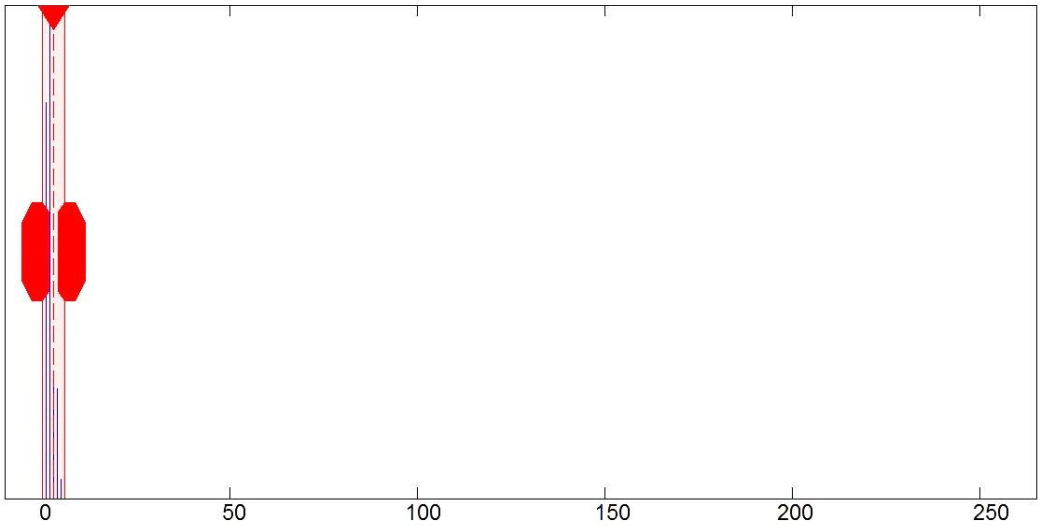

Figure 5.3.2. Histogram corresponding to Figure 4.6.2.

As regards the initial state of dummy sensor, the red shaded region begins from 20 and ends at 65 approximately. Most of the pixels are distributed in the area between 40 and 65 (approx.). On the other hand, the histogram of the dummy SNS that was not protected from soot is totally different. The red shaded area is limited between zero and 10 (approx.),

values that correspond to the darkest shades of grayscale color map. This is attributed to excessive soot deposition.

- Trial air – curtain device with parallel nozzle. Air pressure: 2 bar

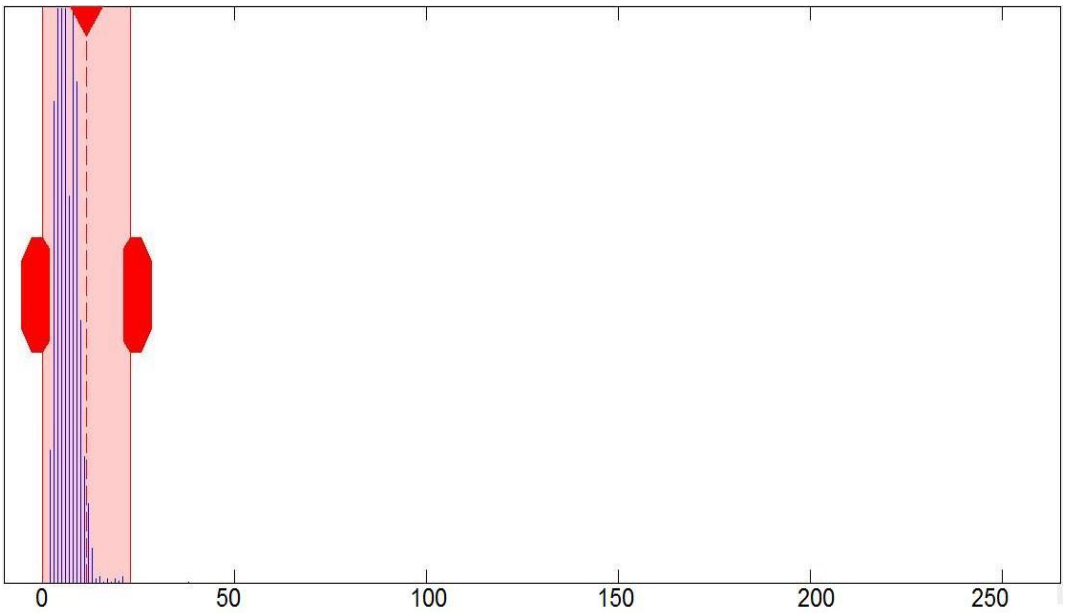

Figure 5.3.3. Histogram corresponding to Figure 4.7.3.

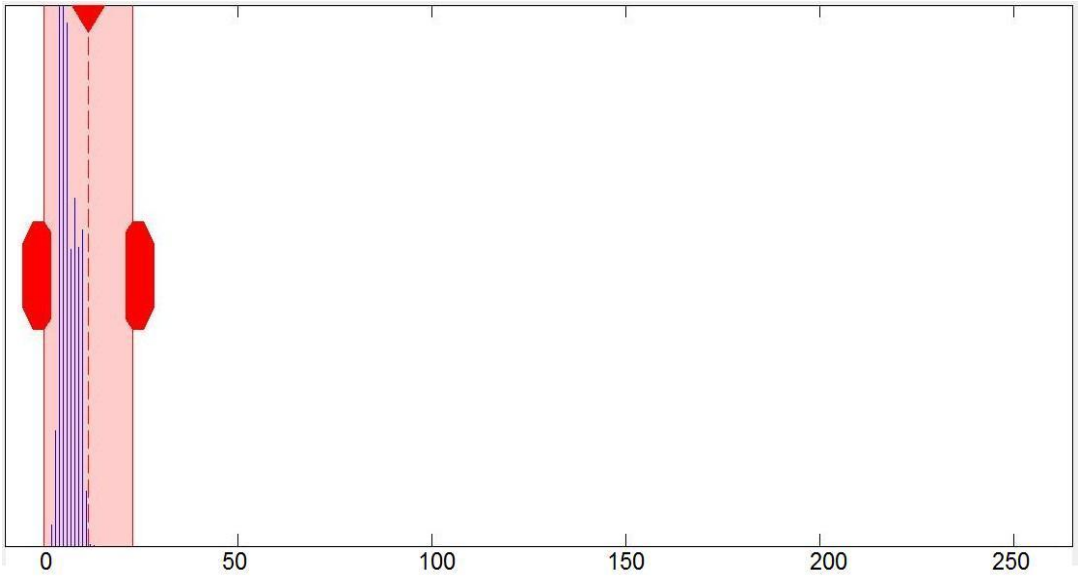

Figure 5.3.4. Histogram corresponding to Figure 4.7.4.

In both histograms, the range of depicted colors is the same (0 - 25) but most of pixels are distributed to lower values (0 – 15). The histogram of the opposite to the nozzle view show that slightly fewer pixels are between 15 – 25. This means that soot deposition had the same rate on both areas of the dummy sensor. It seems that the air – curtain generated by the parallel nozzle protects the whole surface of dummy SNS equally.

- Trial air – curtain device with parallel nozzle. Air pressure: 4 bar

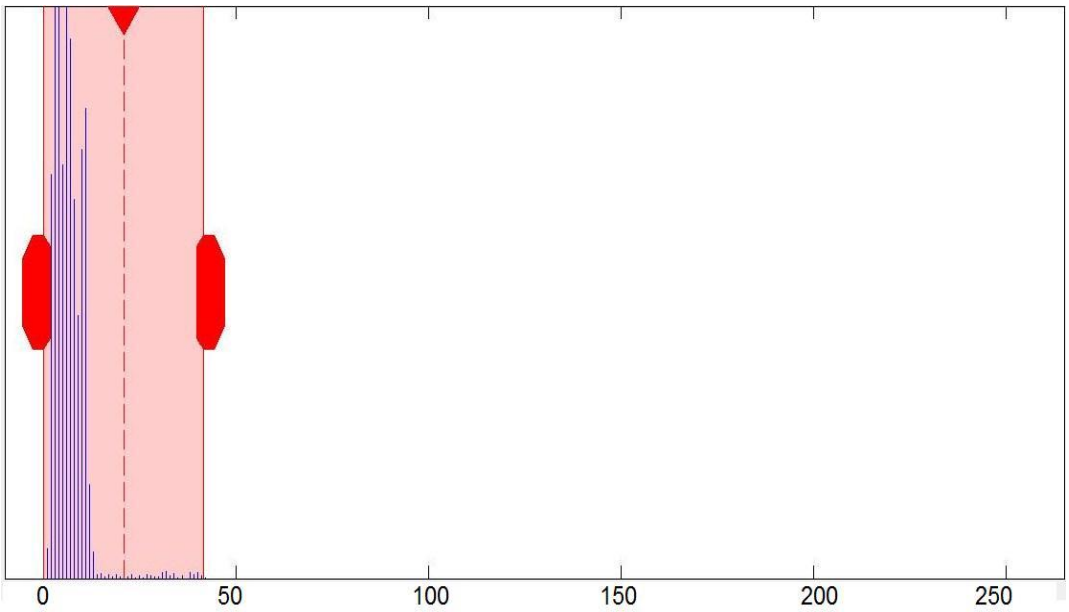

Figure 5.3.5. Histogram corresponding to Figure 4.7.5.

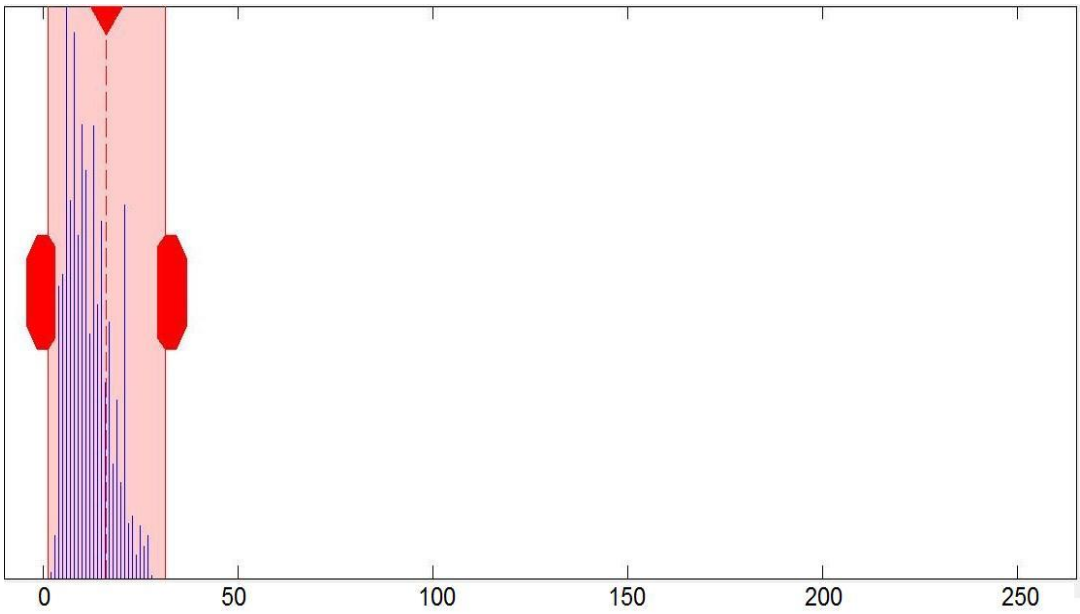

Figure 5.3.6. Histogram corresponding to Figure 4.7.6.

As shown above, the red shaded area of the histogram is wider than this of histograms corresponding to air pressure of 2bar. More specifically, the depicted colors begin from a value slightly bigger than zero and reach approximately the value of 30. However, as in the previous case this area has the same range in both views.

- Trial air – curtain device with inclined nozzle. Air pressure: 2 bar

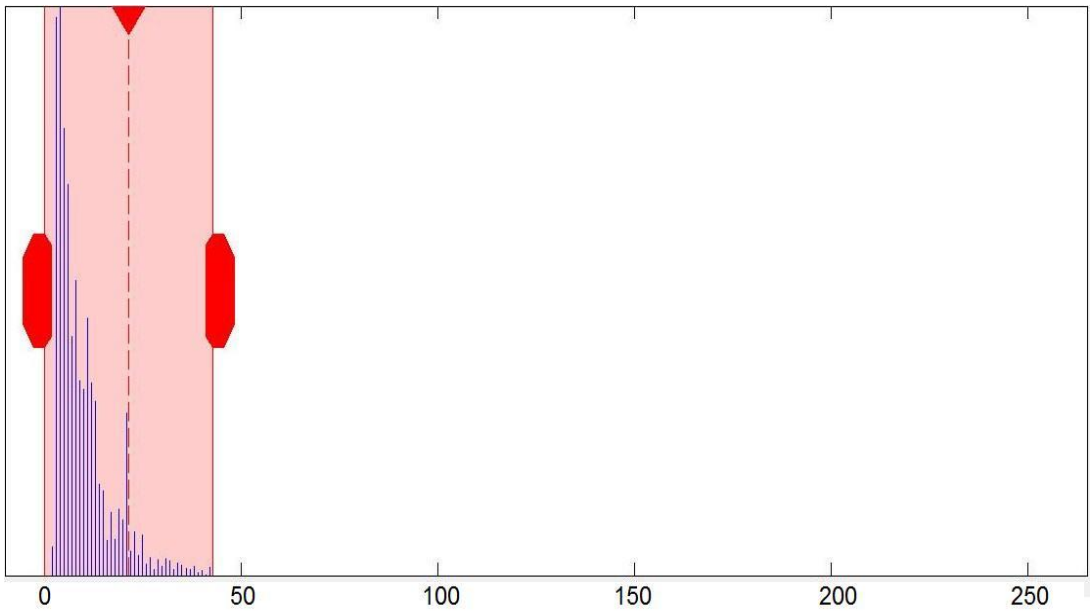

Figure 5.3.7. Histogram corresponding to Figure 4.7.7.

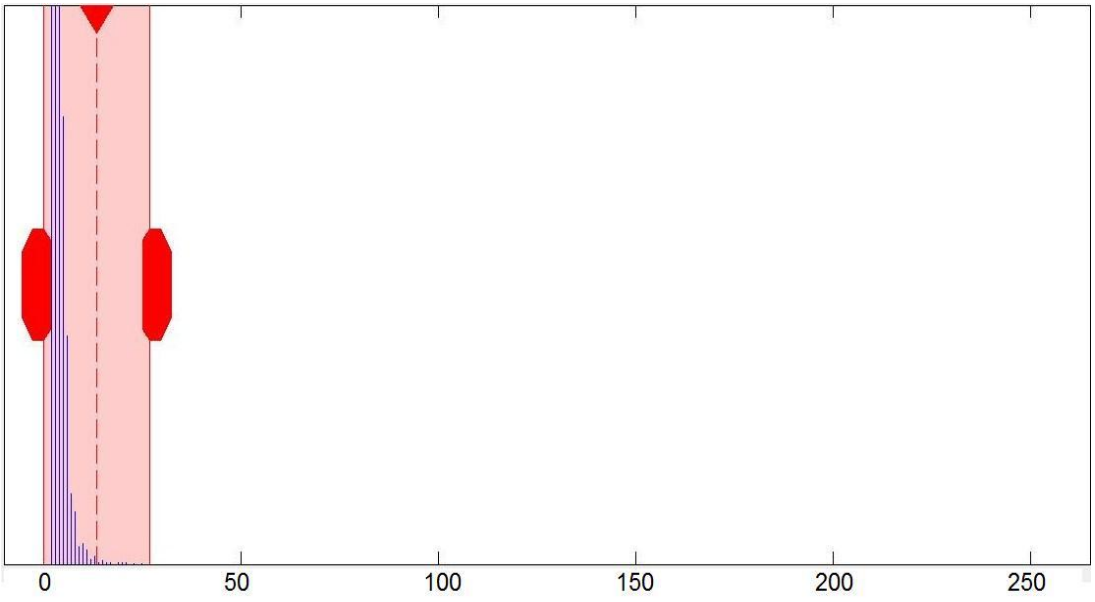

Figure 5.3.8. Histogram corresponding to Figure 4.7.8.

In this case, there is a significant difference between the ranges of depicted colors at each view. In the view adjacent to the nozzle there are pixels of colors between zero and 40. On the contrary, in the opposite view, most of pixels are of colors between zero and 15 and very few pixels are of colors between 15 and 30. Consequently, it can be said that the adjacent view is much more effectively protected than that opposite view.

- Trial air – curtain device with inclined nozzle. Air pressure: 4 bar.

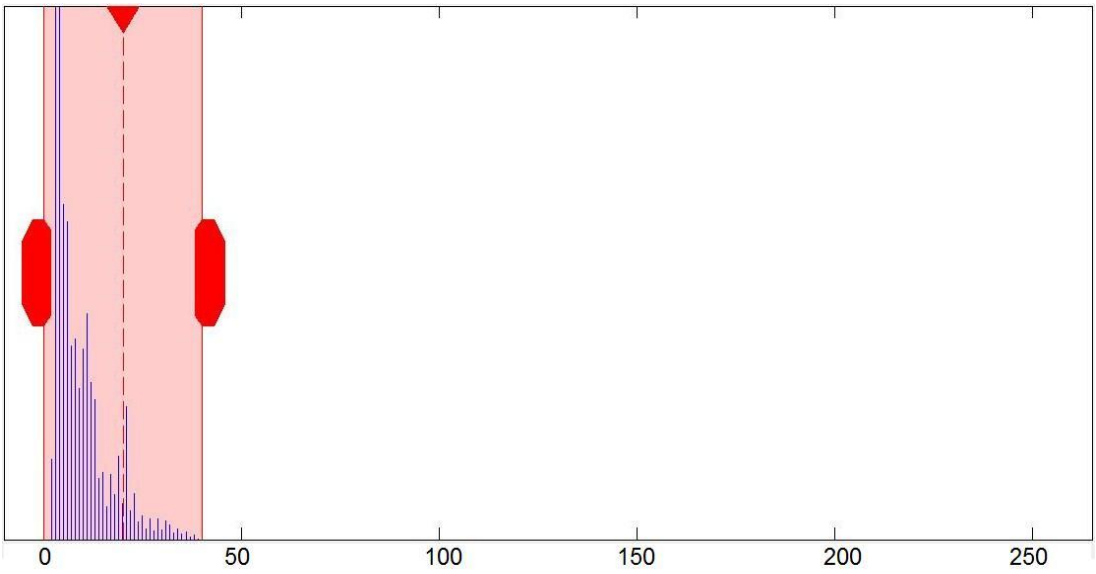

Figure 5.3.9. Histogram corresponding to Figure 4.7.9.

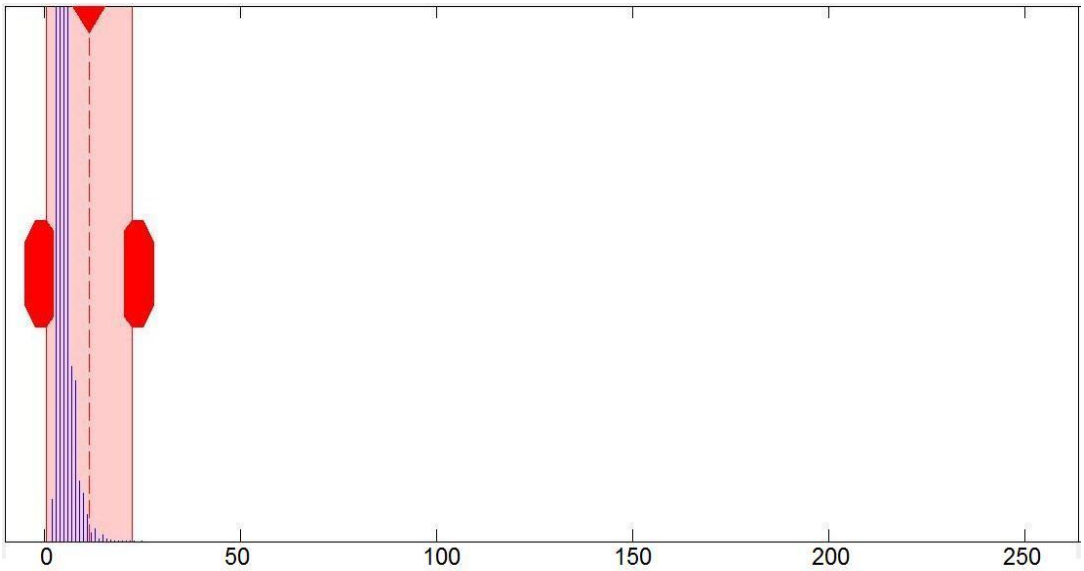

Figure 5.3.10. Histogram corresponding to Figure 4.7.10.

The histograms shown above do not differentiate significantly from the histograms of the previous case. The red shaded region is wider in the histogram of the adjacent view. In the histograms of the opposite view most of pixels are of colors between zero and 15.

5.4 Conclusions

The image processing technique described in this Chapter provided objective facts in order to define which case investigated brings better results against soot deposition. As discussed, the red shaded regions of the histograms enclose the depicted colors of grayscale color map. In all histograms of fouled devices, this region begins from 0, value that corresponds to darkest color, as expected. A large red-shaded zone means that colors lighter than black are depicted and therefore, less soot is loaded in the dummy sensor.

In Figure 5.3.2., it is shown that only the darkest colors are depicted due to the absence of the air curtain device.

As shown in Figures 5.3.7. – 10, the histograms of dummy sensor with the inclined nozzle reveal that the adjacent to the nozzle region is well protected from soot loading but the opposite is not. For both values of air pressure the results are similar.

With respect to the dummy sensor with the parallel nozzle the value of air pressure has a great impact to the results. For the air pressure of 2 bar the histogram is restricted in the area of 0 – 25, when for 4 bar the histogram range is, obviously, broaden. This means that the rate of soot deposition is lower when the air pressure is regulated to 4 bar, as expected.

Finally, since it is important to protect the whole exposed region of the sensor, the parallel nozzle is more preferable. As regards the air pressure, it is proved that 4 bar provided higher level of protection.

6. DESIGN AND MANUFACTURING OF THE FINAL AIR – CURTAIN ARRANGEMENT

6.1 Introduction

The processing of the experiments' results revealed that the air curtain arrangement with a nozzle parallel to the sensor's axis provide better protection to the SmartNO_X Sensor from soot loading. Consequently, the designs of the trial arrangement needed to be modified so that the actual sensor could be fitted in. The required changes concerned the thread through which the SmartNO_X Sensor would be bolted to the arrangement. Also modifications were needed in order to secure the integrity of the SNS's wiring that would be threatened by the high temperature of the exhaust gases.

6.2 Design of the final air – curtain arrangement.

The parts of which the air – curtain arrangement consists are the same with those described in chapter 3. The air pipe and the fitting (BSP G 1 1/2') were parts that did not need any modification. The modified parts of the design are presented below.

- Head of the SNS with the air nozzle

The diameters of the air pipe socket and the air nozzle remained the same. However, the socket of the SNS consists of a threaded hole and a ledge that would stabilize the SNS. The SNS bears a hexagonal nut through which it is bolted to the matrix tightly. The dimensions of the matrix's part that penetrates the probe needed to be change so that the SNS with the hexagonal nut could fit. For the same reason, the depth of the threaded holes for the flathead M5 Allen screw was shortened.

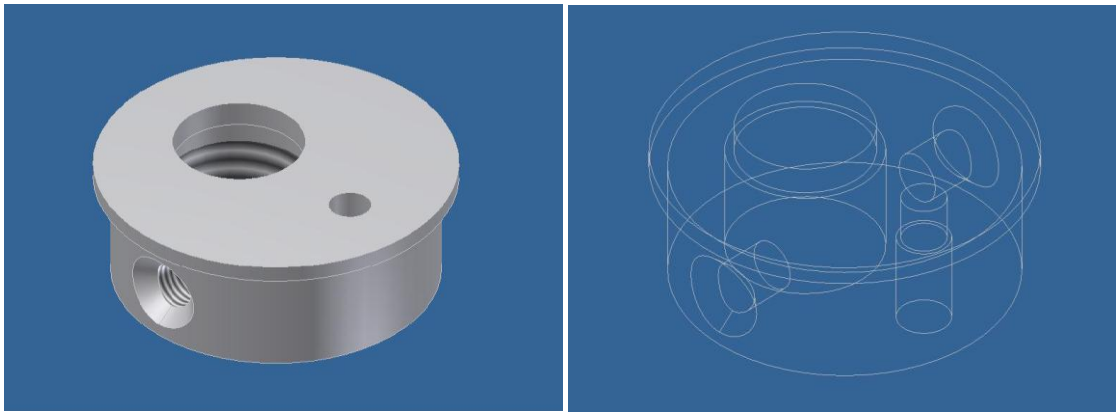

Figure 6.2.1. Design of the final head

- Probe body

As discussed in §3.2, a probe contributes to the correct installation of the sensor in the region of the exhaust duct's section that is specified by the NO_X Technical Code. A part of the probe is exposed to exhaust gases and to high temperature that may surpass 360°C, as shown in §4.2. The manual of the SmartNO_X Sensor specifies that the maximum temperature of measured exhaust gases is 800°C. However, as shown in Figure 3.2.1, the wiring of the SNS is not designed to be located in the exhaust duct. Therefore, four slits on the circumference of the probe were designed. These slits are located in the part of the probe that is outside of the exhaust duct and let the air, that comes from the ventilator of the engine room, to insert the probe and reduce the temperature around the SNS's wiring. Apart from the slits, the inner diameter of the probe, at the tip in which the matrix penetrates, was widened.

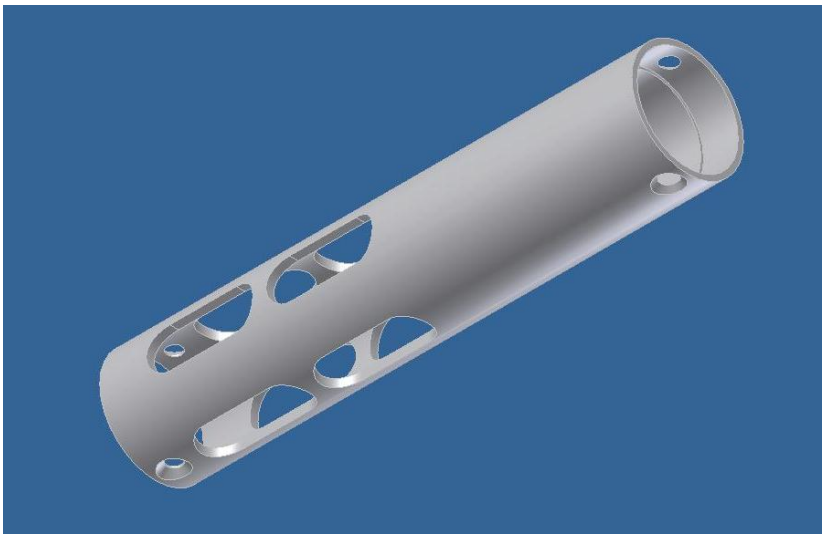

Figure 6.2.2. Design of the final probe with cooling slits.

- Air transfer pipe support

As discussed in §3.2, the relatively long length of the air pipe and the weight of the hose with the quick release fitting may distort the air pipe and the internal compressed air flow. Therefore, it was decided to design a support of the air pipe that would be fitted in the back tip of the probe. In the final arrangement, this support also bears one slot through which the SNS's wiring passes.

Figure 6.2.3. Design of the final pipe support

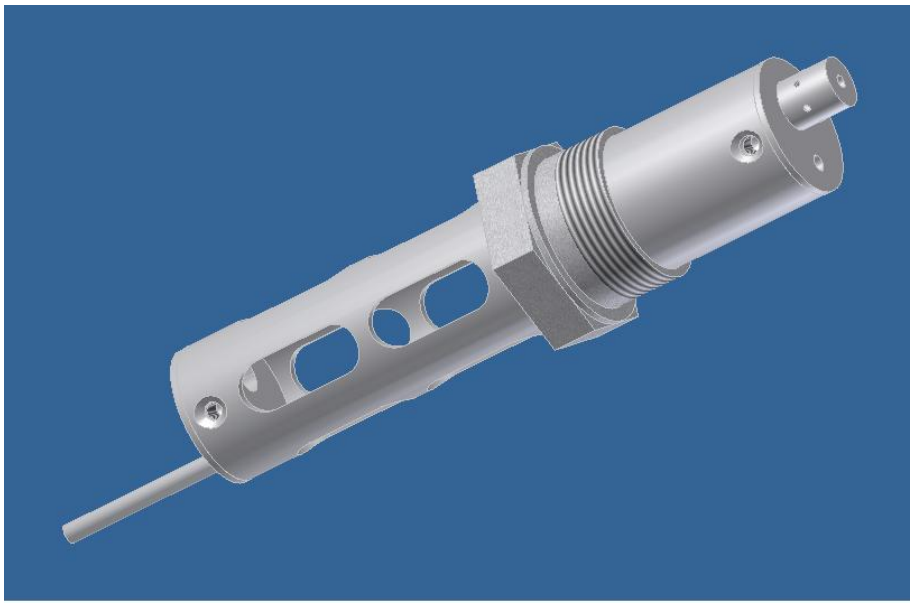

Figure 6.2.4. Design of the final arrangement

6.3 Additional activities for the protection of SNS's wiring from high temperatures.

During the engine runs described in Chapter 4, it was observed that the metal surfaces of the devices were suffering from high temperatures. In the design described in §6.2, the wiring of the SNS is constantly in contact with the walls of the pipe support's slot. The high temperature of the arrangement's surfaces may set the wiring's integrity in danger. It was, therefore, decided to cover the SNS's wiring with a high-temperature resistant material reinforced with glass fibers, as shown in Figure 6.3.1.

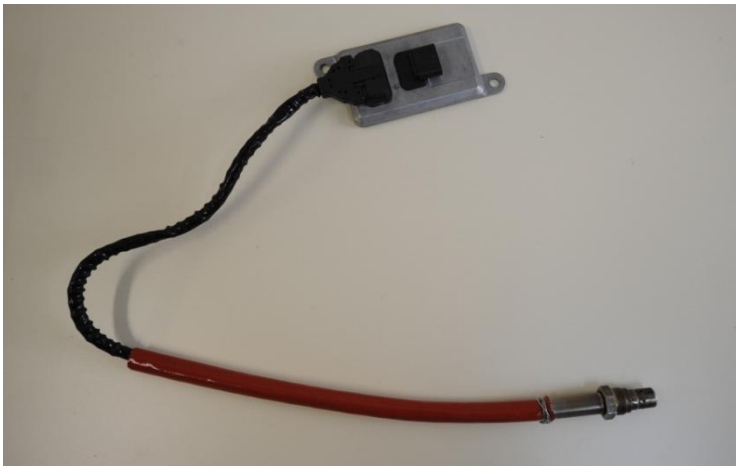

Figure 6.3.1. SmartNO$_X$ Sensor with insulated wiring.

6.4 Conclusions

The design of the final arrangement did not differ significantly from the trial arrangement with the parallel nozzle. The main dimensions of the arrangement remained the same, which means that it is compact, easy to operate and suitable for the sockets of the exhaust duct designed for the trial arrangements. A photo of the final air curtain arrangement with the SNS installed is presented below.

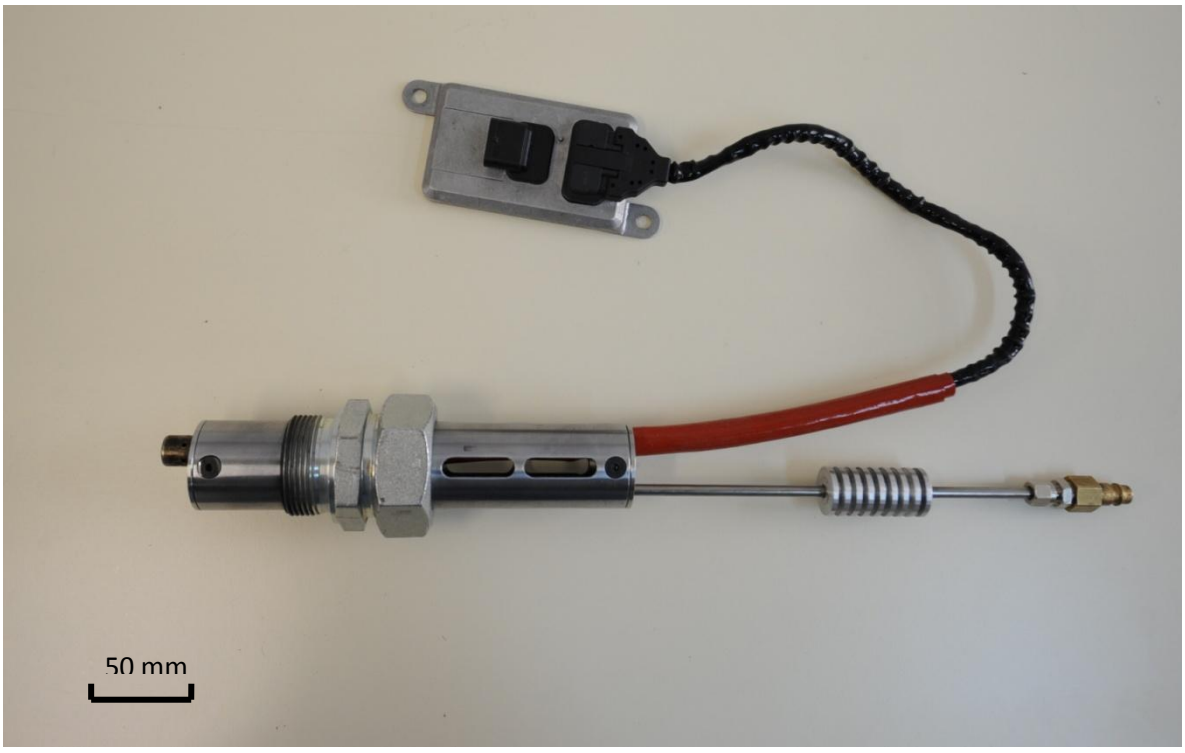

Figure 6.4.1. Final air - curtain arrangement.

7. SIMULTANEOUS NO_X MEASUREMENTS USING CLD ANALYZER AND SmartNO$_X$ SENSOR INSTALLED IN THE AIR CURTAIN ARRANGEMENT

7.1 Introduction

In this chapter, the performance of the SmartNO$_X$ Sensor, that is installed in the air – curtain arrangement, is examined. For this purpose, engine tests were conducted with both the SNS and the CLD reference analyzer installed in the research engine's exhaust duct. In each engine test, measurements from both devices were acquired concurrently. Then, the measurement was stopped, the air curtain arrangement was switched on and the engine kept on operating. After each test, the air curtain arrangement was extracted from the exhaust duct and the amount of soot deposited was evaluated through image processing, as described in chapter 5. Finally, engine tests were conducted in order to compare the SNS's output with the air curtain arrangement on and off operation.

7.2 Description of experimental setup

7.2.1 EcoPhysics CLD 700 RE ht analyzer.

The measuring principle of the CLD analyzer used is presented in §2.3. In this paragraph, the main components of the analyzer are described.

- Detector unit

The CLD analyzer measures both the NO and NO_X concentrations. For this purpose, the analyzer features two separate reaction chambers with a shared light detector. This detector is a cooled photomultiplier (PMT) with a multialkali-photocathode. The chemiluminescent light is collected by an optical imaging system from the chambers and is projected onto the photocathode. The optical imaging system is, in fact, a cylindrical lens mirrored on one side. The position of this mirror alternates between imaging the NO and NO_X chambers through the stepper rotation of a motor to which the cylindrical lens is connected. In certain measuring cycles the mirror is positioned to a covered position, in order to adjust zero point.

Since the output of chemiluminescent type detectors is sensitive to the exhaust gas mass flow, a high precision stainless steel flow restrictor is part of the detector unit. The flow restrictor monitors the inlet gas pressure and the value is used for signal correction. Apart from the inlet pressure, it is necessary to control the temperature of the gases that enter the reaction chambers. The ozone temperature remains constant (55°C) in the reaction chambers and the sample gas passes through a heated tube in which the temperature remains constant, too (190°C). The PMT is cooled and thermally insulated from the

environment and the heated reaction chambers. The inside of the cylindrical lens is flushed with dry air to prevent condensation.

The detector's output is, also, influenced by parameters such as chamber pressure and temperature, sample gas flow and ozone generator high voltage, are constantly monitored.

- Ozone generator

As discussed in §2.3, the ozone concentration in the reaction chambers must be in excess. The ozone is generated by the ionization of atmospheric oxygen. Therefore, the ambient air passes through a drier and, then, through an alternating electrical field. The electrical discharge, through which the ionization of oxygen is accomplished, is created by a constant-frequency stabilized high voltage

- Converter.

The reduction of NO_2 to NO is accomplished through a converter (according to eq. 2.3.5) which uses a metal catalyst with large specific surface. The converter consists of a heated and thermally isolated steel block that bears the converter cartridge. Since, the converter materials are consumed from the use, they are easily replaceable.

- Heated tubing inlet

In order to prevent water and hydrocarbons of the sample gas condensing in the instrument, all gas-contacting parts have constant temperature of 190°C. Therefore, the tubing system downstream of the sampling probe is heated [4].

Some of the performance and physical characteristics of the analyzer are presented below:

NO_X Measuring range	0 – 10,000 ppm
Min. detectable concentration	0.1 ppm
Noise at zero point	0.05 ppm
Sample flow rate	1.2 lt/min
Dry use rate (O_3 generation)	0.55 lt/min
Power required	660VA
Supply voltage	230 V/50 Hz (±10%) optional 115 V/60 Hz (±10%)
Weight	40 kg

Table 7.2.1. CLD700 RE ht performance and physical characteristics

The CLD analyzer used in this set of engine tests is only a part of a group of analyzers which comprise the portable emission measurement unit of NTUA-LME. These analyzers can measure the concentration of different types of emissions, such as SO_X, CO, CO_2, UHCs and O_2. The operation of these analyzers is interrelated and, therefore, the whole set of analyzers had to be transferred to the engine room and connected to one another. The sample gas is extracted from the exhaust duct through a common probe. Downstream of the probe is the heated tube. The probe was installed in the exhaust duct between the two elbows that are downstream of the turbocharger.

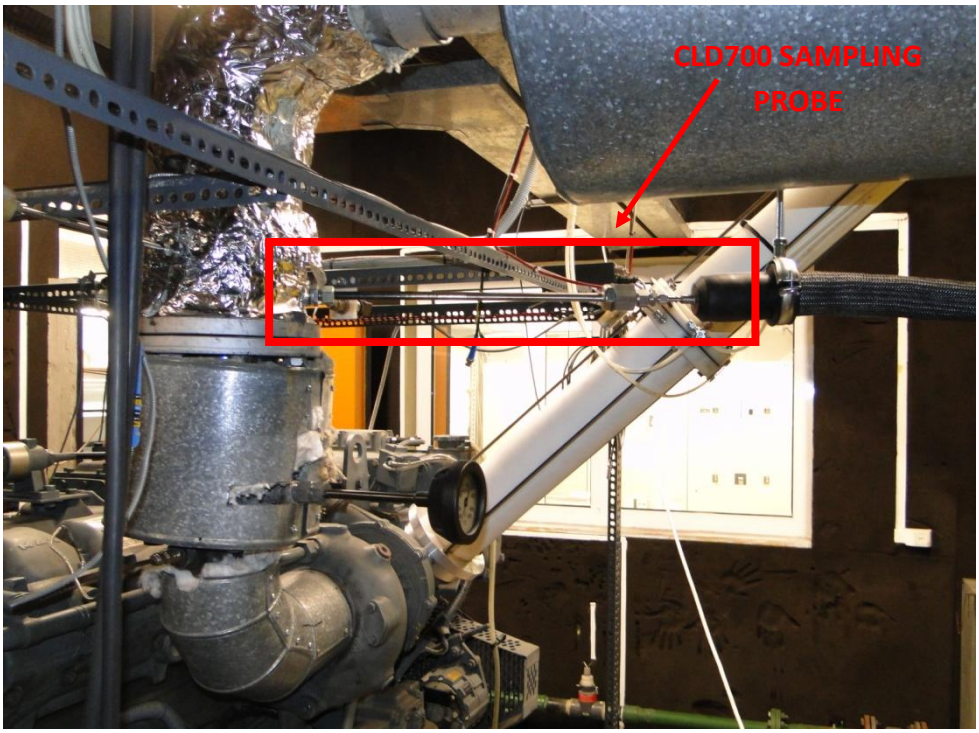

Figure 7.2.1. CLD700 RE ht probe installed in exhaust duct

Regarding the analyzer's operation, it must be mentioned that it has to be calibrated before every use. In the calibration procedure, two types of gases are supplied to the analyzer instead of exhaust gas. Firstly, zero gas, which is gas with zero NO_X concentration, is supplied in order to define zero point. Then, a span gas with specific NO_X concentration is supplied to the analyzer. The value of NO_X ppm is stated through the analyzer's front panel, in order to create a second point. Finally, the calibration curve that connects these two points creates the transfer function from the electrical signal to NO_X ppm.

It must be mentioned that the procedures of pre-heating and calibration lasts at least 30 minutes.

A.

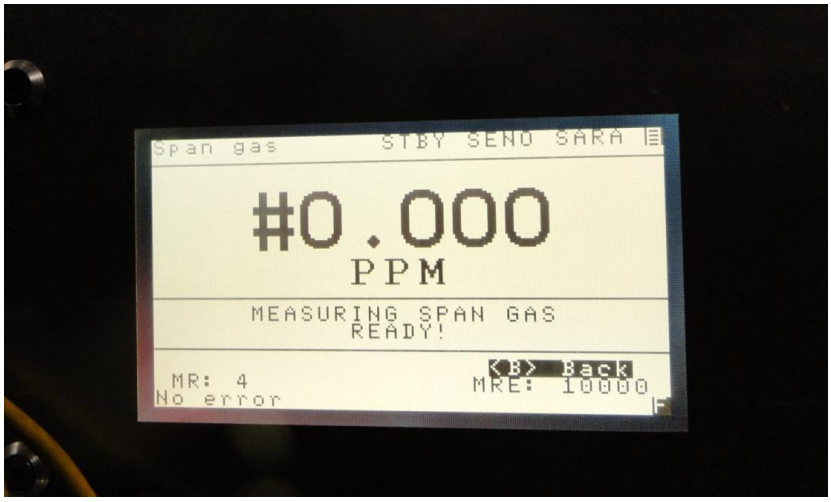

B.

Figure 7.2.2. A. CLD analyzer's front panel during calibration procedure. B. CLD analyzer during span gas supply

7.2.2 SmartNO_X Sensor

The operating principle and the major parts of a typical amperometric sensor, such as the SNS, is described in §2.2. The sensor is connected to an electronic control unit (ECU) by a wiring harness. This ECU provides not only the power control for heating the sensor to operating temperature but, also, the measured gas concentrations digitally via CAN bus. The regulation for the amperometric operation of all pumping cells to determine NO_X concentration is realized in an Application-specific integrated circuit [2].

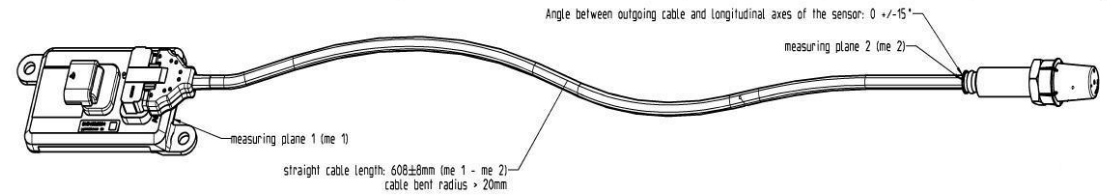

Figure 7.2.3. SmartNO$_X$ Sensor assembly [2]

Some of the performance and physical characteristics of the SNS are presented below:

NO_X measuring range	0 → 3000 ppm
NO_X measuring accuracy	-for new sensor: ±10ppm (at 0ppm) and ±10% (100 - 3000ppm) -for aged sensor: limited values are 10ppm / 10% higher than fresh limit values
NO_X response time	-for new sensor: 1.3 sec -for aged sensor: 1.65 sec
Max. exhaust gas Temp.	800^{o}C (exhaust gas temperature of 950^{o}C allowed up to 100h)
Weight	280 g (ECU incl.)

Table 7.2.2. SmartNO$_X$ Sensor performance and physical characteristics

The operation of the SNS prerequisites the pre-heating of the sensor. The command for the pre-heating is given manually through SNS's specialized software. The procedure of pre-heating lasts five minutes maximum.

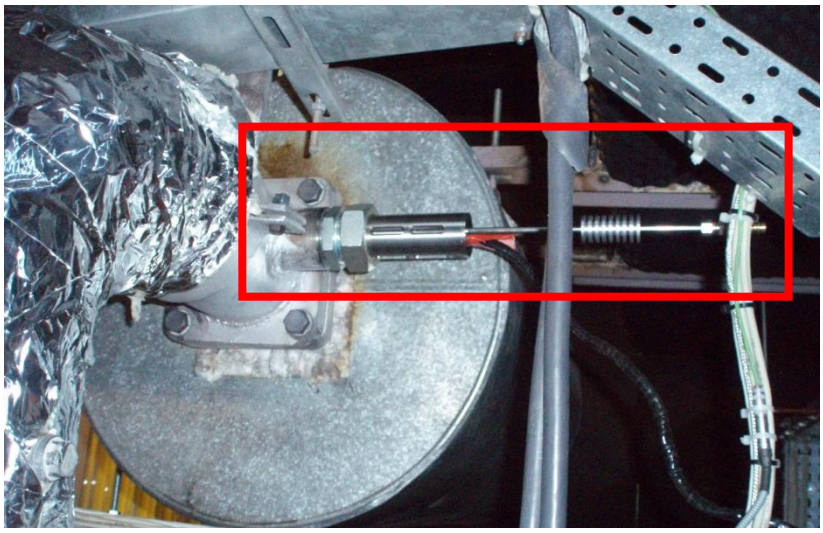

Figure 7.2.4. Final air curtain arrangement with the SNS installed in the exhaust duct

The SNS's output signal was digital (CAN signal). This signal had to be converted to analogue so that all signals from measurement devices could be collected by NTUA-LME's DAQ system and the measured concentrations could be compared directly. To convert CAN signal into analogue, "ATI Canverter" from *Accurate Technologies* was used. The configuration of ATI analog outputs was performed with the "Canverter Configuration Tool" software provided by *Accurate Technologies.*

7.2.3 Recording of measured concentrations.

The analogue outputs of the analyzers and the SNS were collected by a set of three data acquisition cards. These cards convert the analogue signals into digital, in order to be imported to a pc. The recording of the SNS's and analyzer's outputs required the elaboration of a virtual instrument in LabView® platform (Figure 7.2.4).

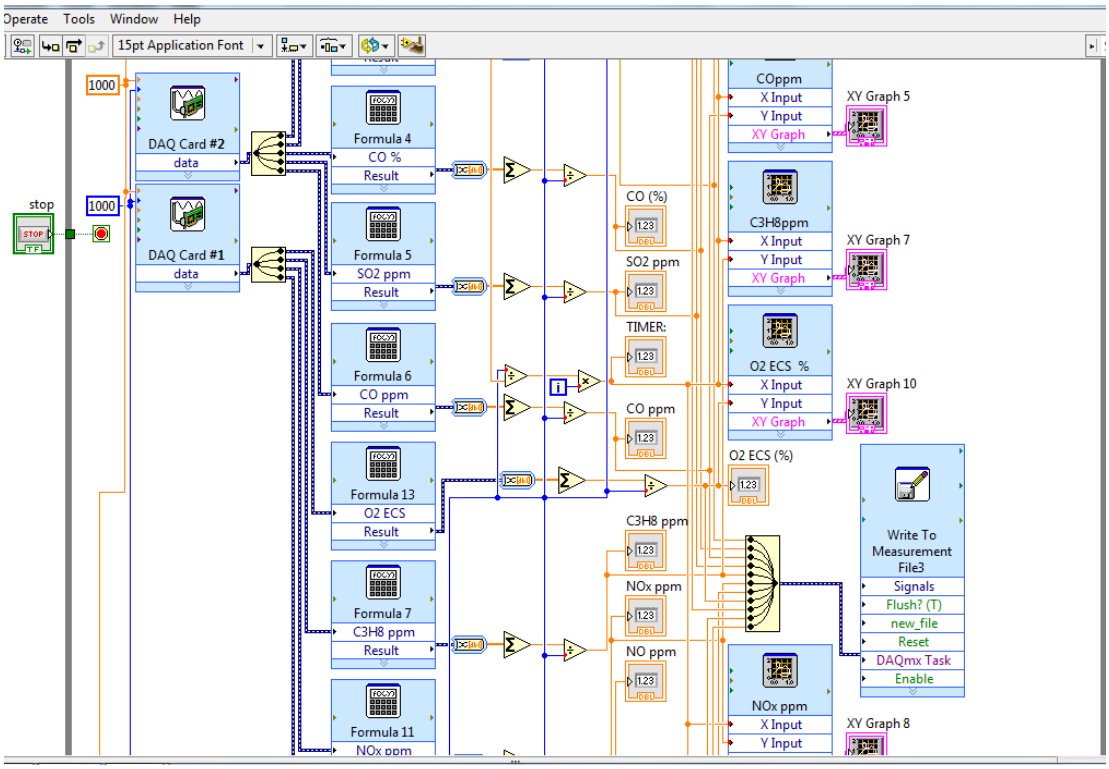

Figure 7.2.5. Block diagram of virtual instrument in LabView®

In this virtual instrument the data acquisition cards and the trasfer function of each signal were stated. Then, the measured concentrations and the corresponding time points were recorded to a file of '.xml' extension.

7.3 Engine tests.

For the experimental investigations of this section five engine tests were performed, each of them lasting for 2 hours. In these tests, the engine remained at idle state for approximately 3 minutes in order to reach stable operating temperatures. Then, the engine was coupled to the electric generator which was paralleled to the electric grid and the engine load was increased to 50% of nominal load (115kW). The engine load was regulated manually through the regulation of the electric generator's power output. Given the fact that the generator's performance ratio is equal to 0.92 (approx.), the selected output value was 105kW.

Figure 7.3.1. Front panel of electric generator's control unit

Continuous NO_X measurements were acquired with the engine operating at idle state, during the transition to 50% load and at constant load for several minutes. Then, the air curtain device was switched on and the measurement recording was stopped. In each test, which lasted for two hours, the air curtain device remained on operation for 90 minutes at least. After two hours of engine operation the engine was switched off and the SNS was uninstalled from the exhaust duct to undergo a photo shoot. The photographs taken, were later processed with the method described in §5.2.

7.4 NO_X and O_2 measurements with SmartNO_X Sensor and analyzers

As discussed in §7.3, five tests were executed in different dates. Each test lasted for 2 hours during which the engine speed was constant at 1500 rpm. The engine remained at idle state for almost 3 minutes and then the load was increased to 115 kW (50% of nominal load). The data acquisition system stopped recording NO_X and O_2 concentrations after several minutes when the air curtain device commenced. Before making any comparison between the outputs of the SNS and the analyzers, it must be mentioned that the SNS and the analyzers were not installed in the same sampling position. The SNS's sampling position was located downstream of the CLD700 sampling position.

- NO_X measurements

The NO_X concentrations recorded simultaneously form SNS and CLD700 RE at each test, are presented in Figure 7.4.1. From all tests, it can be observed that the SNS responded faster than the CLD700 at the load increases, by about 3-4 seconds. The faster SNS's response was attributed to the fact that the CLD analyzer extracts sample gas from the exhaust duct which had to travel almost seven meters inside the heated tube and then undergo the treatment described in §2.3. On the contrary, the SNS was able to create its output immediately, since it was located inside the exhaust duct.

After the transition from idle to 50% load, the engine operated constantly at this load (115 kW). The transition period completed at about 300 sec. The outputs of SNS and CLD analyzer from 400 to 600 seconds are presented in Figures 7.4.2. and 7.4.3. respectively. The aforementioned period was selected because the load was increased manually and, therefore, it took several seconds to be stabilized at the selected value.

Between 400 and 600sec the average values of NO_X concentrations recorded by SNS varied from 1712ppm to 1776ppm. Consequently, it can be said that the SNS's maintained the repeatability that showed in previous tests described in §2.4. The maximum variation of recorded values was equal to almost 89ppm, which is equivalent to ±2.5% of the average value. With regards to the CLD analyzer, the recorded concentrations varied from 1548ppm to 1664ppm. The maximum variation was detected at test No4 and was equal to 88.5ppm, which is equivalent to ±2.78% of the average value.

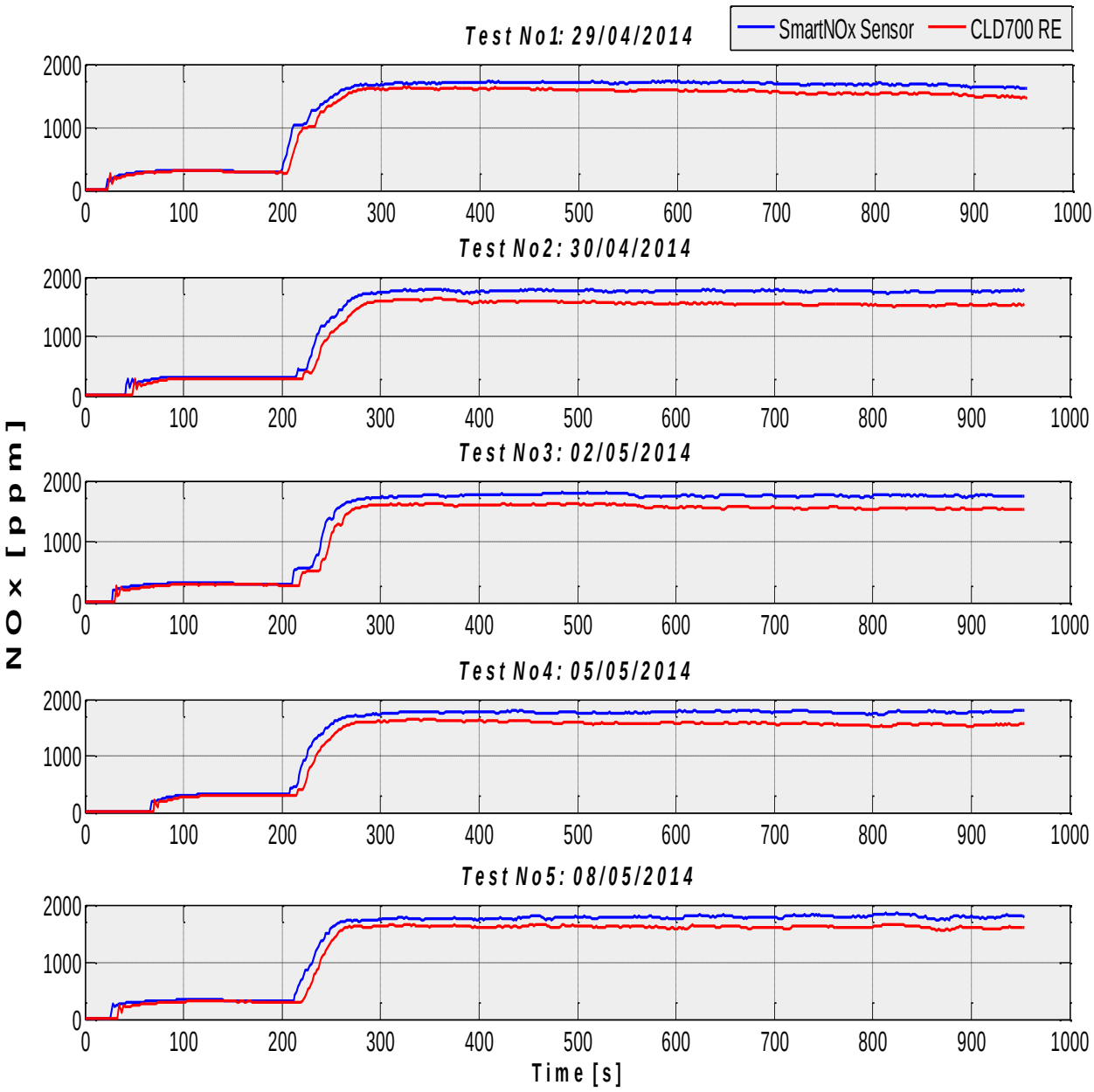

Figure 7.4.1. NO_X concentrations measured by SNS and CLD analyzer

As it can be seen in Table 7.4.2., the deviation between the outputs of CLD analyzer and SNS ranges from 7.14 to 12.2 per cent of the CLD analyzer's output, which is the reference measurement. The maximum deviation appears at Test No2 and the deviation at the last test (No5) is 9.54 per cent. Therefore, it cannot be said that there is a significant increase that would be attributed to the effects of soot deposition on the SNS. It must be mentioned that during the calibration of CLD700, the concentration of the span used was equal to 1500ppm. However, the measured concentrations exceeded 1500ppm. A minor offset in the CLD analyzer's output, due to extrapolation from the calibration curve, can be attributed to this fact. With regards to the SNS, the sensor was purchased at 2009 and took part in a series of tests described in §2.4 during which it was exposed to soot. The

deviation between CLD analyzer's and SNS's output observed in this series of tests was under 10ppm. As described in §2.4, the SNS and CLD analyzer were installed in the same sampling position. On the contrary, in this series of tests, that was executed with a different research engine the sampling position was different..

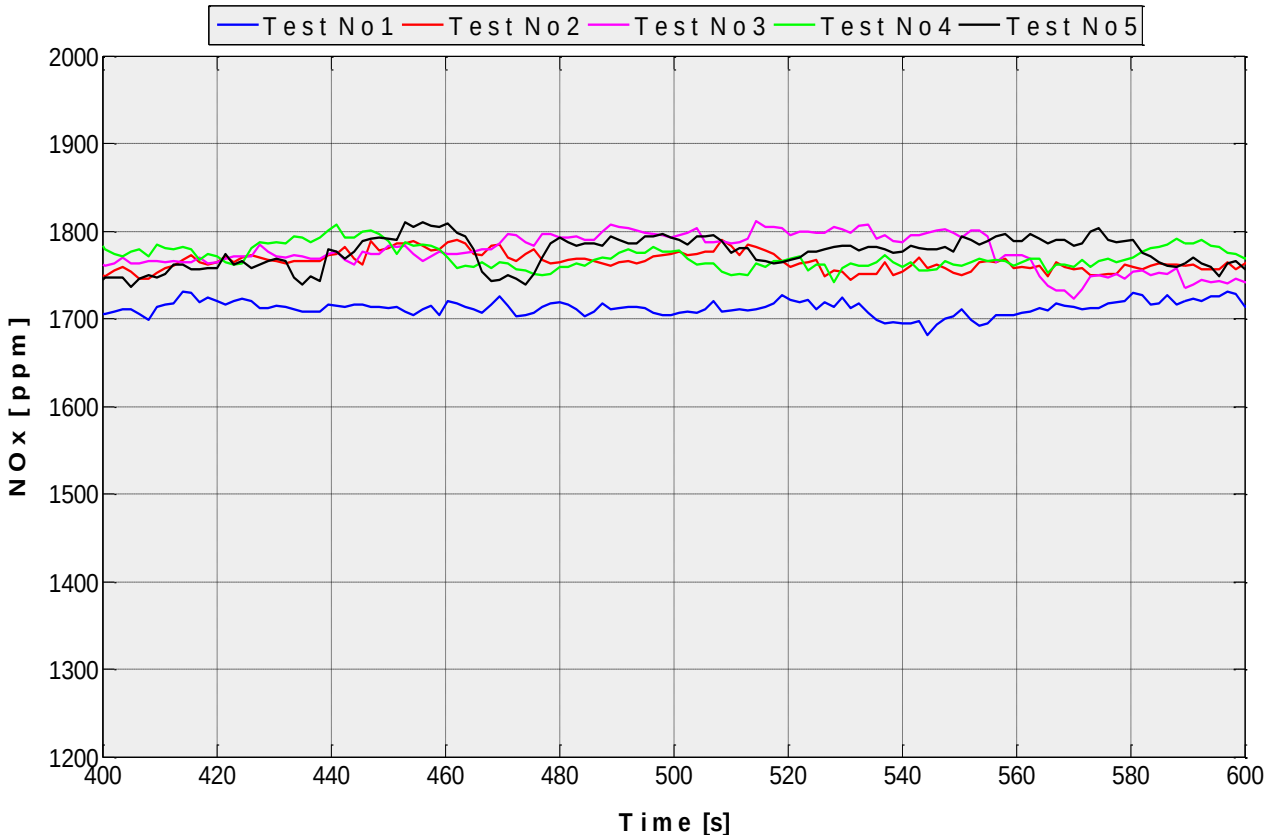

Figure 7.4.2. NO_X concentrations measured by SNS at constant load

NO_X [ppm]					
	SmartNOx Sensor				
	Test No1	**Test No2**	**Test No3**	**Test No4**	**Test No5**
Mean Value	1712.63	1765.56	1776.52	1770.91	1775.88
Standar Dev.	8.82	10.67	21.09	12.88	17.67
Min. value	1681.12	1743.90	1722.31	1741.97	1736.72
Max. value	1731.11	1789.71	1811.35	1807.38	1810.67
Range	49.99	45.81	89.03	65.41	73.96
± %	1.46	1.30	2.51	1.85	2.08

Table 7.4.1. Statistical analysis of SNS output

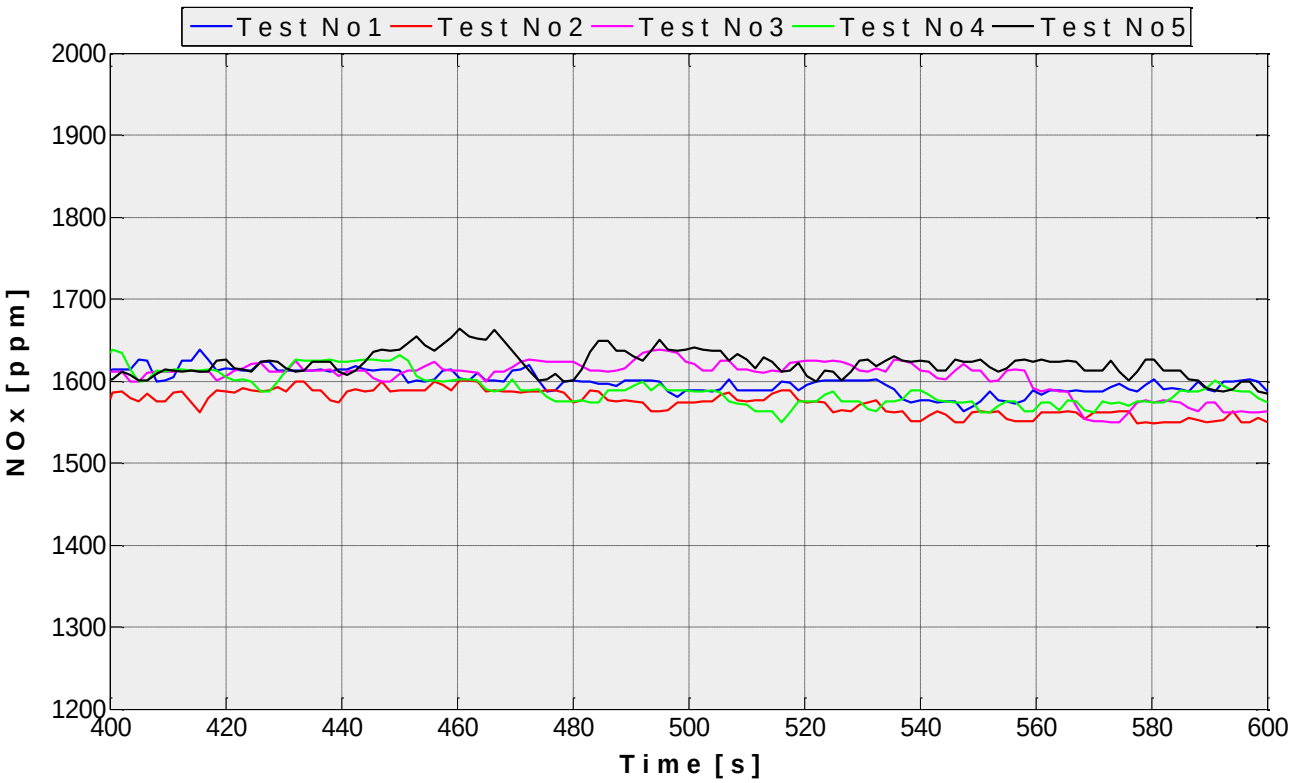

Figure 7.4.3. NO_X concentrations measured by CLD analyzer at constant load

NO_X [ppm]					
	CLD 700 RE				
	Test No1	Test No2	Test No3	Test No4	Test No5
Average	1598.56	1573.55	1605.52	1589.56	1621.19
Standar Dev.	13.99	15.07	21.00	19.52	16.21
Min. value	1563.50	1548.24	1549.80	1549.67	1584.12
Max. value	1638.25	1601.01	1637.96	1638.14	1663.62
Range	74.75	52.77	88.16	88.47	79.49
± %	2.34	1.68	2.75	2.78	2.45

Table 7.4.2. Statistical analysis of CLD700 RE output

	Test No1	Test No2	Test No3	Test No4	Test No5
CLD 700 RE [ppm]	1598.56	1573.55	1605.52	1589.56	1621.19
SmartNOx Sensor [ppm]	1712.63	1765.56	1776.52	1770.91	1775.88
Deviation [ppm]	114.07	192.01	170.99	181.36	154.70
%	7.14	12.20	10.65	11.41	9.54

Table 7.4.3. Comparison between mean values of SNS's and CLD analyzer's output

- O_2 measurements

Apart from NO_X concentration, SNS is capable of measuring O_2 concentration with the measuring principle described in §2.2. The NTUA – LME mobile measurement unit features two analyzers for O_2 concentration measurements, Magnos 206 and Uras 26. In this set of tests Magnos 206 was used. This analyzer measures O_2 concentration using paramagnetic detection (PMD), which is the most reliable and accurate method for this measurement.

As already mentioned, the SNS was installed in the exhaust duct and, therefore, was sampling exhaust gas that contained water vapors. The CLD was sampling exhaust gases through the heated tube without any condensation taking place. Consequently, the SNS and CLD measurements were performed on the so called “wet basis”. On the contrary, the volume of the exhaust gas that was directed to the PMD analyzer was cooled down prior to entering the analyzer. The water vapor of the exhaust gases was extracted within the cooling unit of the emission measurement unit and, therefore, the measurement was on a dry basis. Consequently, the O_2 output of the SNS could not be directly compared to that of the PMD analyzer. In order to have a valid comparison, the output of the PMD had to be corrected using the dry-to-wet correction factor K_{wr} [10]. The calculation of this factor [15] depends on parameters such as intake air pressure, temperature and humidity, the air and the fuel mass flow rate. During the tests, these parameters were not measured and therefore it was unfeasible to calculate this factor. The results of the O_2 measurements are presented in the following Figures (7.4.4 - 6). The SNS output cannot be compared to that of PMD analyzer. However, the responses of the sensor and analyzer and the stability of measured time series can be evaluated. As it was observed in NO_X measurements, the SNS had better response during the engine load increase. Moreover, the repeatability of the SNS’s and PMD’s output showed satisfying repeatability, as shown in Tables 7.4.4 – 5.

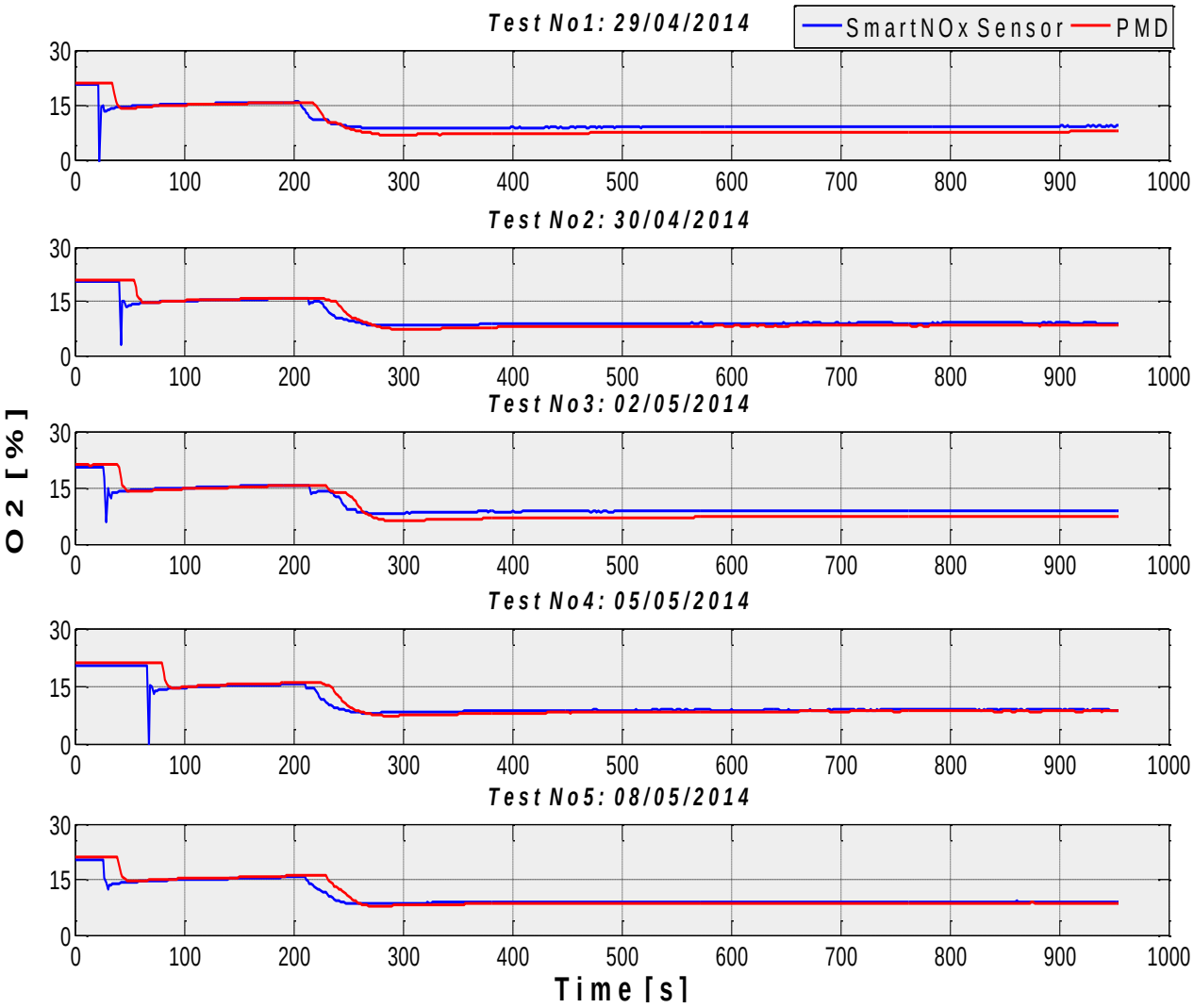

Figure 7.4.4. O_2 concentrations measured by SNS and PMD analyzer

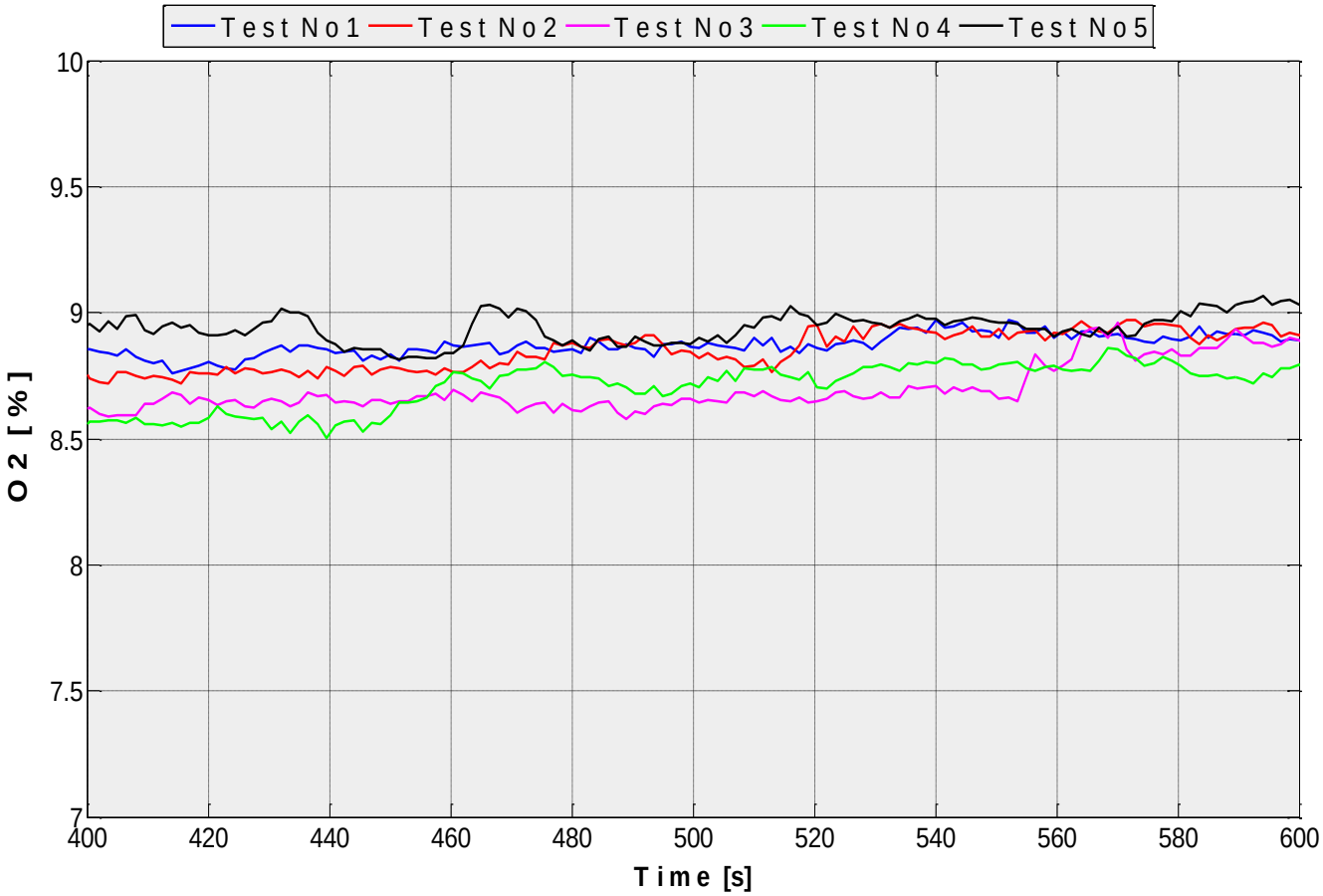

Figure 7.4.5. O_2 concentrations measured by SNS at constant load

O2 [%]					
	SmartNOx Sensor				
	Test No1	**Test No2**	**Test No3**	**Test No4**	**Test No5**
Average	8.87	8.85	8.70	8.71	8.94
Standar Dev.	0.04	0.08	0.09	0.09	0.06
Min. value	8.76	8.72	8.58	8.51	8.81
Max. value	8.97	8.972	8.96	8.86	9.07
Range	0.22	0.251	0.39	0.36	0.25
± %	1.22	1.42	2.22	2.05	1.41

Table 7.4.4. Statistical analysis of SNS O_2 measurements

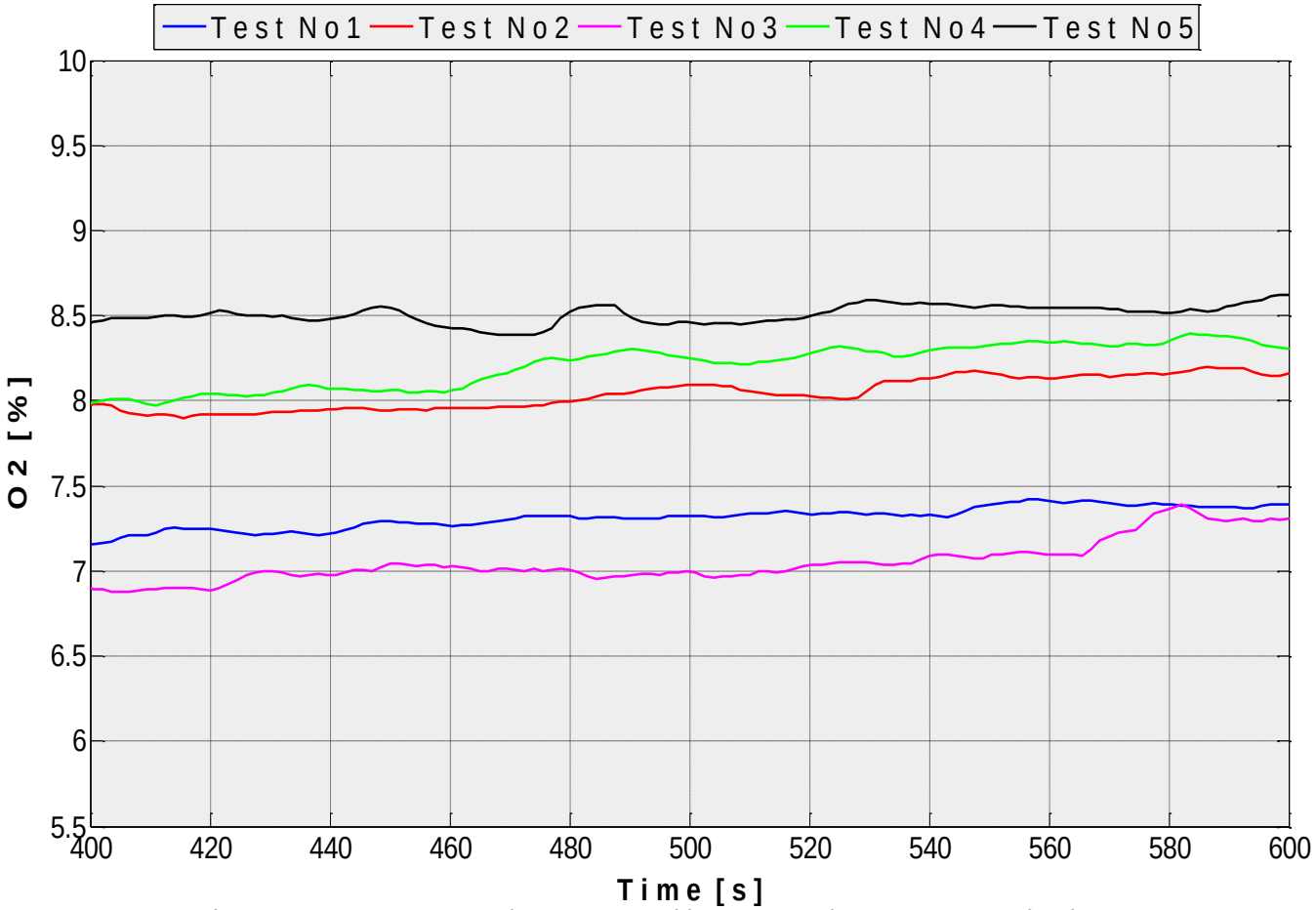

Figure 7.4.6. O_2 concentrations measured by PMD analyzer at constant load

O2 [%]					
	PMD				
	Test No1	**Test No2**	**Test No3**	**Test No4**	**Test No5**
Average	7.32	8.04	7.05	8.21	8.51
Standar Dev.	0.064	0.093	0.125	0.127	0.054
Min. value	7.16	7.9	6.87	7.98	8.39
Max. value	7.42	8.2	7.39	8.39	8.62
Range	0.26	0.3	0.52	0.41	0.24
± %	1.79	1.85	3.65	2.54	1.4

Table 7.4.5. Statistical analysis of PMD O_2 measurements

7.5 Image processing results.

– Initial state

Figure 7.5.1. Initial state of SNS(left) and dummy SNS (right)

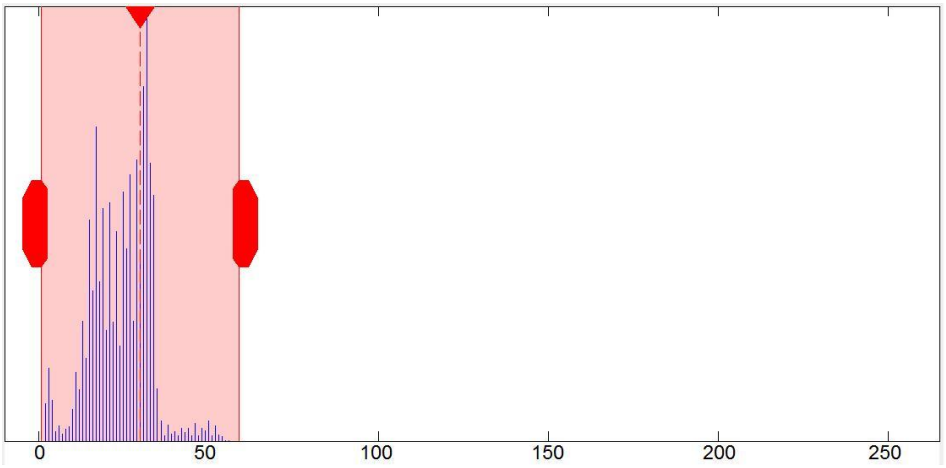

Figure 7.5.2. Histogram of dummy SNS at initial state

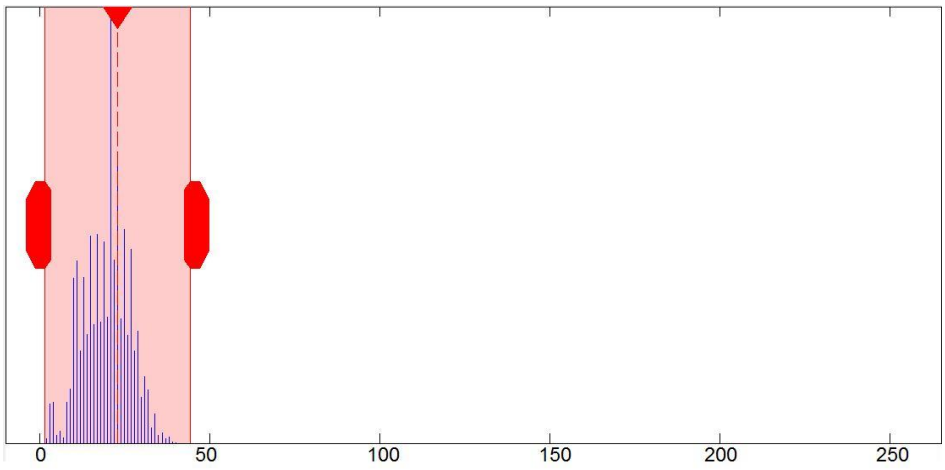

Figure 7.5.3. Histogram of SNS at initial state

– Engine test No1 (2 hours operation)

Figure 7.5.4. SNS (left) and dummy SNS (right) after two hours of engine operation.

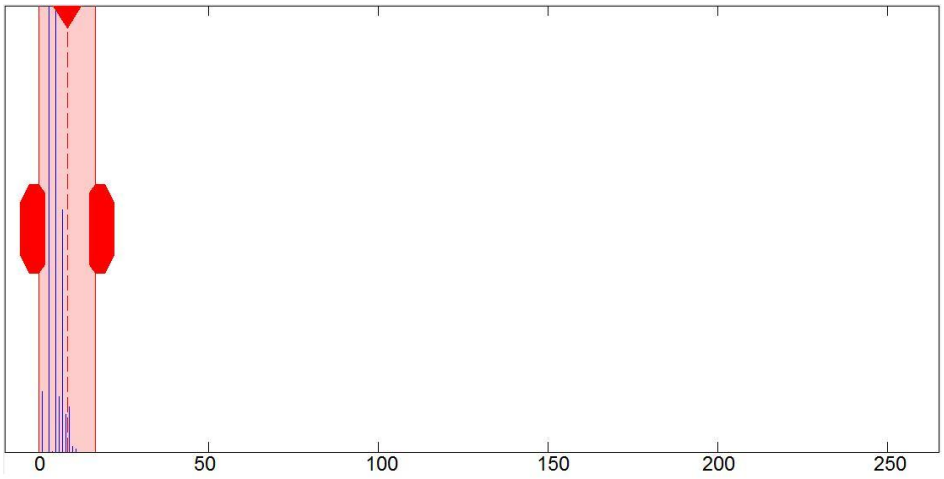

Figure 7.5.5. Histogram of dummy SNS after two hours of engine operation.

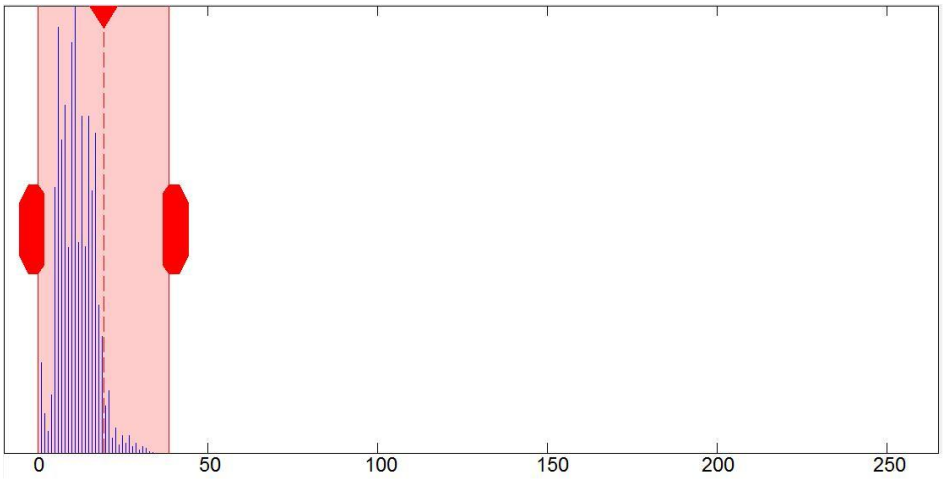

Figure 7.5.6. Histogram of SNS after two hours of engine operation.

– Engine test No2 (4 hours operation)

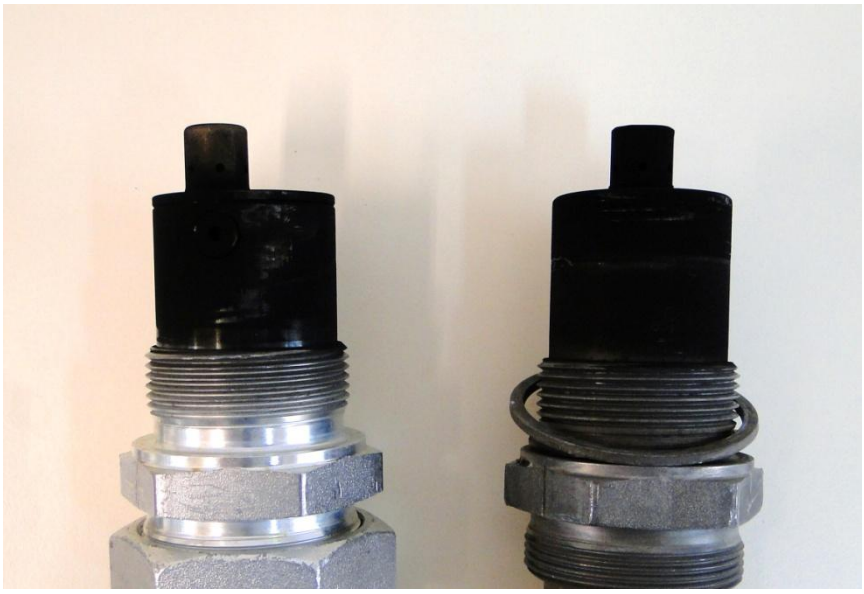

Figure 7.5.7. SNS (left) and dummy SNS (right) after four hours of engine operation.

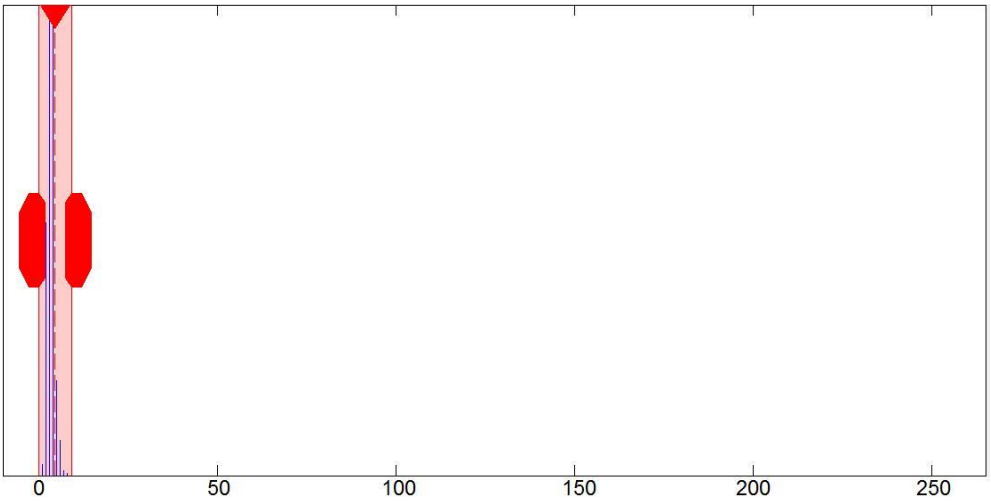

Figure 7.5.8. Histogram of dummy SNS after four hours of engine operation.

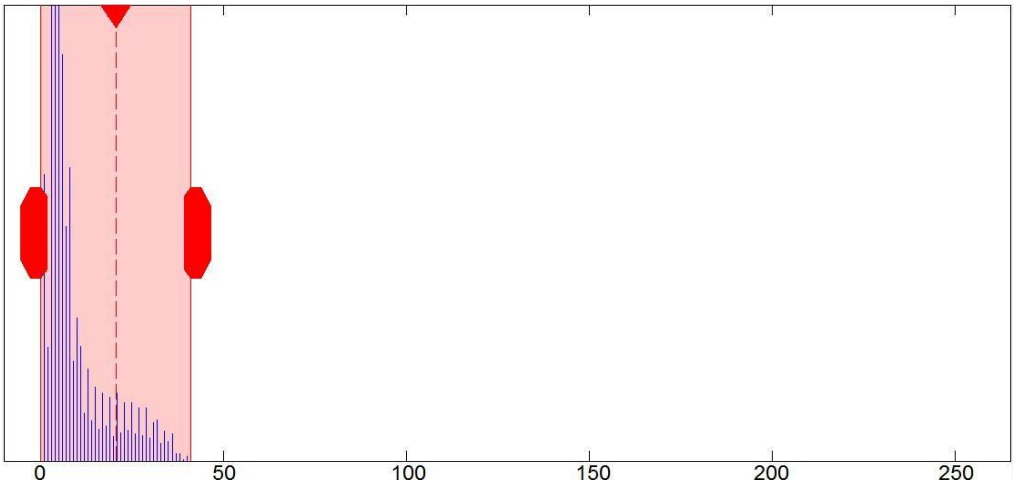

Figure 7.5.9. Histogram of SNS after four hours of engine operation.

– Engine test No3 (6 hours operation)

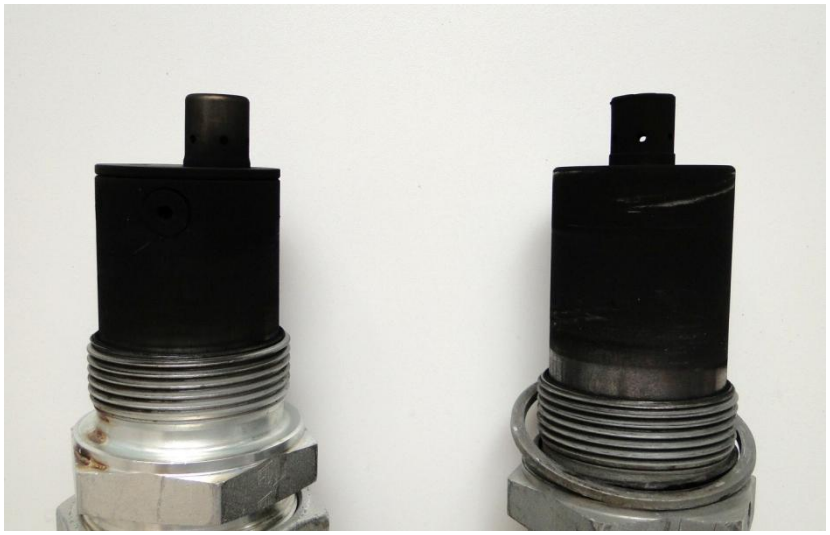

Figure 7.5.10. SNS (left) and dummy SNS (right) after six hours of engine operation.

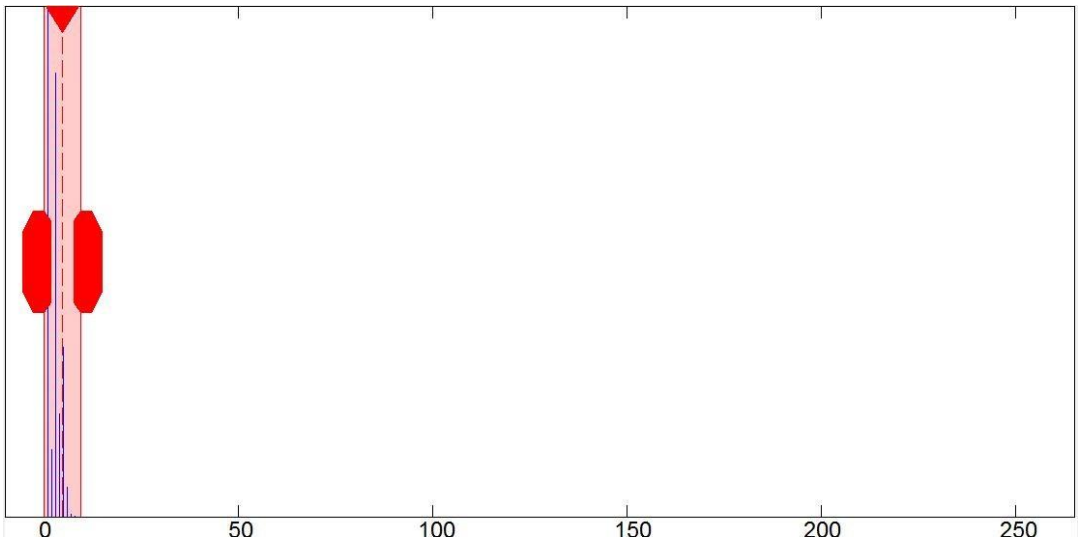

Figure 7.5.11. Histogram of dummy SNS after six hours of engine operation.

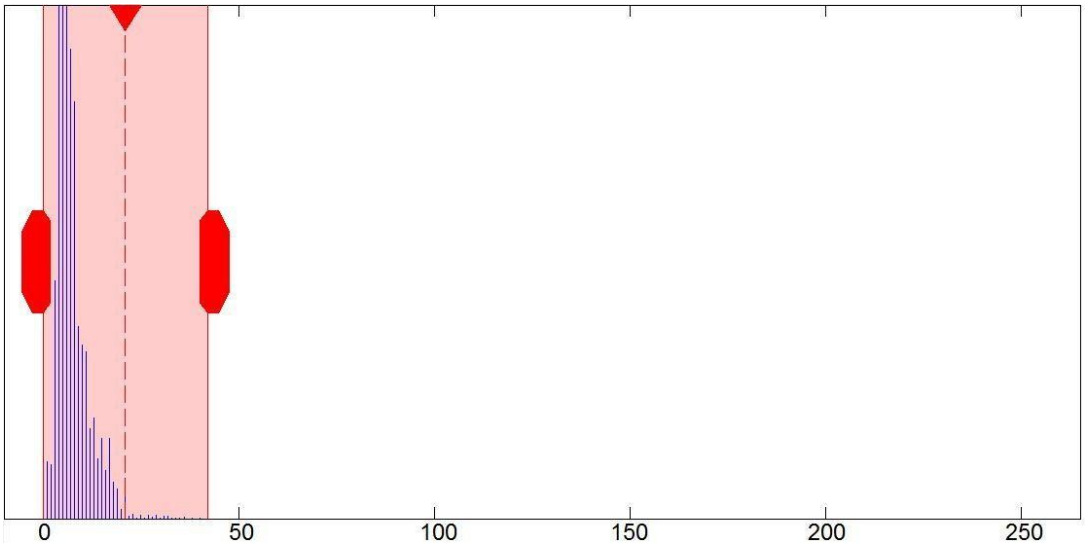

Figure 7.5.12. Histogram of SNS after six hours of engine operation.

– Engine test No4 (8 hours operation)

Figure 7.5.13. SNS (left) and dummy SNS (right) after eight hours of engine operation.

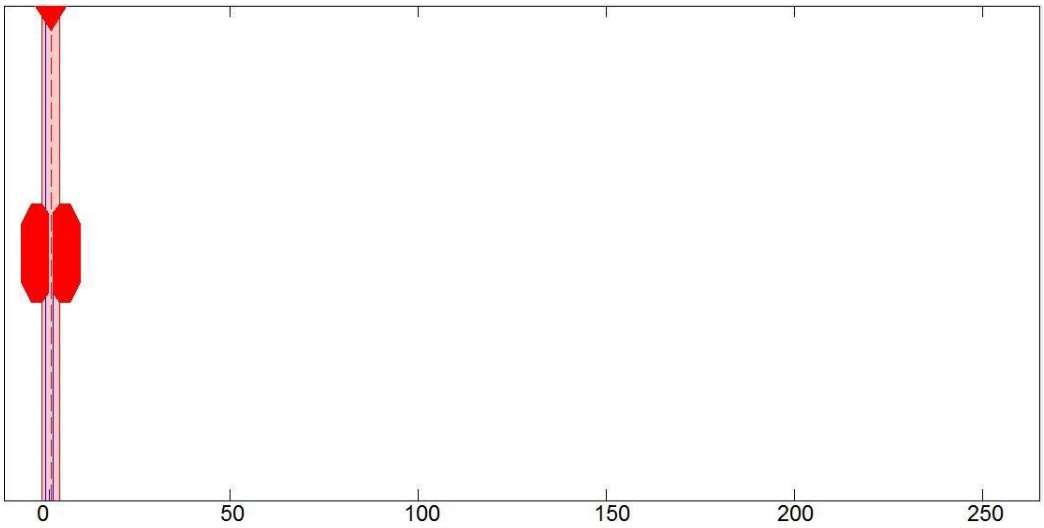

Figure 7.5.14. Histogram of dummy SNS after eight hours of engine operation.

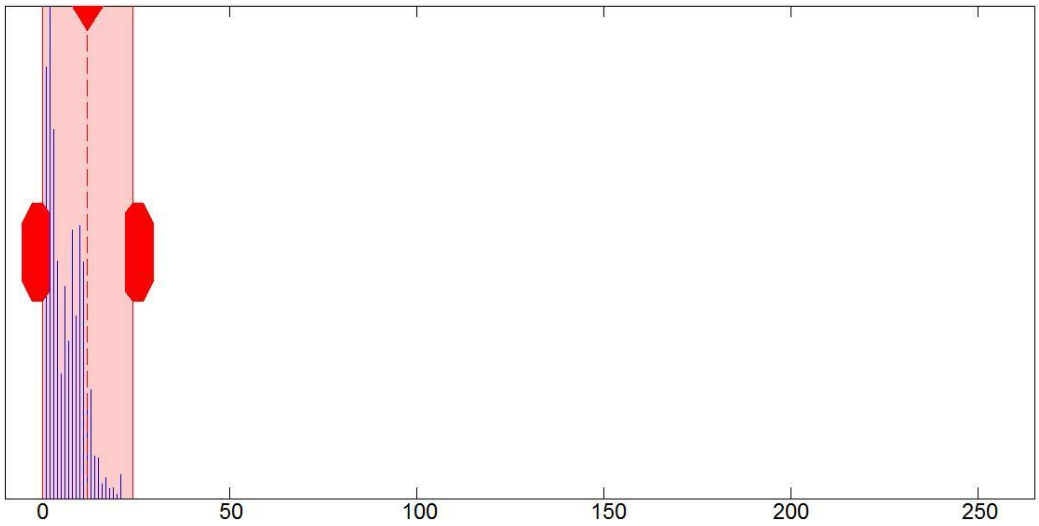

Figure 7.5.15. Histogram of SNS after eight hours of engine operation.

– Engine test No5 (10 hours operation)

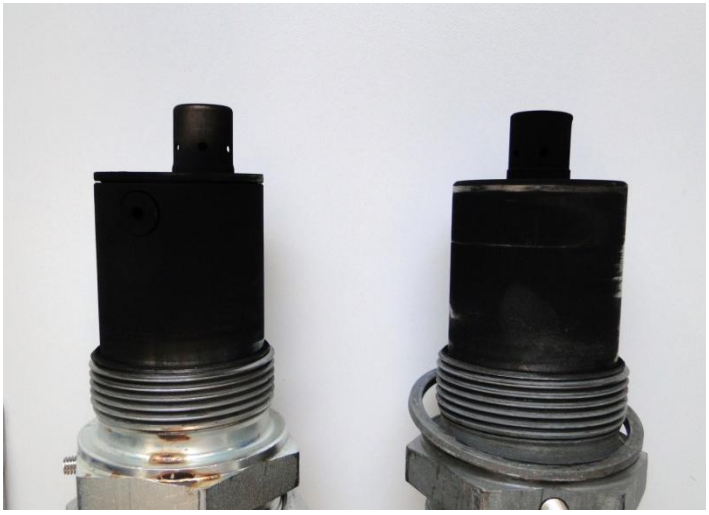

Figure 7.5.16. SNS (left) and dummy SNS (right) after ten hours of engine operation.

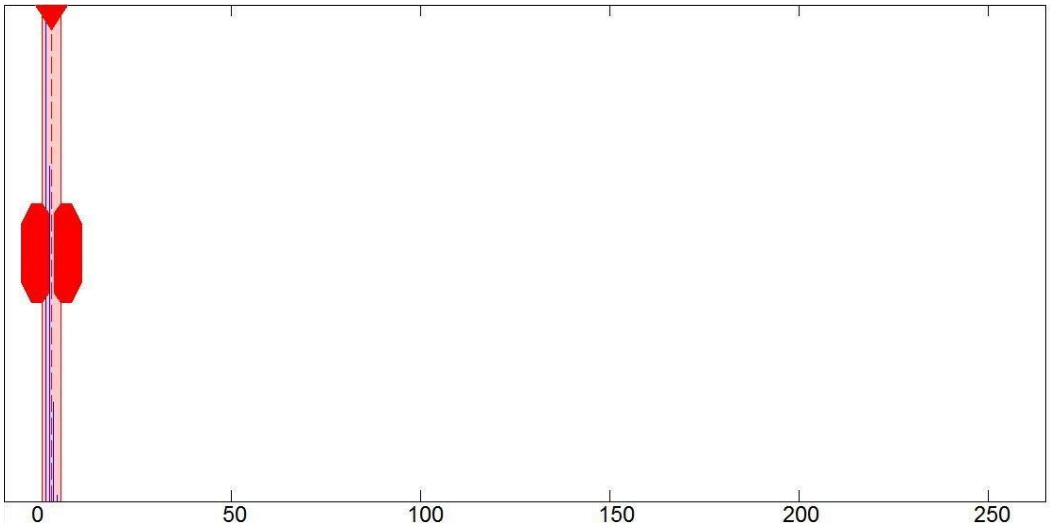

Figure 7.5.17. Histogram of dummy SNS after ten hours of engine operation.

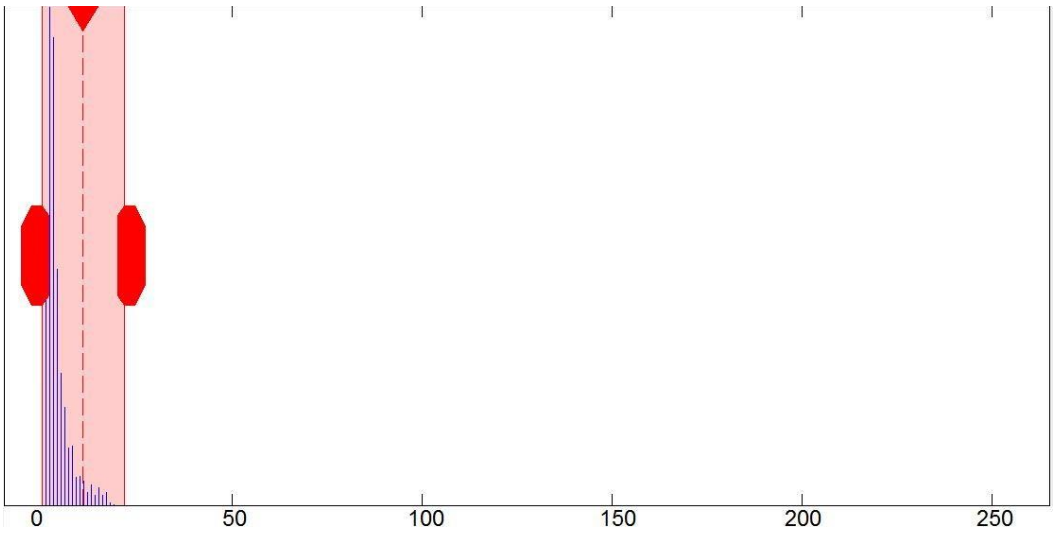

Figure 7.5.18. Histogram of SNS after ten hours of engine operation.

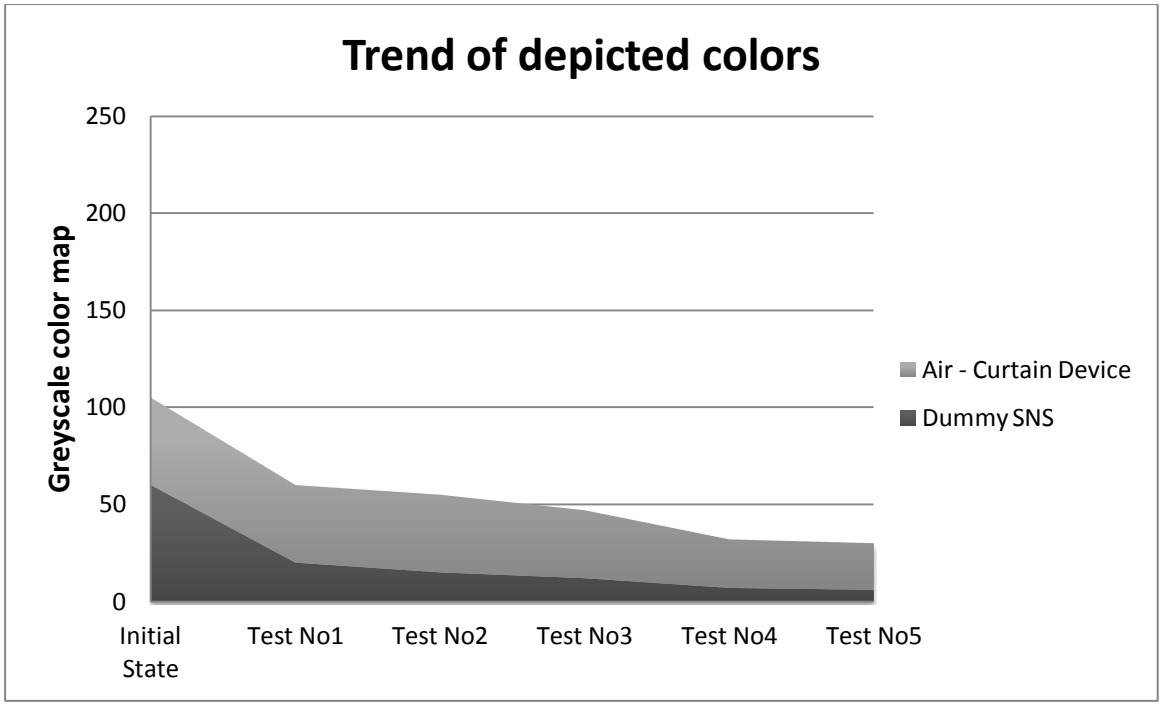

Figure 7.5.19. Trend of depicted colors for dummy SNS and SNS with the air curtain arrangement

7.6 NO_X measurements by SNS with the air - curtain switched on

In order to investigate the impact of air curtain device's operation on the SNS output, an additional engine test was executed. During this test, the engine was set to operate at 50% load and the air – curtain device was initially off operation. Having the engine operation stabilized, the air – curtain device was switched on. After three minutes the air – curtain device was turned off. This procedure was repeated twice again. The DAQ system was recording the SNS's output constantly. The step changes of air – curtain's operation took place at 600, 780, 960 and 1140 seconds.

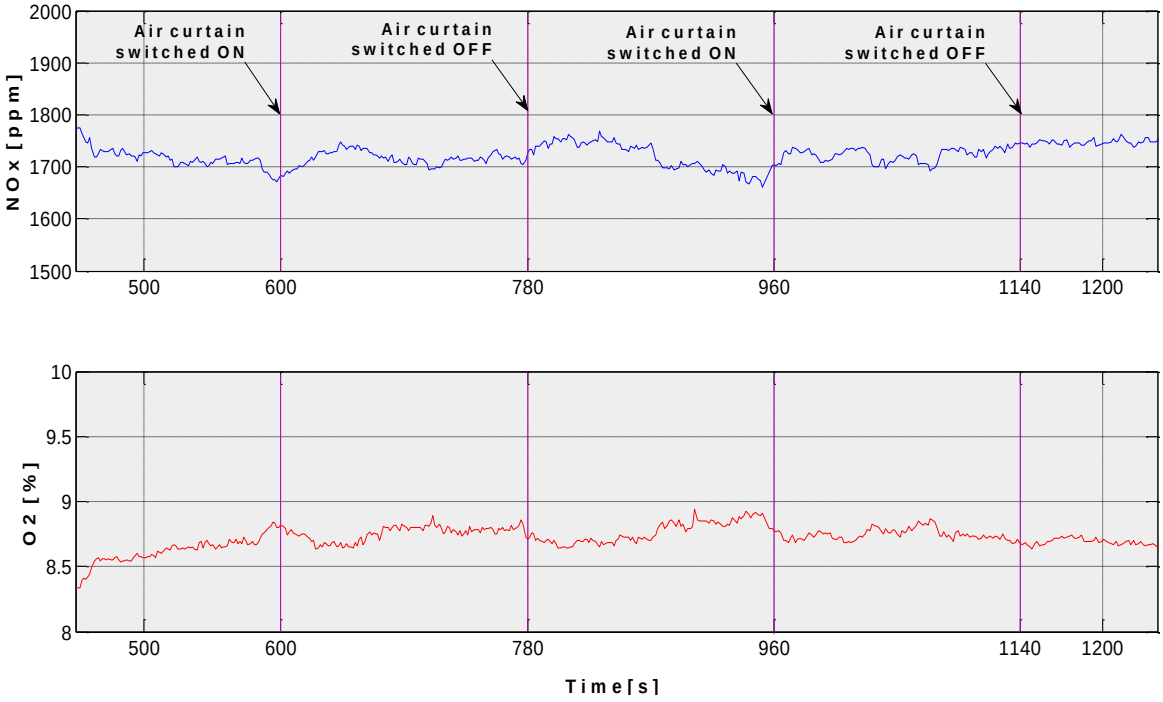

Figure 7.6.1. NO_X and O_2 measurements by SNS with step changes in air - curtain operation

As shown in Figure 7.6.1 the operation of the air curtain device did not affect the SNS output. This means that the air – curtain does not prevent the exhaust gases to enter the sensor. This fact raises concern about the effectiveness of the air curtain arrangement. Since the exhaust gas enters the SNS's cavities it seems rather possible that, also, soot particulates enter the cavities.

As described in §4.3, it is unfeasible to calculate an accurate mean jet trajectory using Equations 2.5.2 - 4. However, it is obvious that greater values of effective velocity ratio r (eq. 2.5.1) lead to better jet entrainment in the cross flow. Using the values of velocity and density calculated in §4.2 (Table 4.2.3) and Appendix.1, the effective velocity ratio r is equal to 20.7, which is a relatively great value. The jet trajectory for $r = 20.7$ is shown in Figure 7.6.2.

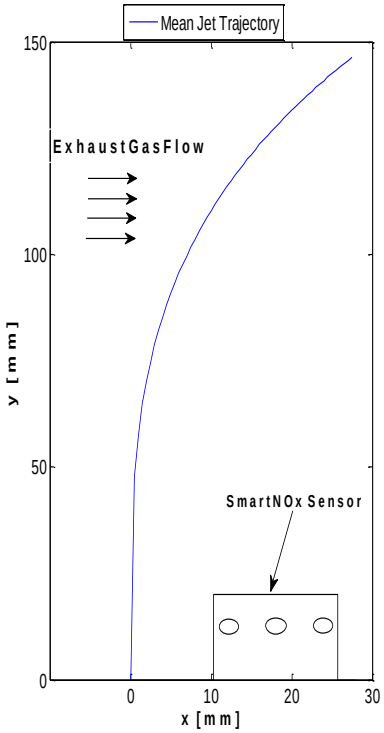

Figure 7.6.2. Mean jet trajectory for r=20.7

It is therefore concluded that the wake of exhaust gas, that consists of the exhaust gas and compressed air enters the SNS's cavities. The proportion of air in the mixture is expected to be low, taking into consideration that the mass flow ratio is

$$\dot{m}_{air}/\dot{m}_{ex} = \dot{m}_{air}/(\dot{m}_{int,air} + \dot{m}_{fuel}) = \frac{0.0167\ kg/s}{0.2645\ kg/s} = 0.06 = 6\%$$

(Appendix 1, Tables 4.2.2-3)

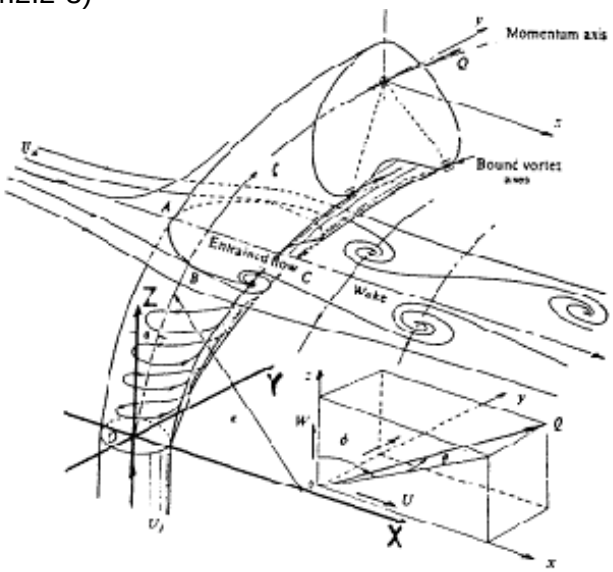

Figure 7.6.3. Flow field description of a round jet in a cross flow [9]

7.7 Conclusions

The activities described in this chapter involved a thorough examination of the effectiveness of the final air curtain arrangement. Engine tests were conducted, in which the outputs of SNS and reference analyzers specified by IMO were compared. The results of this comparison did not reveal any deterioration on the SNS's performance. However, this cannot be attributed to the air curtain device's operation because of the limited duration of this series of tests (10 hours). The deviation between the outputs of SNS and CLD700 RE, which appeared from the first test is attributed to the fact that the SNS was already used in the past for a considerably long period of engine operation (83 hours)[6]. Moreover, it must be mentioned that during the tests the SNS and the analyzer's sampling probe was in different sampling locations along the exhaust duct. However, the SNS showed better response than the CLD analyzer due to the fact that it measures emissions directly in the exhaust duct. Apart from the outputs' comparison, the SNS and the dummy SNS which was also installed, were photographed after each test. The images were processed according the technique described in Chapter 5. The exported histograms revealed that the rate of soot deposition on the SNS surface was significantly lower than that of the unprotected dummy SNS. The final engine test revealed that the flow of compressed air, during operation of the air curtain device, does not affect the SNS's output. This means that exhaust gases do enter the sensor's cavities when the device is switched on. This fact raises concerns about the device's ability to protect the SNS's inner surfaces from soot particles. However, as already mentioned, the rate of soot loading on the SNS's surface is significantly lower and the holes of the SNS's tip remained unblocked. Therefore the results of the air curtain's operation are considered to be successful.

8. CONCLUSIONS – RECOMMENDATIONS

The activities described in this thesis are a part of a general effort to create a novel control system capable of operating the engine at optimal conditions of which the NO_X concentration is a parameter. The analyzers for NO_X measurements specified by the IMO are expensive, delicate and difficult to operate. Those characteristics make CLD analyzers difficult to be used regularly for on-board measurements. On the contrary, the SNS is compact, relatively cheap and significantly easier to operate. On the top of that, it is proved that it has good response at transient engine load and its output at constant load approaches that of CLD analyzer. However, soot deposition may affect SNS's performance and life span by blocking the holes of its tip [6]. The concept of an air curtain arrangement that would protect the SNS from soot loading was thoroughly investigated.

At first, two trial arrangements were tested. The image processing results revealed that the trial arrangement with a nozzle parallel to the sensor offered better overall protection, while the arrangement with an inclined nozzle deterred soot deposition only in a part of dummy SNS's surface. The design of the first arrangement was modified so that the actual SNS could be installed in.

Then, a series of engine tests was conducted during which the output of the SNS and CLD700 RE were compared. The comparison process involved measurements of NO_X emissions during transient and steady state condition. After each recording of measured concentrations the air curtain device was switched on to protect the sensor until the next reading. The results revealed that the SNS showed better response to load changes, although during steady state engine operation the measured concentrations were by almost 10% higher than those of CLD700 RE. This significant deviation was not observed in past engine tests and, therefore, may be attributed to sensor ageing effects. With regards to image processing results, the rate of soot deposition on SNS's surface was lower than on the surface of the unprotected dummy SNS, as expected. It must be mentioned that during the transition from idle to 50% load, when soot generation rates are expected to be intense, the air curtain device was switched off.

However, the results of the last engine test, during which the SNS operated with the air curtain device switched on, revealed that the exhaust gas enters the sensor's cavities despite the operation of the device. Since only one type of test was conducted, the impact of air curtain's flow on the SNS's output needs further investigation.

Finally, it must be mentioned, that due to limited time period of running engine tests for fuel cost reasons, the impact of long term soot deposition on SNS's performance was not confirmed. Also, for the same reason, it was unfeasible to detect the impact of air curtain flow on the ageing effects on the SNS's performance.

Consequently, it is essential to continue the investigation to the directions proposed bellow.

- The air curtain arrangement could be tested with a brand new SNS installed for a longer period, while another brand new SNS with no protection is, also, being installed in the test engine's exhaust duct. Through the comparison of the SNS's output, it would be easier to detect any differences in the ageing effects of both sensors.

- All tests that included the SNS were executed in engines that operate on diesel oil. It is, therefore, proposed to conduct tests with engines that operate in HFO, where the effectiveness of the air curtain can be evaluated in more severe conditions regarding soot loading.

- Apart from a single-nozzle arrangement, designs of less compact arrangements with more than one nozzle can be investigated. The nozzles can be parallel or inclined and distributed around the SNS in a way that they offer total protection from soot loading. It must be mentioned that in this case the needs for compressed air would be even higher (§4.5) and the implementation of such a design on on-board measurements will need significant compressed air amounts. However, these amounts are small compared to the compressed air needs of a ship.

9. REFERENCES

[1] AirClim, Seas At Risk, Bellona Foundation, North Sea -Foundation, Transport & Environment, European Environmental Bureau, November 2011 *Air Pollution From Ships* [Online]. Available from http:// http://www.airclim.org/air-pollution-ships [accessed 7th July 2014]

[2] Goettler, H and Lemire, B., (2008) *Specification Smart NO_X Sensor "Uninox24V"*, Continental Corporation

[3] Romer, E. (2001) *Amperometric NO_X-sensors for Combustion Exhaust Gas Control*, PhD thesis, University of Twente, Netherlands.

[4] Eco Physics (August 1998) *CLD 700RE ht, Users Manual*

[5] Cambustion (n.d.) *CLD Principles* [Online]. Available from: http://www.cambustion.com/products/cld500/cld-principles [Accessed 7th July 2014]

[6] M. Ioannou, G. Papalambrou, N.P. Kyrtatos, H. Dumele , M. Diessner (September 2013) *Evaluation of Emission Sensors for Four-Stroke Marine Diesel Engines,* Journal of Marine Engineering and Technology, Volume 12 No 3

[7] M. Ioannou (2012) *Emission component measurement technologies,* (LRET – COE Task 1.1.1), p. 28

[8] Suman Muppidi, Krishnan Mahesh (2004) *Study of jets in cross flow using direct numerical simulations*, Aerospace Engineering and Mechanics, University of Minnesota, USA

[9] Kavsaoglu, M. S., Akmandor I., Ciray, S., Fujii, K., (April 1993), *Navier-Stokes Simulation of Two and Three Dimensional Jets in Cross Flow, Effects of Grid and Boundary Conditions*, AGARD Meeting on 'Computational and Experimental Assessment of Jets in Cross Flow', Winchester, UK.

[10] *NO_X Technical Code*, *Annex VI of MARPOL 73/78 Regulation for the Prevention of Air Pollution from Ships and NO_X Technical Code*, International Marine Organization (IMO), ISBN 92-801-6089-3

[11] ISO 5167 – 2 (2003) *Measurement of fluid flow by means of pressure differential devices inserted in circular-cross section conduits running full – Part 2: Orifice plates*

[12] University of Oslo, October 2011, *Flow in pipes,* Available from: www.uio.no/studier/emner/matnat/math/MEK4450/h11/undervisningsmateriale [Accessed 7th July 2014]

[13] *ZS25 Vane Wheel Sensor Handbook*, Höntzsch® Flow Measuring Technology

[14] *Compressed Air Receivers* [Online]
Available from http://www.engineeringtoolbox.com/compressed-air-receivers-d_846.html [Accessed 16 July 2014]

[15] ISO 8178–1 (2006), *Reciprocating internal combustion engines – Exhaust gas emission measurement – Part 1: Test bed measurement of gaseous and particulate exhaust emissions*.

APPENDICES

APPENDIX 1. COMPRESSED AIR MASS FLOW CALCULATION

The temperature of compressed air is taken equal to ambient temperature:

$T_{air} = 25℃ = 298.15\ K$

The total pressure of compressed air was regulated to 4 bar: $P_{t,air} = 4 \cdot 10^5\ N/m^2$

Since the exhaust gas pressure upstream of the turbocharger is measured 129.7 kPa (Table 4.2.1), the exhaust gas pressure downstream of the turbine outlet is taken as slightly greater than the atmospheric pressure. $P_{ex} \cong 1.1 \cdot 10^5\ N/m^2$

The absolute pressure ratio is equal to:

$$P_{ex}/P_{t,air} = 1.1 \cdot 10^5/4 \cdot 10^5 = 0.275\ < 0.528$$

The absolute pressure ratio is not greater than 0.528 and therefore the air flow can be characterized as choked. The air velocity is equal to the sonic velocity that corresponds to T_{air} :

$$w = \sqrt{\gamma \cdot R \cdot T_{air}} = \sqrt{1.4 \cdot 287.04\ {m^2}/{s^2 K} \cdot 298.15K} = 346.14 m/s$$

The total temperature of compressed air is calculated as shown below.

$$T_{t,air} = T_{air} + \frac{w^2}{2C_p} = 298.15K + \frac{(346.14 m/s)^2}{2 \cdot 1004{,}64\ {m^2}/{s^2 \cdot K}} = 357.78K$$

The compressed air mass flow $\dot{m}_{air}$ is given according to the following equation:

$$\frac{\dot{m}_{air}}{A \cdot P_{t,air}} \cdot \sqrt{\frac{R \cdot T_{t,air}}{\gamma}} = M \cdot \left[1 + (\gamma - 1) \cdot \frac{M^2}{2}\right]^{-\frac{1\gamma+1}{2\gamma-1}}$$

Where, M is the mach number and A is the cross sectional area of the orifice.

Since the flow is choked, the mach number is $M = 1$.

The cross sectional area of a round orifice with a diameter of 5mm is equal to:

$A = \pi \cdot \left(\frac{d}{2}\right)^2 = \pi \cdot \left(\frac{0{,}005m}{2}\right)^2 = 1.96 \cdot 10^{-5}\ m^2$

Finally, the air mass flow is calculated from the above equation: $\dot{m}_{air} = 16.7\ {gr}/{s}$.

Also, $\dot{V}_{air} = A \cdot w = 1.96 \cdot 10^{-5} m^2 \cdot 346.14 \frac{m}{s} = 6.8 \cdot 10^{-3}\ m^3/s = 24.4\ {m^3}/{h}$

The air density for total pressure of 4 bar is given below:

$$\dot{m}_{air} = \rho_{air} \cdot w \cdot A\ \Rightarrow\ \rho_{air} = \frac{0.0167 \frac{kg}{s}}{346.14 \frac{m}{s} \cdot\ 1.96 \cdot 10^{-5}\ m^2} = 2.462\ kg/m^3$$

For air pressure regulated to 2 bar the calculations give the following results.

$w_2 = 156\,{}^{m}/_{s}$

$\dot{m}_{air,2} = 6.9\,{}^{gr}/_{s}$

$\dot{V}_{air,2} = 11.01\,{}^{m^3}/_{h}$

APPENDIX 2. MANUFACTURING DRAWINGS

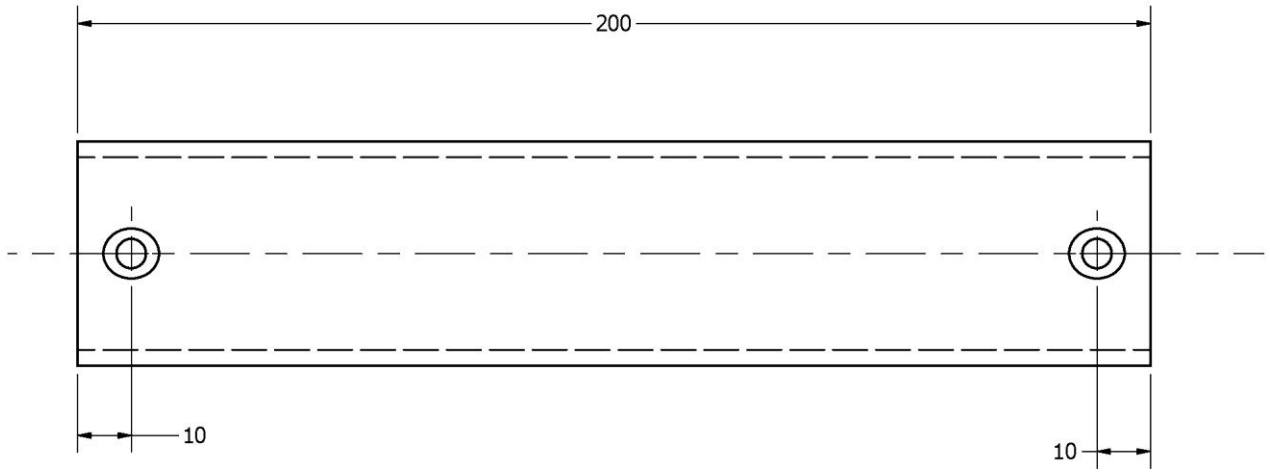

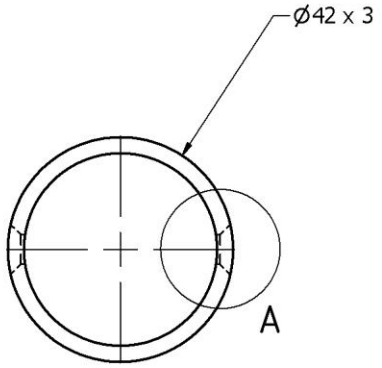

A (4 : 1)

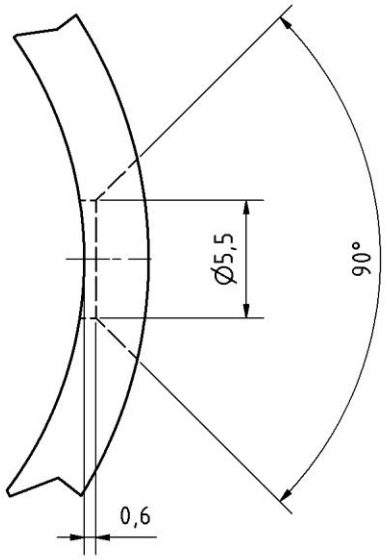

DRAWN Rizos Lampros	1/7/2013	NTUA - LME
CHECKED		TITLE: Probe of trial air - curtain devices
QA		
MFG		
APPROVED		
		SIZE A3 / Material St 37 - 2 / REV 1
		SCALE / SHEET 1 OF 1

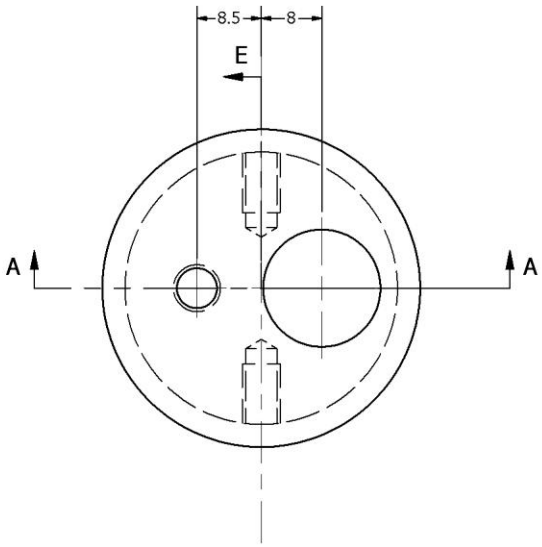

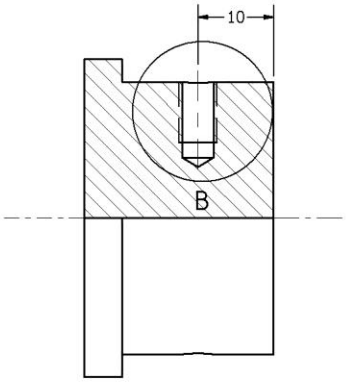

SECTION E-E
SCALE 2 : 1

B (4 : 1)

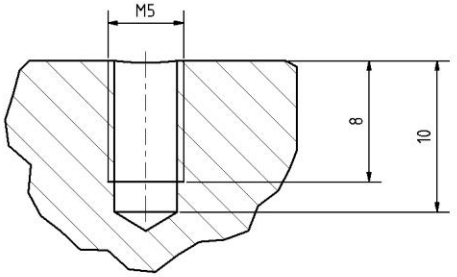

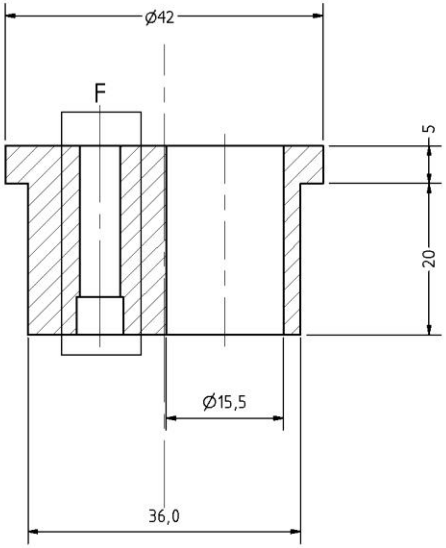

SECTION A-A
SCALE 2 : 1

F (4 : 1)

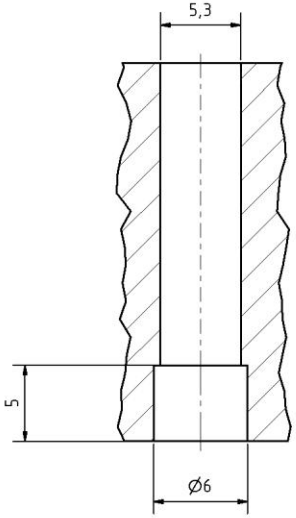

DRAWN Rizos Lampros	1/7/2013	NTUA - LME	
CHECKED		TITLE	
QA		Dummy SmartNOx Sensor Matrix with parallel nozzle	
MFG			
APPROVED		SIZE A2	Material DIN X5CrNi18.9
		SCALE	SHEET 1 OF 1

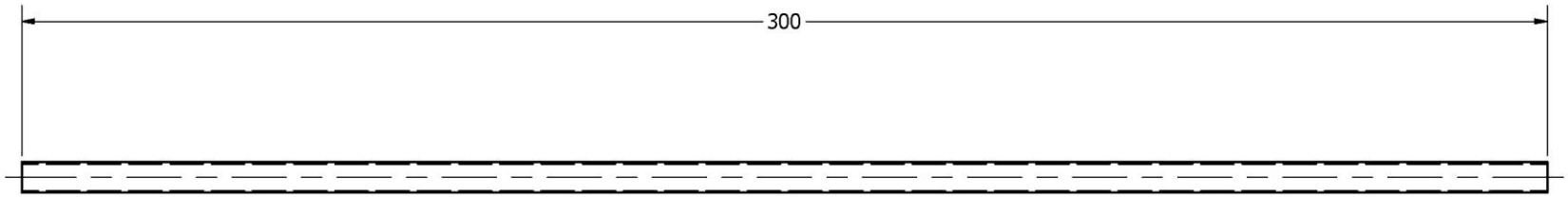

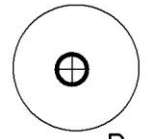

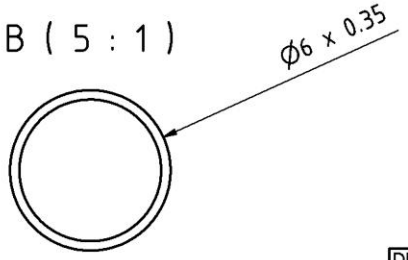

DRAWN Rizos Lampros	29/6/2013	NTUA - LME
CHECKED		TITLE: Compressed air pipe
QA		
MFG		
APPROVED		
		SIZE: A3 · Material: DIN X5CrNi18.9 · REV: 2
		SCALE · SHEET 1 OF 1

SECTION B-B
SCALE 2 : 1

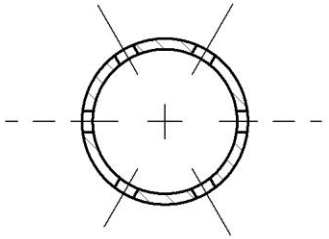

SECTION A-A
SCALE 2 : 1

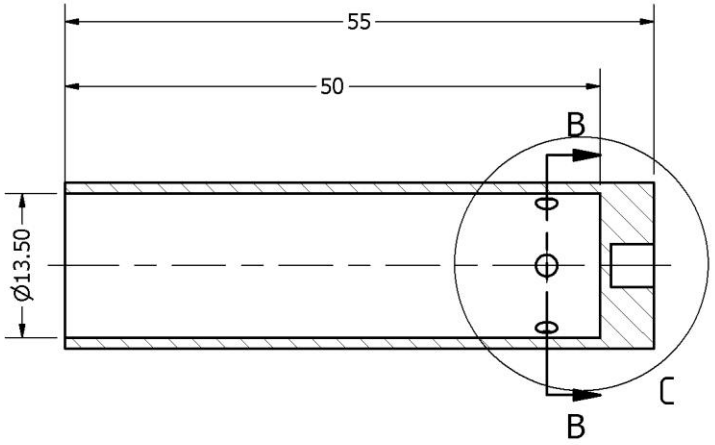

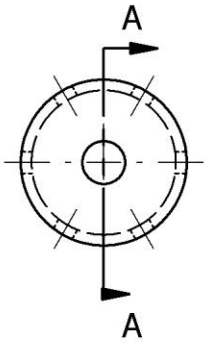

C (4 : 1)

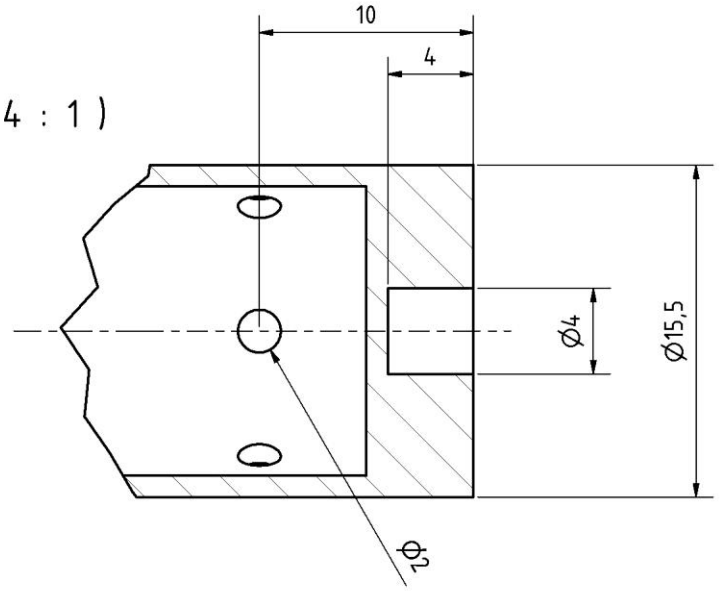

DRAWN Rizos Lampros	1/7/2013	NTUA - LME
CHECKED		TITLE: Dummy SmartNOx Sensor
QA		
MFG		
APPROVED		
SIZE A3	MATERIAL DIN X5CrNi18.9	REV 2
SCALE		SHEET 1 OF 1

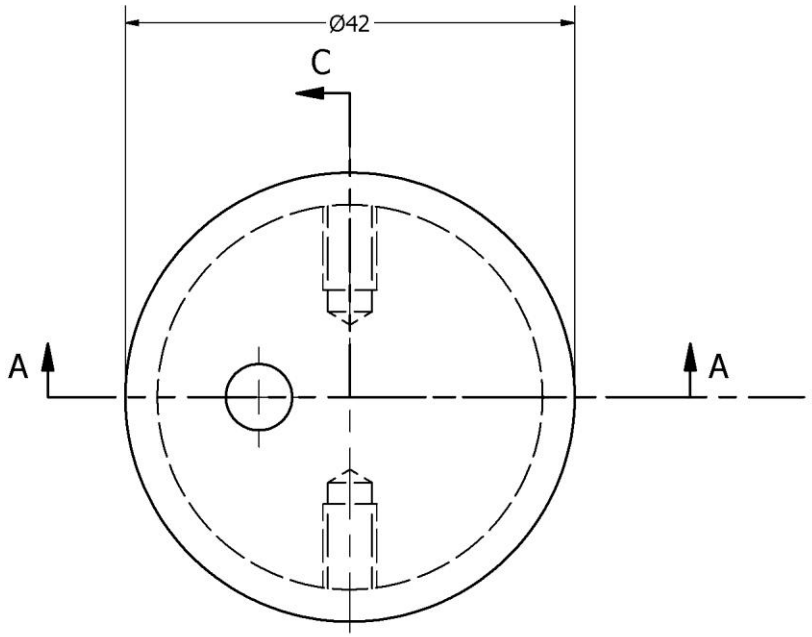

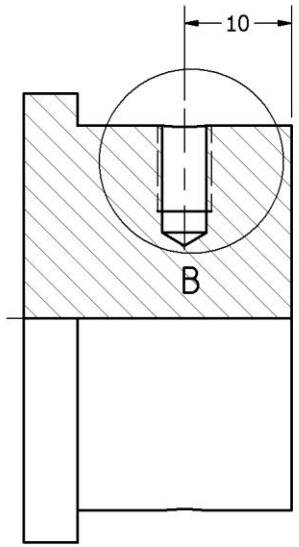

SECTION C-C
SCALE 2 : 1

B (4 : 1)

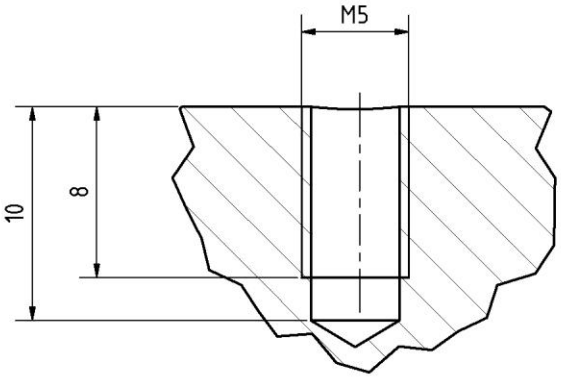

SECTION A-A
SCALE 2 : 1

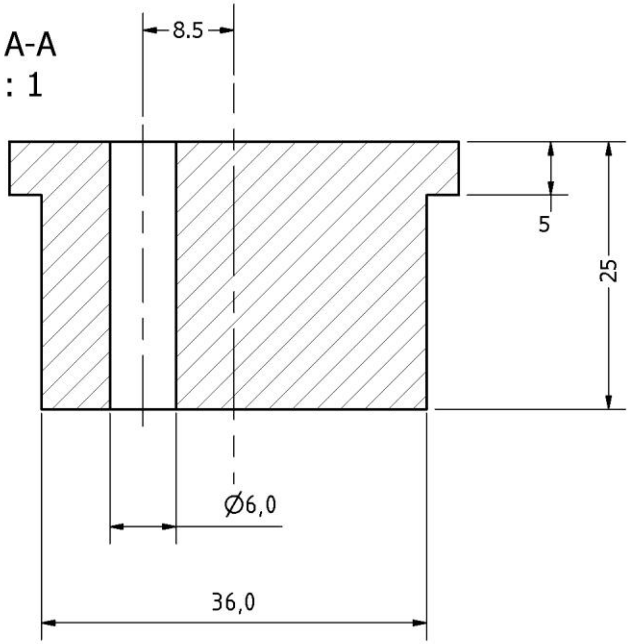

DRAWN Rizos Lampros	1/7/2013	NTUA - LME
CHECKED		TITLE: Air pipe support for trial air-curtain device with parallel nozzle
QA		
MFG		
APPROVED		
		SIZE A3 | Material St 37 - 2 | REV 1
		SCALE | SHEET 1 OF 1

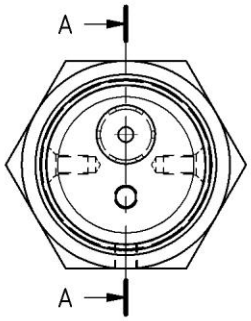

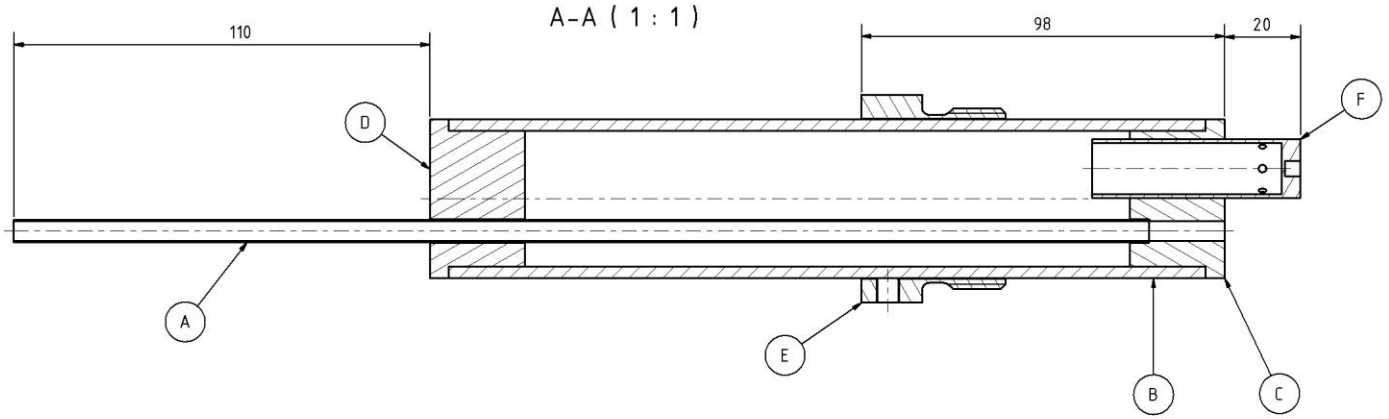

PARTS LIST			
ITEM	QTY	DESCRIPTION	MATERIAL
A	1	Air Pipe	DIN X5CrNi18.9
B	1	Probe	St. 37-2
C	1	Matrix of DUMMY SNS with air nozzle	DIN X5CrNi18.9
D	1	Air pipe support	St. 37-2
E	1	Fitting BSP 1 1/2'	St. 37-2
F	1	DUMMY SNS	DIN X5CrNi18.9

DRAWN Rizos Lampros	3/12/2013	NTUA - LME
CHECKED		TITLE: Assembly of DUMMY SNS with parallel air nozzle
QA		
MFG		
APPROVED		
		SIZE A2 / DWG NO
		SCALE / SHEET 1 OF 1

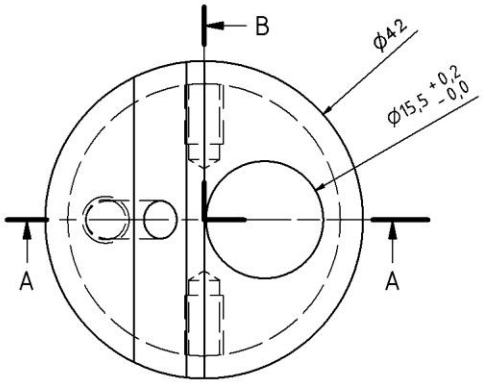

B-B (2 : 1)

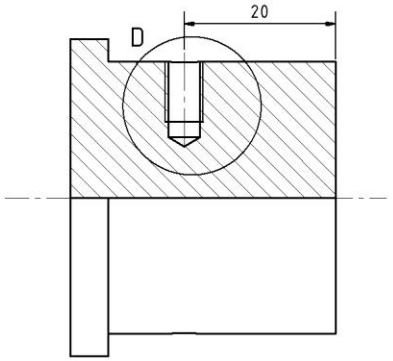

D (4 : 1)

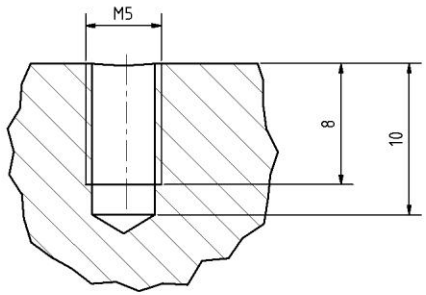

A-A (2 : 1)

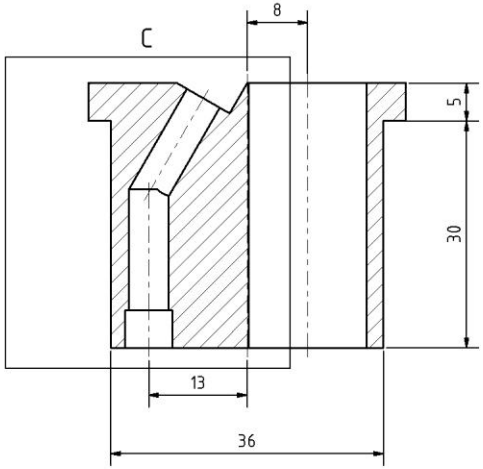

C (4 : 1)

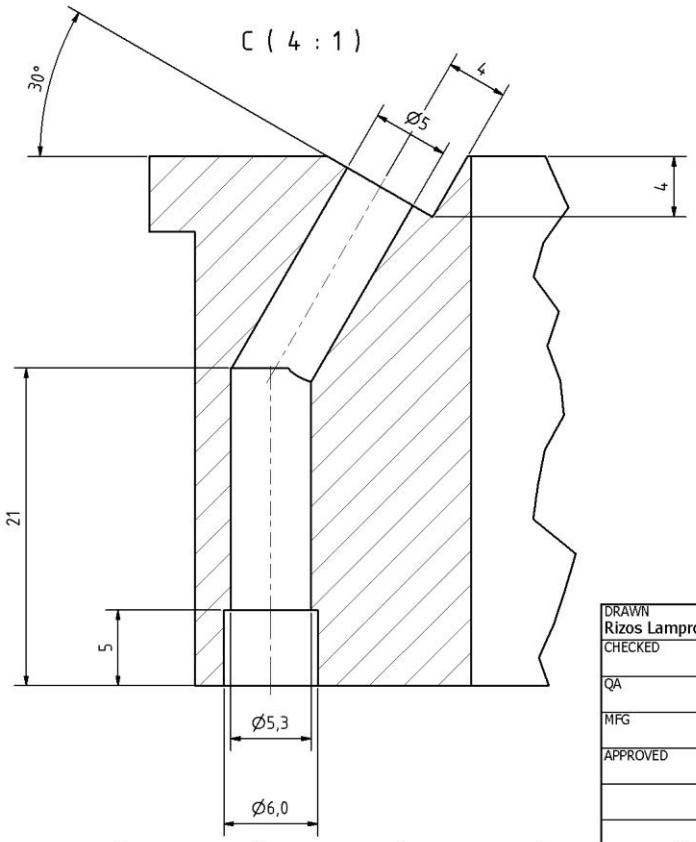

DRAWN Rizos Lampros	10/7/2013	NTUA - LME	
CHECKED		TITLE	
QA		Dummy SmartNOx Sensor Matrix with inclined nozzle	
MFG			
APPROVED			
		SIZE A2	Material DIN X5CrNi18.9 REV
		SCALE	SHEET 1 OF 1

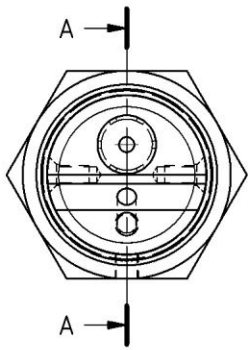

A-A (1 : 1)

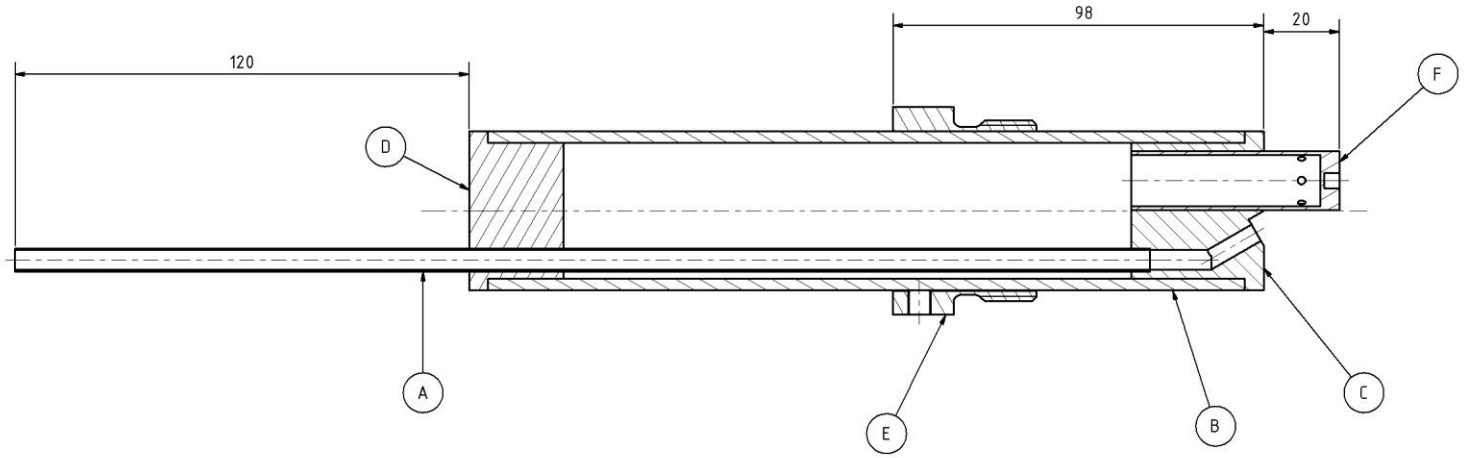

PARTS LIST			
ITEM	QTY	DESCRIPTION	MATERIAL
A	1	Air Pipe	DIN X5CrNi18.9
B	1	Probe	St. 37-2
C	1	Matrix of DUMMY SNS with inclined nozzle	DIN X5CrNi18.9
D	1	Air pipe support	St. 37-2
E	1	Fitting BSP 1 1/2'	St. 37-2
F	1	DUMMY SNS	DIN X5CrNi18.9

DRAWN Rizos Lampros	3/12/2013	NTUA-LME
CHECKED		TITLE: Assembly of DUMMY SNS with inclined nozzle (30 deg)
QA		
MFG		
APPROVED		
		SIZE A2 / DWG NO / REV
		SCALE / SHEET 1 OF 1

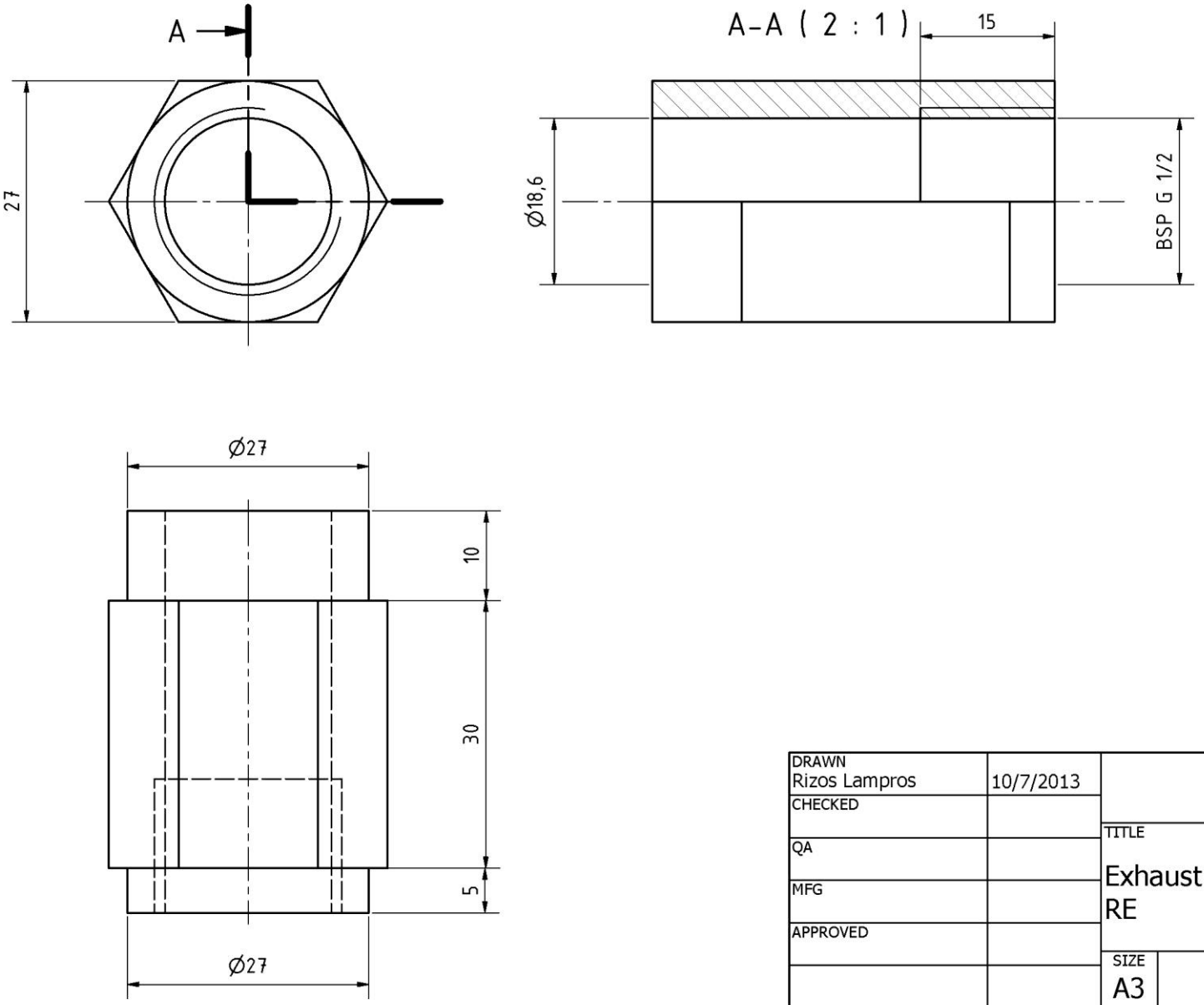

DRAWN Rizos Lampros	10/7/2013	NTUA - LME
CHECKED		TITLE: Exhaust duct socket for EcoPhysics CLD700 RE
QA		
MFG		
APPROVED		
		SIZE A3 | Material St. 37 - 2 | REV 1
		SCALE | SHEET 1 OF 1

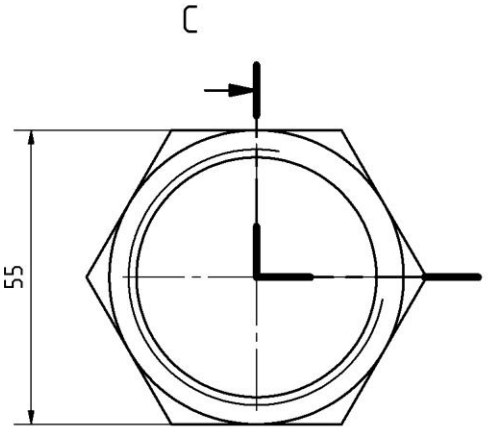

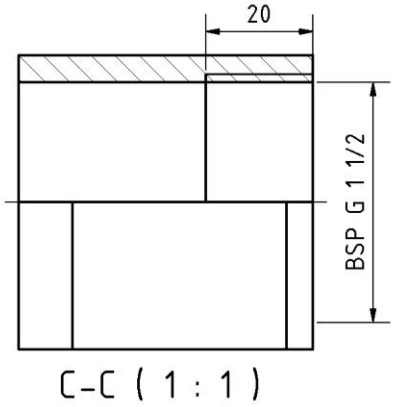

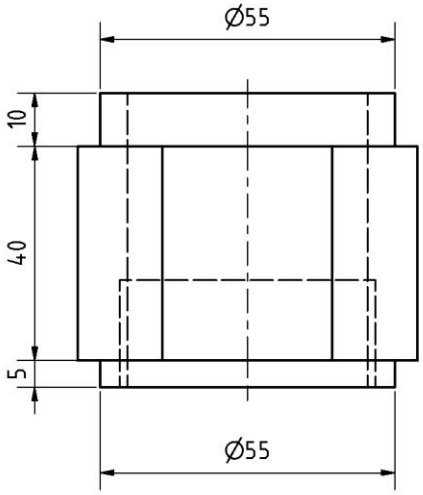

DRAWN Rizos Lampros	1/7/2013	NTUA - LME
CHECKED		TITLE: Exhauxt duct socket for SmartNOx Sensor/Air curtain devices
QA		
MFG		
APPROVED		
		SIZE A3 | Material St 37 - 2 | Rev. 2
		SCALE | SHEET 1 OF 1

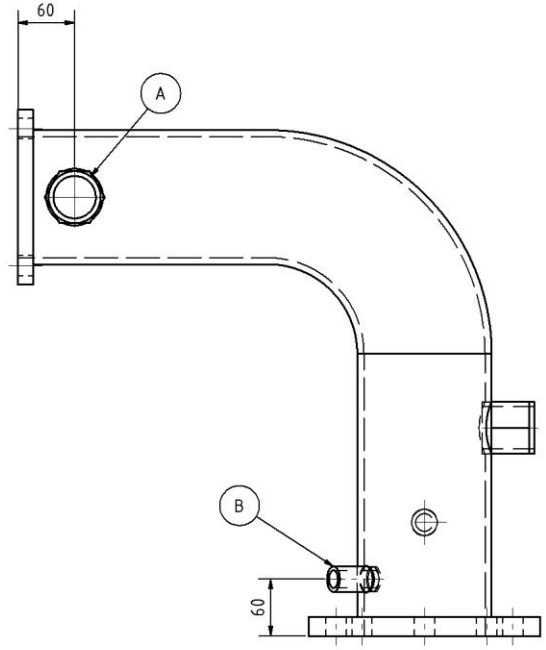

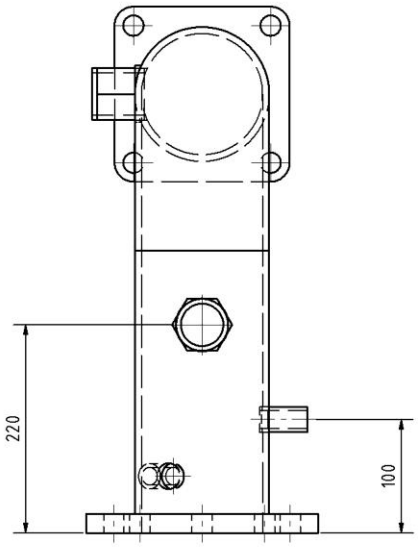

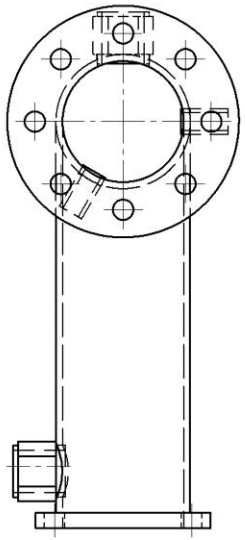

PARTS LIST		
ITEM	QTY	DESCRIPTION
A	2	SNS socket
B	1	EcoPhysics CLD700 socket

DRAWN Lampros Rizos	3/12/2013	NTUA - LME	
CHECKED			
QA		TITLE Modified Exhaust Gas Duct	
MFG			
APPROVED			
		SIZE A2	DWG NO / REV
		SCALE	SHEET 1 OF 1

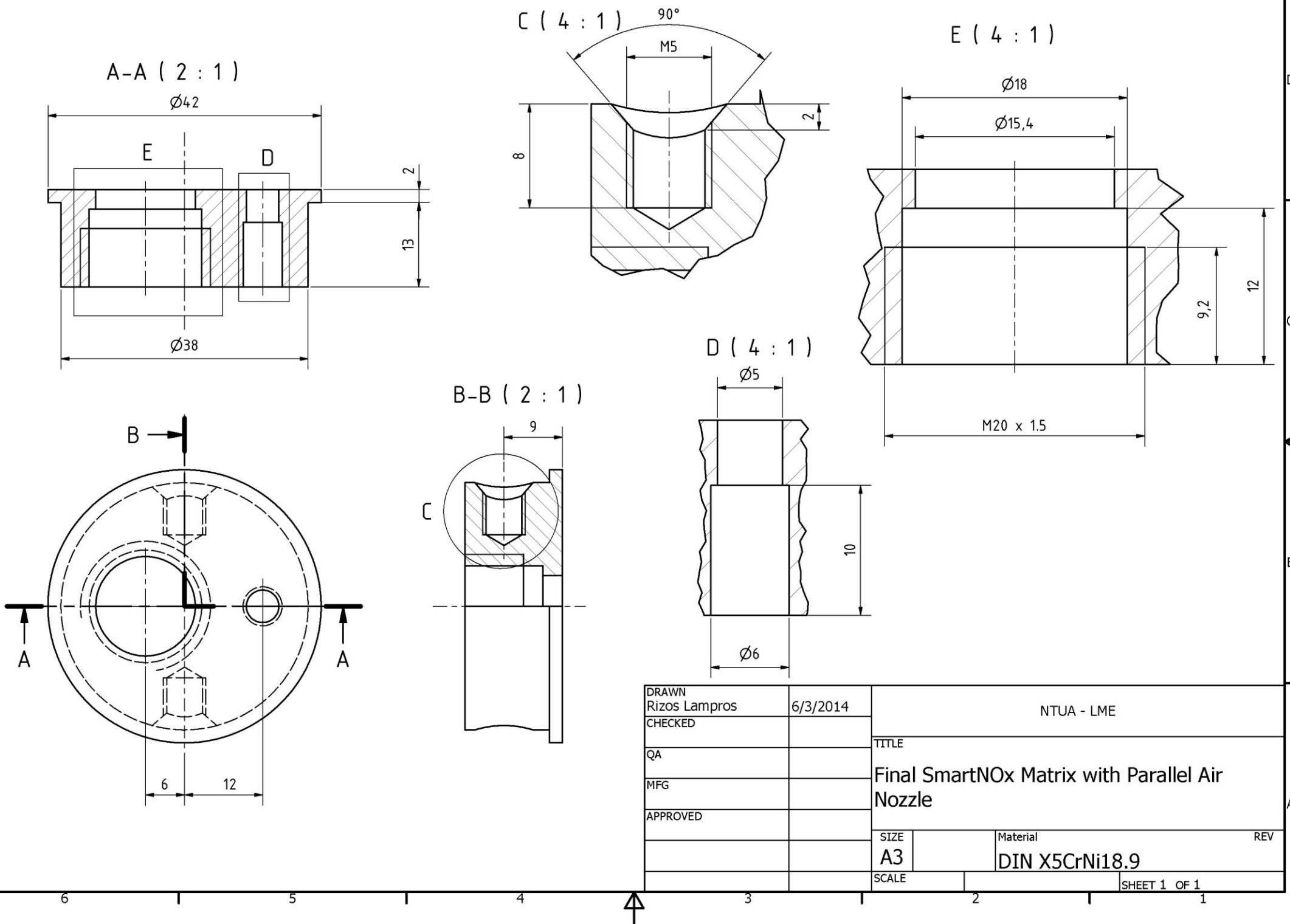
A-A (2 : 1)
Ø42
E
D
2
13
Ø38
C (4 : 1)
90°
M5
8
2
E (4 : 1)
Ø18
Ø15,4
9,2
12
M20 x 1.5
D (4 : 1)
Ø5
10
Ø6
B-B (2 : 1)
9
C
B
A
A
6
12
DRAWN
Rizos Lampros
6/3/2014
CHECKED
QA
MFG
APPROVED
NTUA - LME
TITLE
Final SmartNOx Matrix with Parallel Air Nozzle
SIZE
A3
Material
DIN X5CrNi18.9
REV
SCALE
SHEET 1 OF 1

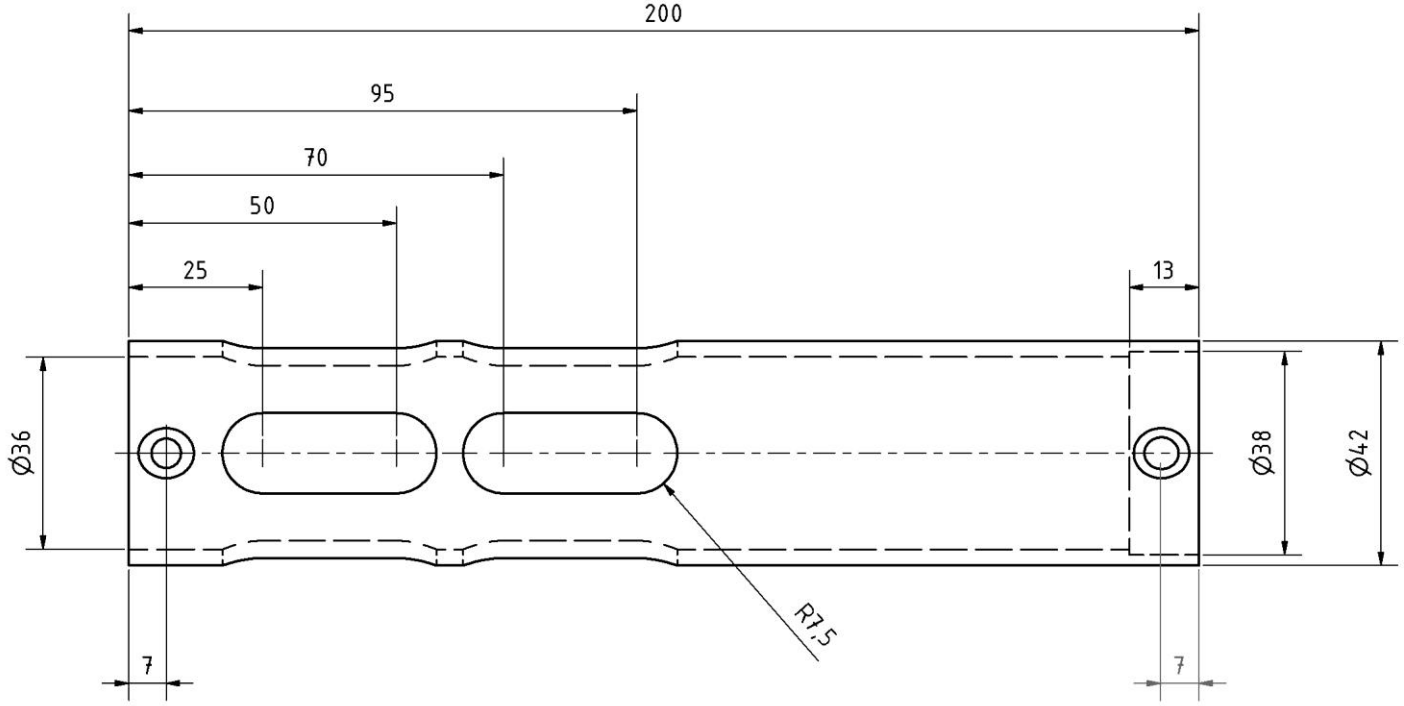

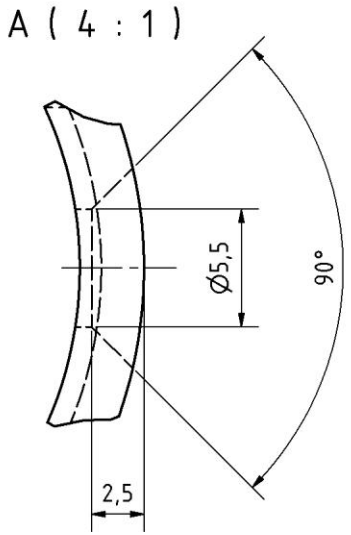

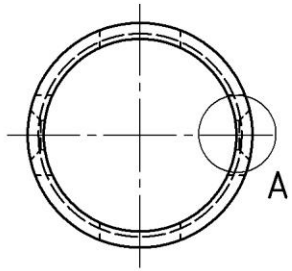

DRAWN Rizos Lampros	6/3/2014	NTUA - LME
CHECKED		TITLE: Probe of final air - curtain device
QA		
MFG		
APPROVED		
		SIZE A3 / Material St. 37 - 2 / REV 1
		SCALE / SHEET 1 OF 1

A-A (2 : 1)

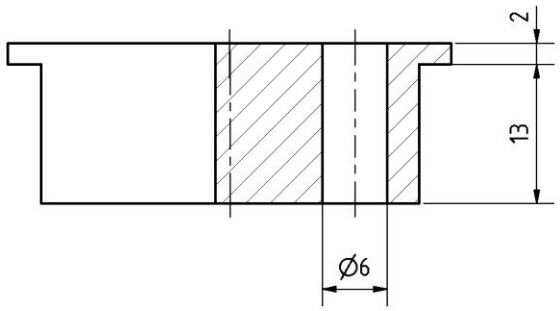

C (4 : 1)

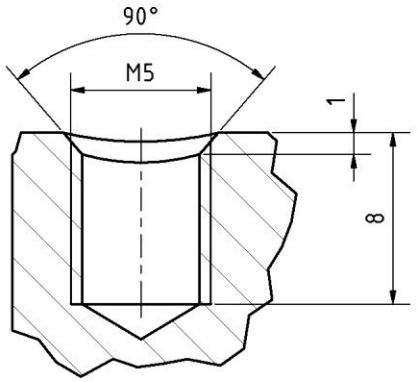

B-B (2 : 1)

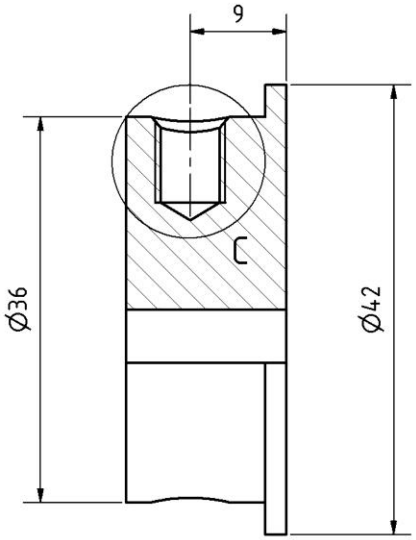

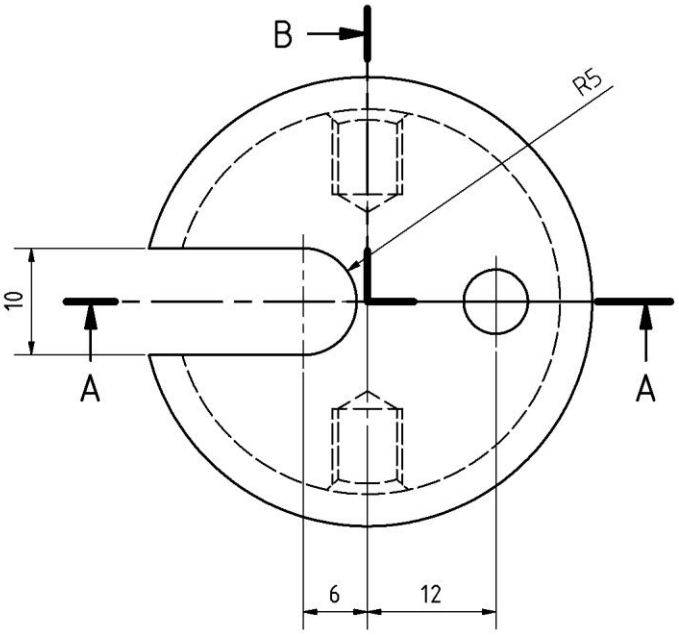

DRAWN Rizos Lampros	6/3/2014	NTUA - LME	
CHECKED		TITLE	
QA		Air pipe support of final air - curtain device	
MFG			
APPROVED			
		SIZE A3	Material St 37 - 2 / REV 1
		SCALE	SHEET 1 OF 1

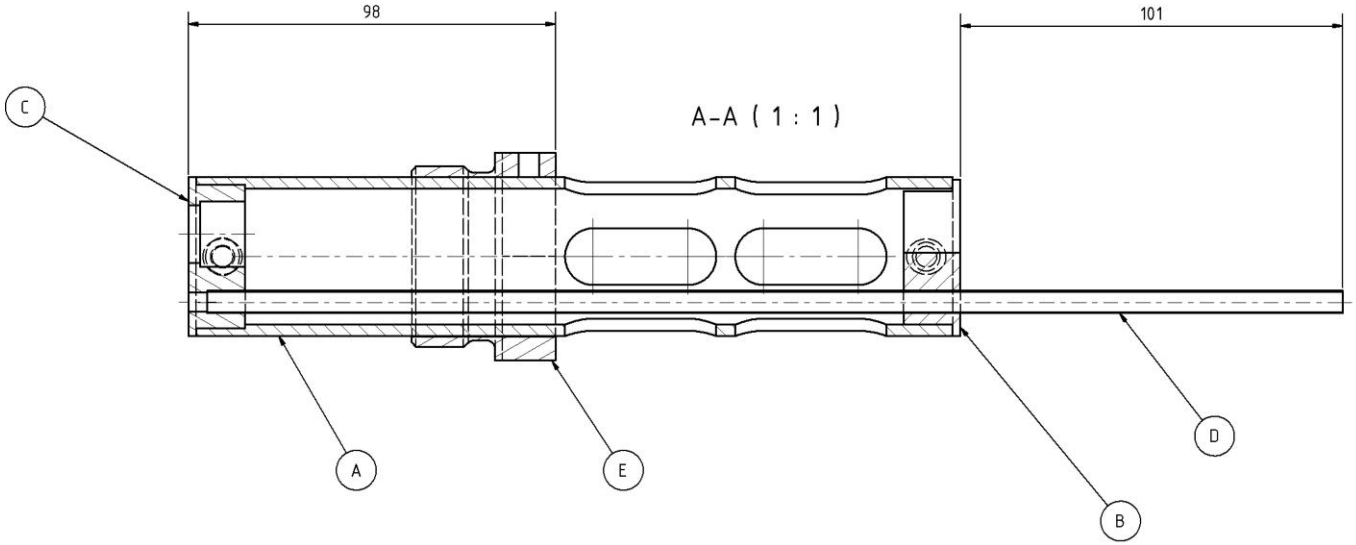

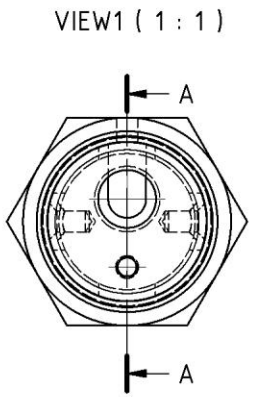

PARTS LIST			
ITEM	QTY	PART NUMBER	MATERIAL
A	1	Probe	St 37 -2
B	1	Air pipe support	St 37 - 2
C	1	SNS matrix with air nozzle	DIN X5CrNi18.9
D	1	Air pipe	DIN X5CrNi18.9
E	1	Fitting BSB G 1 1/2'	St 37 - 2

DRAWN Rizos Lampros	6/3/2014	NTUA - LME
CHECKED		TITLE: Final air - curtain device
QA		
MFG		
APPROVED		SIZE A2 | DWG NO final assembly-1 | REV
		SCALE | SHEET 1 OF 1